U.PORTO
FEUP FACULDADE DE ENGENHARIA
UNIVERSIDADE DO PORTO

Master Thesis in Mechanical Engineering

Determination of the cohesive law of structural adhesives using the direct method

Author:

Beatriz Duarte Simões

Supervisor:

Prof. Dr. Lucas F. M. da Silva

Co-Supervisor:

Dr. Eduardo A. S. Marques

Paulo D. P. Nunes

Dr. Ricardo J. C. Carbas

Master in Mechanical Engineering

March, 2022

Para a Milai

Abstract

Adhesives have grown in popularity in many industrial sectors, particularly in the automotive and aerospace industries. When compared to traditional mechanical joining methods, such as fastening or riveting, adhesive bonding technology is seen as more advantageous, since it can join different materials, as well as produce tougher joints, with a more uniform stress distribution, resulting in structures that are lighter and that consume less energy. The development of cost-effective and reliable bonded products requires a thorough understanding of the materials being used, so the experimental procedures used to determine their properties should be as simple as possible, in order to minimize the iterations and computational effort and maximize the accuracy of the data. As a result, the direct method emerges as a highly viable choice to obtain the essential parameters for characterisation of adhesive fracture behaviour.

The present work aimed to characterize the fracture behaviour of structural adhesives through the application of the direct method. This approach was implemented using the J-integral together with the Digital Image Correlation (DIC) technique. Furthermore, a Python script was developed for process optimization. The Mode I cohesive law of two adhesives was attained and some exploratory work on Mode II was performed.

The bulk specimens were used to predict the adhesives' strength, and the tests were carried out at two different loading rates, replicating the strain rate shown by Double Cantilever Beam (DCB) tests. The fracture energy results were obtained using the J-integral approach, as well as DCB and End-Notched Flexure (ENF) tests. The fracture toughness of each adhesive was determined by comparing these values to the Compliance Based Beam Method (CBBM). Then the cohesive law for Mode I was estimated, by differentiating the J values with respect to the crack tip opening displacement (CTOD).

The attained results were implemented in a cohesive zone model (CZM) to validate the direct method, by making a direct comparison between experimental and numerical results. Although the damage mechanism was not precisely described, this approach could still predict the main features of the cohesive law.

The obtained cohesive law was also used to simulate the fracture behaviour in a different geometry, in order to assess the effect of test specimens on the results. The data suggest that the direct method is influenced by the joint geometry and the adhesive's constraining conditions.

Resumo

O uso de adesivos é cada vez mais comum em aplicações industriais, mais concretamente nos sectores automóveis e aeroespaciais. A tecnologia de ligações adesivas, apresenta-se mais vantajosa do que as juntas mecânicas tradicionais, como ligações aparafusadas ou rebitadas, pois permite ligar materiais distintos e produzir juntas mais resistentes, com uma distribuição de tensões mais uniforme, resultando em estruturas mais leves e que consomem menos energia. O desenvolvimento de produtos duráveis e com uma boa relação custo-desempenho, requer um profundo conhecimento dos materiais envolvidos. Como tal, os procedimentos experimentais usados para determinar as suas propriedades devem ser simples, com o menor número de iterações e esforço computacional possível, permitindo obter informação mais precisa. Como tal, o método direto surge como uma escolha altamente viável para a obtenção dos parâmetros essenciais de caracterização do comportamento à fratura dos adesivos.

O presente trabalho tem como principal objetivo a caracterização do comportamento à fratura de adesivos estruturais, recorrendo ao uso do método direto. Esta abordagem foi implementada utilizando o Integral-J, juntamente com a técnica de correlação digital de imagem (DIC). Ademais, foi desenvolvido um algoritmo em linguagem Python, com o propósito de optimizar o processo. A lei coesiva de dois adesivos, em Modo I, foi determinada, sendo também realizado algum trabalho exploratório em Modo II, para os mesmos adesivos.

Os provetes *bulk* foram utilizados para prever a resistência dos adesivos, tendo sido executados a duas velocidades de carregamento, de forma a replicar a taxa de deformação existente nos testes Double Cantilever Beam (DCB). Os resultados da energia de fratura foram obtidos aplicando a abordagem do Integral-J, utilizando testes DCB e End-Notched Flexure (ENF). A resistência à fratura de cada adesivo foi determinada comparando estes valores com os obtidos pelo Compliance Based Beam Method (CBBM). Por fim, a lei coesiva em Modo I foi estimada, derivando os valores de J em função da abertura da ponta da fenda (CTOD).

Os resultados alcançados foram implementados num modelo de zona coesiva (CZM), de modo a validar o método direto, por comparação direta entre os resultados experimentais e numéricos. Embora o mecanismo de dano não tenha sido descrito com precisão, esta abordagem ainda permitiu prever as características principais da lei coesiva.

A lei coesiva obtida foi também utilizada para simular o comportamento à fratura numa geometria diferente, visando uma avaliação do efeito dos provetes de teste nos resultados. Os dados obtidos sugerem que o método direto é fortemente influenciado pela geometria da junta, assim como pelas restrições aplicadas ao adesivo.

Contents

List of Figures

List of Tables

List of acronyms

CBBM	**C**ompliance **B**ased **B**eam **T**heory
CBT	**C**orrected **B**eam **T**heory
CCM	**C**ompliance **C**alibration **M**ethod
CTOD	**C**rack **T**ip **O**pening **D**isplacement
CZM	**C**ohesive **Z**one **M**odel
DCB	**D**ouble **C**antilever **B**eam
DIC	**D**igital **I**mage **C**orrelation
ENF	**E**nd-**N**otched **F**lexure
FEA	**F**inite **E**lement **A**nalysis
FEM	**F**inite **E**lement **M**ethod
FPZ	**F**racture **P**rocess **Z**one
LEFM	**L**inear **E**lastic **F**racture **M**echanics
LVDT	**L**inear **V**ariable **D**ifferential **T**ransducer
TENF	**T**apered **E**nd-**N**otched **F**lexure
TDCB	**T**apered **D**ouble **C**antilever **B**eam

1 Introduction

1.1 Background and motivation

The use of adhesives in the industrial sphere has been significantly increasing, namely in the automotive and aerospace fields [1, 2]. Compared to classic mechanical joints, such as fastening or riveting, the bonding technology is shown to be more advantageous, since it can join different materials and allows for a greater design flexibility, allowing for tougher joints with a more uniform stress distribution [3], which is translated into structures with reduced weight, less energy consumption, and fewer vehicle emissions [2, 3].

The development of cost-efficient and reliable products demands extensive knowledge of the materials [4] and thus the experimental procedures used to determine their properties should be as simple as possible, with the minimum number of iterations, and the lowest computational effort, in order to obtain the most accurate date. Hence, the direct method turns out to be an extremely relevant option to reach the necessary parameters that enable the characterization of the adhesive fracture behaviour.

In regards to the fracture resistance of the adhesive joints, researchers have recurrently used the Double Cantilever Beam (DCB) test to obtain the critical energy release rate, G_{IC}, for Mode I [5, 6], while for Mode II, the End Notched Flexure (ENF) test has been the most commonly used to determine the critical energy release rate G_{IIC} [6]. In this manner, the Digital Image Correlation (DIC) technique provides essential information for the estimation of the cohesive laws. Furthermore, the application of the J-integral enables the determination of the cohesive laws, even when the initial crack length, as well as the stress in the crack tip, are unknown, avoiding the limitations of the Linear Elastic Fracture Mechanics (LEFM). Besides that, the direct method shows the potential to automatize this process, allowing for a more expedite collection of information about the adhesive behaviour in the respective joint.

Although the study of adhesive behaviour through DCB and ENF testing is widely disseminated, the use of these tests to implement the direct method, with the DIC technique, is not yet considered a preferential approach.

1.2 Objectives

The present work serves two main purposes. The first is the validation of the use of the direct method application in the estimation of the cohesive law. It should be accomplished using the J-integral with resort to displacement fields obtained through the DIC technique. Moreover, the process should be validated for Mode I, and some exploratory work on Mode II should be conducted. The second relates to the development of a code in Python language that enables to automate the process of estimating the cohesive law for structural adhesives.

1.3 Research methodology

To achieve the referred purposes, the following research methodology was used:

- Thorough literature review with the aim of learning the state of the art related to the application of the direct method using the DIC technique and the J-integral to estimate the cohesive law in structural adhesives.
- Development of a code in Python language to automate the processing of the collected data through DIC.
- Execution of experimental fracture tests, namely DCB and ENF with two different structural adhesives.
- Application of the cohesive laws obtained through experimental tests in numerical simulations.
- Validation of the experimental data in a different test geometry, namely block specimens.

1.4 Thesis outline

The thesis is divided into eight sections. The first chapter provides a brief overview of the problem being addressed, as well as the background and motivation for this work and its goals.

The second chapter presents a literature review that encompasses a survey of adhesive joints, accompanied by the most relevant failure prediction approaches. Considering that the aim of this work is to characterize the fracture behaviour of structural adhesives, using the direct method, this section includes an extensive description of fracture and damage mechanics. The former is focused on reviewing the state of the art of the J-integral approach, whereas the latter thoroughly describes the cohesive zone modelling process. The last part of the chapter describes the cohesive parameter estimation and the digital image correlation technique.

The third chapter sheds light on the experimental procedures offering a description of the materials and performed tests, as well as an explanation of the data processing strategy. The fourth chapter describes the finite element modelling details and a numerical validation of the inputted softening laws.

The fifth chapter informs about the exploratory work that was conducted in Mode II, comprising the test configuration, experimental results, and the final remarks.

The sixth chapter provides the summary of the appended paper, with its objectives and conclusions.

Finally, the seventh chapter discusses the conclusions reached upon the finalization of this work while the eighth chapter puts forward suggestions for future work.

2 Literature review

2.1 Survey of adhesive joints

Adhesives are ubiquitous in nature [7] and, for several centuries, they were made from various natural products, such as bones, skins, fish, and plants. Nevertheless, the use of this joining method in highly technological applications only became significant in the last 70 years. The reason behind this is the arrival of advanced synthetic polymers, which were only developed in the mid-forties and allowed the development of durable high performance adhesives [8].

An adhesive is a material capable of joining more than one substrate – the materials joined by the adhesive [8] – through the process of surface attachment [9]. It possesses the quality to form bonds between two surfaces, with relatively small quantities, comparing to the final weight of the objects [10]. When two substrates are held together by an adhesive layer, an adhesive joint is created [11]. These joints can be composed of similar or dissimilar materials and, after bonding takes place, the substrates are then designated as adherends [2].

The phenomenon of adhesion is transversal to multiple areas, but its main application is in adhesive bonding, which has been the scope of intensive research over the past few years [12]. Although there is no consensual definition of adhesion among research peers, it may be defined as the state in which two surfaces are held together through interfacial forces. When both surfaces are in contact, the attraction between them can only be reversed resorting to work [11].

Applications in which the substrates are subjected to high stresses, up to their yield point, require the use of a structural adhesive. Moreover, these bonds must be capable of transmitting stress without compromising its integrity along the process [10]. This category of adhesives has been developed within the last 100 years [2] and one of its landmarks was the emergence of the epoxy resins [13]. Thus, the adhesives based on synthetic polymers, like epoxies, are now considered as viable alternatives for other joining methods, such as welding, mechanical fastening and riveting [2, 14]. The different stress distributions provided by these joining methods can be observed in Figure 1.

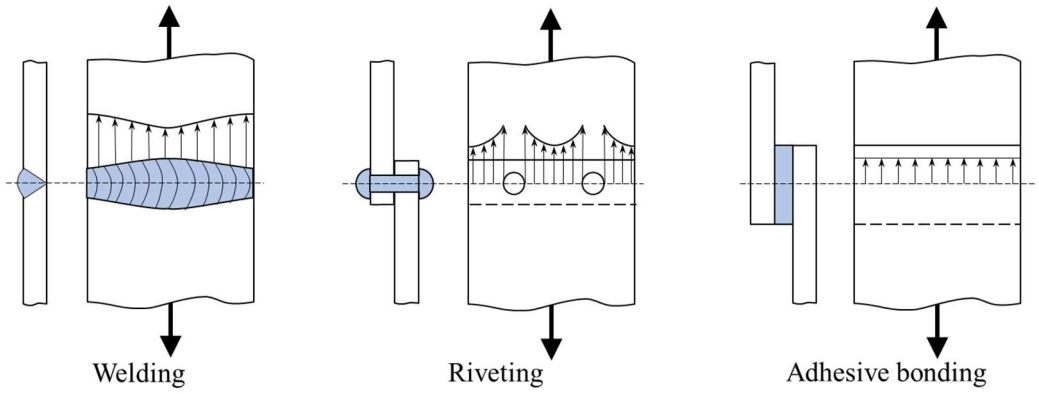

Figure 1 - Comparison of the stress distribution between the different joining techniques.

The advantages and disadvantages of this technology are summarized in Table 1.

Table 1 - Advantages and disadvantages of the adhesives [7, 10].

Advantages	Disadvantages
• Uniform stress distribution and large stress-bearing area • Excellent fatigue resistance • Vibration damping and shock absorption • Minimizes and prevents galvanic corrosion between dissimilar metals • Flexibility in the design allowing the emergence of new design concepts • Seals joints and isolate them from several environments • Joins many combinations of materials • Usually cheaper and/or quicker than mechanical fastening • Prevents damage to the metal parts when heat is required to set the joints • Attractive strength/weight ratio • Possibility to automate the formation process • Improves the stiffness of the joints • Joins thin metal sheets	• Difficult visual examination of the bonded area • Requires careful surface preparation, frequently with corrosive chemicals, to obtain a durable bond • Long cure cycles, mainly with low curing temperatures • Demands specific equipment (e.g., holding fixtures, presses, ovens, and autoclaves) • Limited upper service temperature • Rigid process control, namely, cleanliness • The service life of the adhesive joint is dependent on the exposure environment • Requires prevention of peel and cleavage stresses resulting in a low strength of the joint • May require specific training • Usually involves high temperatures to better hardening • Health problems due to exposure to solvents used for cleaning

2.1.1 Classification of adhesives

The classification of adhesives can be done via several methods, but the most general way to distinguish them is through their origin: natural or synthetic. Since this categorization is too broad, the industry adopts other categories, according to its objectives [15], commonly opting for polymer base, functionality in the polymer "backbone", physical form, functional type, chemical family, and method of application [2, 8]. Somehow, all the classifications considered above eventually overlap [7, 12].

The polymer base can be natural or synthetic. The natural group encompasses animal glue, casein- and protein-based adhesives, and natural rubber adhesives. Most of these are of organic origin, yet there are some adhesive systems which fully originate from inorganic elements. The synthetic group may be divided into industrial and special compounds. The former comprises acrylics, epoxies, and silicones, while the latter includes pressure sensitive adhesives [7, 10, 15].

The functionality in the polymer "backbone" further groups the adhesives as thermosetting, thermoplastic, elastomeric, or hybrid. The cure cycle of the thermosetting adhesives is a process which occurs through chemical reactions at room temperature or at high temperatures, depending on the adhesive type. However, these adhesives cannot be heated or softened repeatedly after the initial cure cycle is completed [11, 15]. Moreover, they may be offered as one-part or multiple-part systems: the former mostly demands high cure temperatures and exhibits a reduced shelf-life; the latter usually cures at room temperature and has a longer shelf-life than its counterpart [2]. Contrarily to thermosetting adhesives, the thermoplastic ones do not cure or harden with heat, nor do they show cross-linking during the process, such that they can be melted without significantly altering their properties. These adhesives are presented as a one-part system and harden upon cooling from a melted state, or by evaporation of a solvent or water vehicle [11, 15]. In a different manner, elastomeric adhesives have their own classification due to their peculiar rheological characteristics and are composed of polymers with rubber properties, which can be synthetic or natural, granting the adhesives with high values of tenacity and strain [15]. Finally, hybrid adhesives are a combination of thermosetting, thermoplastic, or elastomeric resins and were developed with the purpose of obtaining the more convenient properties from each component. Stiff and brittle resins are commonly combined with tough and flexible elastomeric or thermoplastic adhesives, with the aim of improving their peel strength and energy absorption [7, 15].

When it comes to physical form, the adhesives may be supplied in liquid, paste, film or tape, or powder form, and each form determines the application method [11]. Liquid adhesives tend to flow and spread during the cure cycle, mainly at high temperatures, due to

their low viscosity, and therefore, must be applied by means of mechanical spreaders such as rolls, sprays, or brushes. The paste ones have high viscosity and, for this reason, are destined for gap-filling, a process in which its anti-sagging properties are crucial, allowing their application on vertically oriented surfaces. Hence, they should be applied with spatulas, syringes, mastic pistols, or pneumatic equipment. Tape and film adhesives provide uniform bond line thickness, since they are supported by a paper sheet, a fabric, or a glass or nylon mesh, which help controlling the adhesive layer thickness and ensure stress distribution. Lastly, powder adhesives require previous heating or activation with solvents, so they can be converted into liquid form and acquire the ability to flow [11, 15].

The functional type separates the adhesives into structural and non-structural. The former should ensure high strength and performance, while the latter, such as pressure sensitive adhesives, hot melt adhesives, water based adhesives, among others, do not have the capacity to resist high loads [2, 15].

Within the very diverse chemical families of adhesives, the most significant ones are the epoxies for thermosetting adhesives, polyamides for thermoplastic adhesives, and polyurethanes for elastomeric adhesives. The epoxies are considered the most important and versatile family of structural adhesives because they exhibit excellent tensile and shear strength. Additionally, they present low peel strength, unless they are modified with a more ductile polymer. Fully imidized aromatic thermoplastic polyamides are linear polymers which show a good thermomechanical performance and are used in high temperature applications (>230°C). Nonetheless, these are expensive and require large cure temperatures. On the contrary, polyurethanes may be cured at room temperature or high temperature, and they are flexible and demonstrate good peel and shear strength. Furthermore, this adhesive remains tough and flexible, even at low temperatures, although it is sensitive to moist and heat [2, 8, 15].

2.1.2 Failure modes and joint design

The primary function of a structural adhesive joint is to transmit external loads to the different structural parts. If the joint malfunctions, it will suffer damage which may consist of complete failure of the bonded structure or some degree of plastic deformation. That being said, for successful design of bonded joints is fundamental achieve a relationship between the loads applied to the joint and a parameter that will adequately describe the criteria for structural failure [10].

In a general way, there are three failure modes in adhesive joints: cohesive failure in the adhesive, adhesive (interfacial) failure, and cohesive failure in the substrate. The first

occurs when the internal adhesive strength is weaker than the bond between the substrate and the adhesive, or than the substrate itself [15], after which the surfaces of both substrates remain covered with adhesive. This process can be driven by excessive thermal stresses, gross void defects, or inadequate overlap length [2]. The second failure mode generally happens due to inadequate preparation of the surfaces, since the joint needs to be projected in a manner that prevents adhesive failure. Consequently, when the design and conception of the joint are properly executed, the collapse of the joint will result from substrate failure [15]. Figure 2 shows the different types of failure modes in bonded joints.

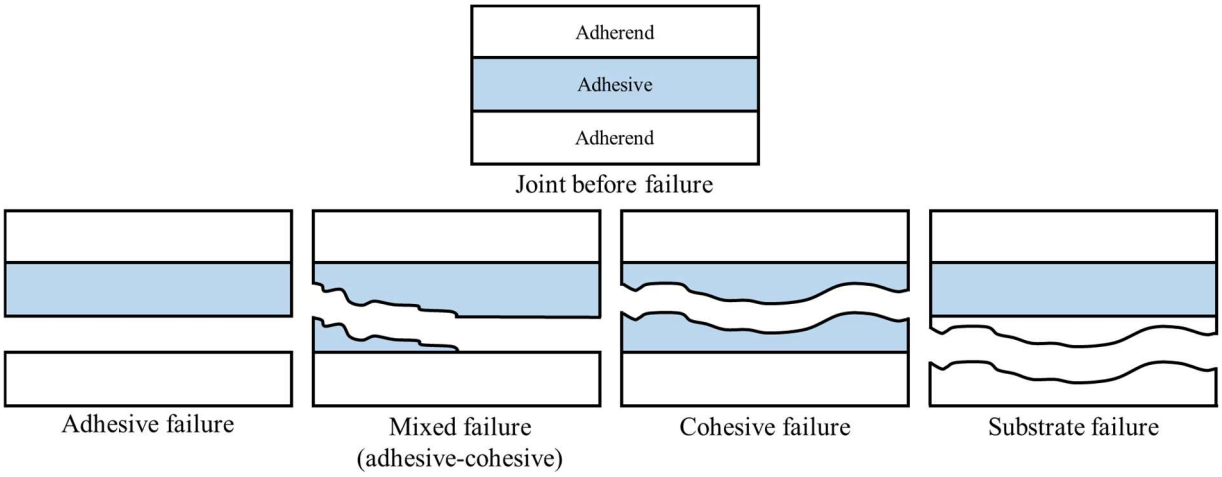

Figure 2 - Different failure modes for adhesive joints.

Adhesive joints can be subjected to several types of stress during service, which affects the adhesive layer in different manners. In order to guarantee a successful design, it is imperative to comprehend those stresses, in addition to the differences between them [13]. Essentially, there are four fundamental modes of loading: shear, tension, cleavage, and peel, which can be observed in Figure 3. In practice, these modes can be found in different combinations or variations [15].

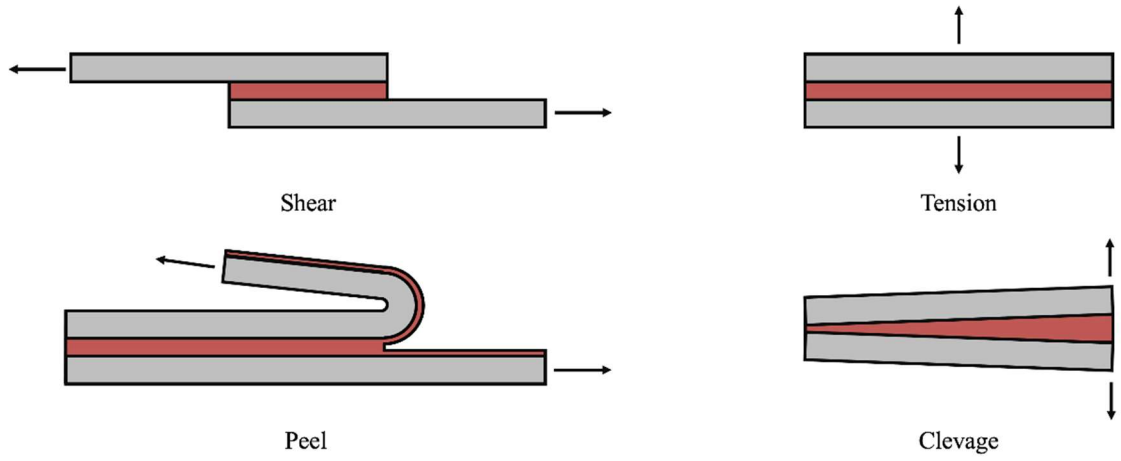

Figure 3 - Modes of loading in the adhesive joints.

The most common joints are single-lap joints, double-lap joints, scarf joints, and stepped-lap joints [15]. The selection of the adhesive must take into consideration the design of the bonded joint, for two main reasons. The first and most important one, refers to the way the load travels along the adhesive joint. For instance, a joint that is subjected to high levels of peel and/or cleavage will require a toughened system of adhesive that can handle those loads, whereas high levels of shear or tension will be better handled with a stiffer adhesive system. The second reason concerns the way the joint must be assembled. When joints are very large, the working life of the adhesive, prior to the cure cycle, must be long enough to provide sufficient time for adhesive application [8]. Figure 4 provides some examples of the used adhesive joints.

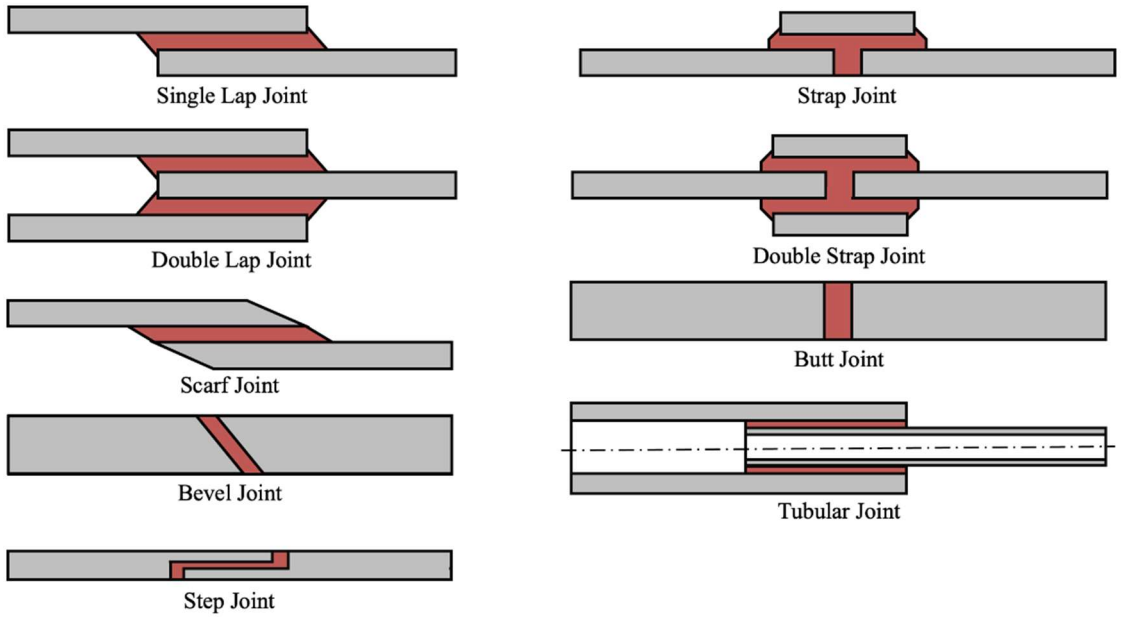

Figure 4 - Examples of joint configurations.

2.2 Failure prediction approaches

As we have seen above, adhesive joints may be subjected to diverse loading conditions and peel and shear stresses are usually the most important stress components for the analysis of joint strength. An ideal design presupposes tensions within the adhesive layer that are dominated by in-plane shear. However, the eccentricities of the applied loads existent in the real joints create bending moments with a significant potential to generate severe peel stresses that must be accounted for [13]. These peel and shear stresses exhibit peaks at the edges of the adhesive, with values that tend to infinity when the thickness of the adhesive tends to zero. Thus, the failure of the joints usually begins at the edge of the adhesive [8]. There are three approaches to assess the strength of the adhesive joint: continuum mechanics, fracture mechanics, and damage mechanics, which is a combination of the previous two [16].

2.2.1 Continuum mechanics

When the maximum stresses are determined and the allowable stresses are calibrated, the failure criterion based on the continuum mechanics may be used to predict the failure of the adhesive joint, namely through the maximum stress criterion, Von Mises criterion, and Tsai-Wu criterion [8]. In this approach, adhesives and substrates are modelled using continuum finite elements and assume a perfect connection between them [2], with no consideration for the interface properties between adhesive and substrate [16]. Nevertheless, due to the presence of singularities in the proximity of an adhesive edge, the approach referred above is not able to accurately predict the failure of the adhesive joint [2, 8]. These singularities are shown in Figure 5. According to the linear elastic analysis, these singularities have correspondent infinite stress values and, as a result, the use of the Finite Element Analysis (FEA) impedes the existence of a convergence due to the increasing stresses, as the mesh gets progressively refined. Several authors have tried to overcome this problem, but the solutions are only applicable to continuum structures and cannot be utilized to describe defects or different materials [2, 16].

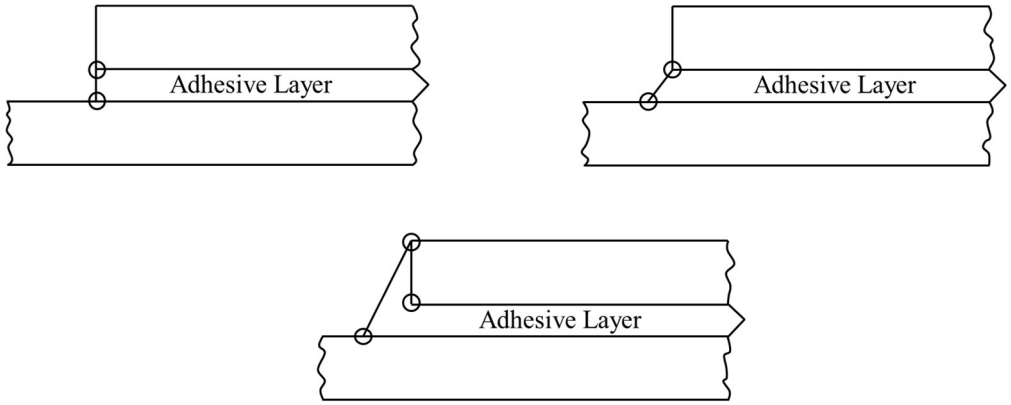

Figure 5 - Singularities in the proximity of an adhesive edge. Adapted from [16].

2.2.2 Fracture mechanics

The failure criteria previously mentioned are based on the theory of the Strength of Materials, which describes this material as exempt of defects. On the other hand, Fracture Mechanics assumes that a structure may contain defects caused by the manufacturing process or by an accident during its functioning, an aspect that violates the principles of continuum mechanics. Furthermore, it evaluates if the existent defects will remain under a critical dimension, even though they may propagate in a stable manner, or if they will cause a catastrophic failure [15-17]. More specifically, delamination, debonding, cracks, and other imperfections in the materials, usually make up stress concentration points and become initiation and propagation fracture zones that may cause component failure. The Fracture

Mechanics approach is based on two main criteria: the stress intensity factor criterion e the energy criterion [16].

Energy release rate approach

The initial progress in Fracture Mechanics was achieved by Griffith [18], upon the conclusion that all materials possess a defect distribution and that a potential fracture will occur from the most critical ones. More specifically, the researcher determined that whenever a load is applied, an internal defect propagation will occur, when the available energy at the edge of this defect (G – Energy Release Rate) becomes equivalent to the necessary energy for crack propagation (G_c – Critical Energy Release Rate), being the latter a material property [15, 17]. Then, the critical condition to prevent crack propagation is [16]:

$$G \leq G_c. \tag{2.1}$$

Griffith's theory was first developed for ideally brittle materials. Still, even in these materials, there are energy dissipation mechanisms, associated to an inelastic deformation in the crack tip, which occur in the so-called fracture process zone (FPZ). This zone must be substantially smaller than the crack length, a, to admit the application of the Linear Elastic Fracture Mechanics (LEFM) principles. In all cases, these dissipation mechanisms can be embodied in an energy per crack surface unit, being that the energy release rate for a plate with constant thickness is given by the following equation [15, 17]:

$$G = \frac{1}{B}\left(\frac{dW}{da} - \frac{dU}{da}\right) \tag{2.2}$$

in which W represents the work done by exterior loads, U represents the internal elastic deformation energy of the solid, B stands for the thickness of the solid, and a stands for the length of the crack. The Equation 2.2 shows that the deformation energy release rate is equal to the variation of the potential energy due to an increment in crack propagation [17].

Stress intensity factor approach

The stress intensity factor represents a scale factor that defines the change in the stress state in the vicinity of the crack tip and is given by [15-17]:

$$K = Y\sigma_R\sqrt{\pi a} \tag{2.3}$$

where Y is an adimensional factor dependent on the geometry and load distribution, σ_R stands for the applied remote stress, and a stands for the crack length. There will be crack propagation when the following condition is reached:

$$K = K_c \tag{2.4}$$

where K_c stands for the fracture toughness and is a material property [13, 15-17].

Irwin [19] resorted to the analysis of the virtual crack closure technique to obtain the relationship for a plane stress state:

$$G = \frac{K^2}{E} \tag{2.5}$$

and the following relationship for the plane strain state:

$$G = \frac{K^2(1-\nu^2)}{E} \tag{2.6}$$

These relationships remain valid for the critical values K_c and G_c [15-17].

As shown in Figure 6 - Fracture modes: Mode I (left), Mode II (middle), and Mode III (right)., there are three modes according to which the crack can propagate. Mode I represents an opening mode and both Modes II and III represent shear modes. In Mode II, the crack surfaces have relative displacement perpendicular to the crack front, while in Mode III, the same movement is parallel to the crack front [15, 16].

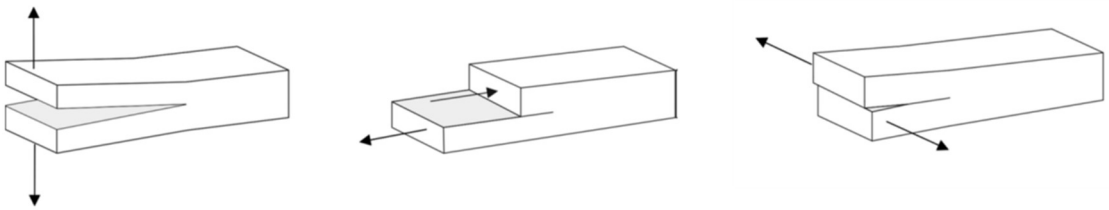

Figure 6 - Fracture modes: Mode I (left), Mode II (middle), and Mode III (right). Adapted from [16].

There are diverse advantages associated to the use of energy release rate instead of the stress intensity factor, from which two may be highlighted. First, G presents a physical meaning related to the process of energy absorption; second, it is very difficult to calculate the value of K, especially if the crack is located in an interface or within its vicinity. Considering that adhesive joints are known for being non-homogenous, Ripling, et al. [20] proposed the use of the energy release rate for this type of joint, in order to describe their fracture process.

For bulk materials, crack tends to propagate in Mode I. However, under service conditions, bonded joints are not usually loaded in pure loading conditions. Furthermore, the substrates also restrict deformation and originate a triaxial stress state. Hence, the characterization and analysis in Mixed Mode are very important for this type of joints, being fundamental the adequate use of energetic criteria. One criterion that is utilized assumes that the Mixed Mode

fracture energy envelope represents a simple sum of the normalized adhesive components [13, 15]:

$$\left(\frac{G_I}{G_{Ic}}\right)^A + \left(\frac{G_{II}}{G_{IIc}}\right)^B = 1 \tag{2.7}$$

where G_{Ic} and G_{IIc} are the critical energy release rates for Modes I and II, respectively, and A and B are exponents. The most used criteria are the linear ($A = B = 1$) and the quadratic ($A = B = 2$) [15, 16]. The Mixed Mode fracture ratio, highly used in planar problems, may be defined as [16]:

$$\varphi = tan^{-1}\sqrt{\left(\frac{G_{II}}{G_I}\right)} \tag{2.8}$$

J-integral approach

For the cases in which the LEFM principles are not applicable, there are alternative approaches that enable the computation of the fracture toughness of the material [21], namely the J-integral approach [21-25]. The J-integral, of which the formulation was developed by Cherepanov [26] and Rice [27] for elastic materials, results from the application of a contour integral, with the following formulation for two-dimensional problems:

$$J = \int_{\Gamma} (w\,dy - T\frac{\partial u}{\partial x}ds) \tag{2.9}$$

where w represents the elastic deformation energy, T is the traction vector perpendicular to the integration contour Γ, and u is the displacement vector.

Rice also demonstrated that the J-integral is independent of the contour for any elastic or elasto-plastic material, as long as deformation theory of plasticity is used [28]. Therefore, several researchers were able to apply this approach while studying ductile materials [22, 29-34], such as Li and Chandra [29], who focused on the crack growth and the plasticity in the crack tip in ductile materials, whereas Ikeda [31] investigated the failure of ductile adhesive layers constrained by stiff substrates, and analysed the effect of the adhesive layer thickness in the J-integral values. The authors noticed an increase of the J value proportional to the increase of the bond line thickness for ECP (Edge Cracked Plate) specimens, contrarily to the tendency verified in TDCB (Tapered Double Cantilever Beam) ones. In this case, the J values were independent of the bond line thickness, since most of the deformation energy was not stored in the adhesive region, but in the substrates. Additionally, they concluded that it was not expectable for the stress distribution near the crack tip to be dependent on the specimen shape, but only on J-integral and bond line thickness, maintaining the CTOD of a crack, in an

adhesive joint, a unique relationship with the J-integral [24], Rosendahl, et al. [35] measured the Mode I fracture properties for a structural silicone with a thick layer and found that the use of specimens with 6 mm and 12 mm of adhesive thickness yields a reliable value for fracture toughness. Also, Goutianos and Sørensen [24] applied the J-integral in materials with a non-linear stress-strain behaviour and concluded that even though there was some unloading in a small region behind the crack tip, the DCB substrates did not show macroscopic unloading during the crack opening and its propagation. Moreover, the researchers observed a difference between the stable value, J_{ss}, and the critical energy release value, J_c, lower than 16%, which constitutes a lower value than the usual scatter, when the fracture toughness is experimentally calculated. Therefore, this method was validated for fracture toughness and for cohesive laws in materials with large scale yielding.

In order to maintain its independence property, the contour must obey to three conditions: surround the crack tip, the elastic deformation energy should not be explicitly dependent on the x coordinate, and no other object that may alter the body energy if it is moved in the x direction, should be inside the contour [4]. Considering this property, Biel and Stigh [4] used the J-integral approach and several alternative contours. As a result, the authors observed that the two contours which assumed elastic deformation in the substrates in the presence of plasticity were less accurate. Also, the method with a lower number of assumptions was considered to be the most precise and allowed for the presence of plasticity.

Besides the fact that the J-integral is independent of the selected contour, it also permits monitoring the adhesive stress evolution in the crack tip. This aspect may be achieved by measuring macroscopic quantities through experimental procedures, such as the applied loads or the evolution of the crack tip displacement. However, this approach has some downsides like not being applicable to time-dependent materials or being dependent on the load history [36]. Furthermore, the use of the J-integral in materials with a non-linear stress-strain relation is only valid as long as there is no unloading in any point of the material, so that the stress-strain relation could be considered non-linear elastic [24]. Nevertheless, when the material is under monotonically increasing loading, there is no way to distinguish between a stress-strain relation for in-elastic materials or elastic materials [4]. In case of elastic materials, the J-integral value increases until it reaches a peak when the crack tip opening reaches a critical value. From then on it remains constant during the subsequent stable crack propagation. However, the materials with non-linear stress-strain relations may exhibit a different behaviour in which, after the initial crack propagation, there is an increase in fracture resistance followed by a value stabilization into a steady-state value [24]. Additionally, it has been demonstrated that the increase of the dependence of the crack tip resistance, regarding

geometry size and load of ductile material, is due to the combined effects of plastic dissipation and expended energy in the creation of the new surfaces [29].

The J-integral has been used in diverse cases of the study of materials, for the purpose of obtaining their fracture toughness. Kimpfbeck, et al. [23] used this approach to assess the fracture toughness of welded polymeric components through their comparison to fracture tests in bulk sheets of the same material. Consequently, they noted a difference in the fracture behaviour for both specimens, in terms of the critical J values as well as the resistance curve, which are rate sensitive. In addition, Scheel and Ricoeur [37] estimated the J-integral of a matrix crack, when it is present in the cohesive interface edge and in a central crack, followed by the study of their contribution to energy dissipation and to the cohesive zone theory. The analysis of a matrix crack tip loading in the presence of a weak interface revealed that the energy release rate does not necessarily decrease due to the energy dissipation in the cohesive zone. Moreover, it was observed that for a sufficiently low stiffness, the matrix crack tends to grow towards the interface, such that, when damage occurs, the effect of the deflection is amplified. Also, the influence of delamination was demonstrated through a model with a hole and with an inclusion bonded by an interface, resulting in the matrix crack growth in the direction of the hole, with no damage in the interface. Notwithstanding, an increase in delamination leads to the matrix crack growth towards the interface. Finally, Leitão and Gilabert [38] proposed a methodology to obtain the energy release rate from stress-strain fields that can be applied to any notched-plate specimen, not only in FEM models, but also in experimental results extracted from DIC. This approach is based on J-integral formulation and admits a precise analysis of the specimens that are under an intense dynamic loading. More specifically, it represents a more general and flexible approach through which the energy release rate value is directly obtained from the displacement field, with no need for complementary models or complex strategies of field mapping. Regarding the numerical simulation, the authors developed a robust tracking algorithm that permits to dynamically reckon the J-integral value, as the crack propagates.

Given that this approach allows to overcome some LEFM limitations [5, 16, 21, 23, 39, 40], it has been employed in the characterization of fracture processes involving large FPZs [21, 22, 41]. Furthermore, it has also been used in the estimation of cohesive laws [24, 36, 42-45] through the computation of the obtained data related to the J-integral and to the crack tip opening. Besides that, the J-integral can be applied in all loading modes: Mode I [5, 24, 29, 35, 42, 46], Mode II [4, 30, 47, 48], and Mixed Mode [34, 36, 49, 50].

Sørensen and Jacobsen [42] aimed to develop a robust approach to obtain the cohesive law from test specimens and then predict the strength of the same adhesive for other geometries.

The J-integral method yielded very good results, providing a shape of the law that suits the micromechanical model in the problem of cross-over bridging. For this problem, as well as the quantitative prediction of the strength of the bonded joint, good agreement between predicted and measured strengths was accomplished.

Upon the study of the cohesive properties and the crack tip opening displacement (CTOD) for different rates in Mode I in structural adhesives, Sun, et al. [51] found that, in the case of a toughened epoxy, the J_c and strength values escalate as the loading rate increases, displaying a cohesive law which follows a trapezoidal shape. When it comes to a ductile adhesive, such as polyurethane, the use of a loading rate above or under a critical value generates a decrease or an increase, respectively, in the parameters mentioned above. Desai, et al. [43] determined the cohesive laws for interfacial failure in Mode I, at different loading rates, and concluded that the rate dependency in the overall response of the joints, observed in cohesive laws derivate from the J-integral and CTOD values, is a result of the adhesive material sensitivity to the rate.

A study in Mode I, in which G_c, J_c, and the cohesive laws were simultaneously ascertained, Sun and Blackman [5] utilized several methods to obtain the fracture toughness of three distinct adhesives and assessed their applicability in each situation. The authors learned that for the brittle adhesive and toughened epoxy, all the values of G_c obtained through the LEFM method were in accordance with the J_c values, evidencing their validity. On the other hand, for a ductile polyurethane adhesive, the G_c values were 15% higher than the J_c indicating that the same methods are not valid. Moreover, the same authors resorted to the DIC technique to automatize the measurement of the crack length and fracture toughness in Mode I with structural adhesives. They found out that the CBBM and the Corrected Beam Theory (CBT) with a crack length extended to the compression zone yielded G values very similar to J, for all the three adhesives. More specifically, they observed almost identical values for all cases in CBT and one adhesive in CBBM, while the remaining two showed an increase of 6% in relation to the J values.

Biel and Stigh [4] compared different contours to compute the J values and then experimentally obtained the cohesive laws for Mode II, finding that the results for the substrates which suffered elastic deformation were very similar. On the contrary, for the substrates which deformed plastically, two of the three contours showed reasonable results, and it was noted that both the fracture energy and strength were related to each type of specimen and the chosen contour.

Jia, et al. [30] calculated the fracture toughness of several adhesives through the application of the J-integral, when loaded in Mode II, and assessed the effect of a high strain

rate and of low temperatures. The use of this approach allowed the use of a ductile adhesive, with plastic deformation in the substrates of ENF specimens. A significant effect of the strain rate and temperature on the fracture toughness in Mode II was observed. Moreover, this material property decreased drastically as the loading conditions changed from quasi-static to high rate. Furthermore, in high strain rate condition, the adhesive exhibited an increase in the fracture toughness, as the temperature decreased. Specifically, a -40 °C at a 3 m/s loading rate yielded a 130% increase in the fracture toughness comparing to the same test at room temperature and 2 m/s. Nevertheless, this method requires additional research since the measurement of the rotation in the loading point using DIC proved to be quite challenging.

Pérez-Galmés, et al. [41] introduced a methodology based on the J-integral approach to obtain interlaminar fracture toughness in End-loaded Split (ELS) tests without the restriction of small FPZs and displacements, which might be applied to the adhesive joints. This new method proved to be more objective than the ones based on LEFM, with no need for measurement or estimation of the crack length and acknowledging the effect of high deflections. A comparison between this method and the LEFM approach revealed a difference of less than 2.3% in the interlaminar fracture toughness values, confirming that the former is suitable for the evaluation of this parameter.

Sarrado, et al. [21] proposed a data reduction method, using the J-integral approach for the Mixed Mode bending (MMB) test. A comparison between this method and the one proposed by the standard, based on LEFM, was performed taking into consideration the accuracy and uncertainty of the results. It was concluded that this new method has a quite superior range of applicability than the ones based on LEFM, since it could be applied using MMB tests with large FPZs. Moreover, the results for Fibre Reinforced Polymer (FRP) specimens demonstrated a satisfactory degree of concordance when compared to the standardized test. Additionally, the proposed test were shown to have a lower associated uncertainty due to reduced need for the input of information and the fact there is no need for measuring the crack length, to determine the fracture toughness values. Sadeghi, et al. [22] assessed the suitability of data reduction scheme based on the J-integral for the fracture toughness determination of a ductile adhesive. When compared to the values of FEA, DCB, and MMB tests, as well as to the load-displacement curve, the obtained values proved to be accurate. The authors considered that the proposed method has high potential for adhesive joints applications.

Loh and Marzi [50] proposed a new methodology to determine fracture envelopes in mixed Mode I + III, however, there are only a few studies investigating this type of loading. The authors argue that the main advantage of this study arises from the possibility to separate the fracture energy modes which are coupled through the sum $J_c = J_{Ic} + J_{IIIc}$. Furthermore, it was

proposed a regulation for the J values instead of displacements or forces, allowing to compute nearly in real time the J values, as well as the contribution of each mode to the obtained results. Thus, it would be possible to prescribe mode mixity or J-integral versus time.

2.2.3 Damage mechanics

The methods based on fracture mechanics are limited because they do not consider the initiation phase, assuming that damage occurs in a single planar crack propagating through undamaged material. However, this may not reflect what happens in reality. On the other hand, a damage mechanics-based approach aims to solve some of these problems, enabling the modelling of progressive degradation and failure. Therefore, both initiation and propagation phases are represented in the model [8]. In general, a cohesive zone model (CZM) is adopted for this kind of study [2].

CZMs were initially developed as a numerical tool to study fracture [52]. However, today they are increasingly used for theoretical studies, in simulation of decohesion of structural joints or delamination in composite laminates [53], and thus, became the most adequate method for the modelling of adhesive joints in static and fatigue models [36]. In this approach, the volumes correspondent to the substrates remain intact, while inside the volume correspondent to the adhesive layer initiation and propagation processes of fracture take place. The adhesive layer is eliminated from the general equilibrium equations and replaced by interface forces that act between the two substrates. These forces are dependent on the relative displacement of the substrates, dynamic effects, loading history, and environmental effects. CZM is very efficient in the analytical description, as well as in the Finite Element (FE) simulation of the adhesive layer behaviour, given that the separation surface is known and the thickness and the material properties on the process zone are constant from point to point [53]. Furthermore, this modelling approach has been used in several material systems, such as polymers [54], metals [33], ceramics [55], concrete structures [56], multi-materials [57], and composites [58]; different loading types, such as static [59], dynamic [60], cyclic [61], and impact [62]; or also in the different modes, Mode I [40], Mode II [63], and Mixed Mode [21].

The basis of CZM is a cohesive law that describes the increasing initial elastic response, which reaches a maximum stress and then decreases until it eventually reaches a zero value, enabling full decohesion [29, 64]. The concept of cohesive law was developed for monolithic materials in the 60's by Barenblatt [65] and Dugdale [66] and describes the local fracture process near the crack tip as a gradual phenomenon where the separation takes place across a cohesive zone [67, 68]. While studying concrete and cementitious composites, Hillerborg, et

al. [56] was the first to apply the work developed by these researchers in the use of FEM analysis.

The idea of this approach is that the fracture process can be described as a relationship between local stress-relative displacement and the fracture process zone (FPZ). This relationship represents a constitutive law of the material, i.e., the so-called cohesive law [67]. There are several designed cohesive laws, such as linear, bilinear, trapezoidal, polynomial, and exponential, to simulate fracture using the parameters that were obtained experimentally or numerically, as shown in Figure 7 [47]. Although there are four main characteristics that define cohesive law – stiffness, strength, fracture energy, and shape [34] – two independent parameters suffice in its description, excepting the trapezoidal law. Regarding fracture energy, cohesive strength, or separation length, any two of the three may be used to characterize the constitutive law of the material [29], as the same exception applies. Moreover, the stiffness and strength of the cohesive law are difficult to obtain experimentally, nevertheless, they can be estimated empirically or by assuring concordance between the simulation and experimental data. The fracture energy can be obtained through classical fracture mechanics tests [34].

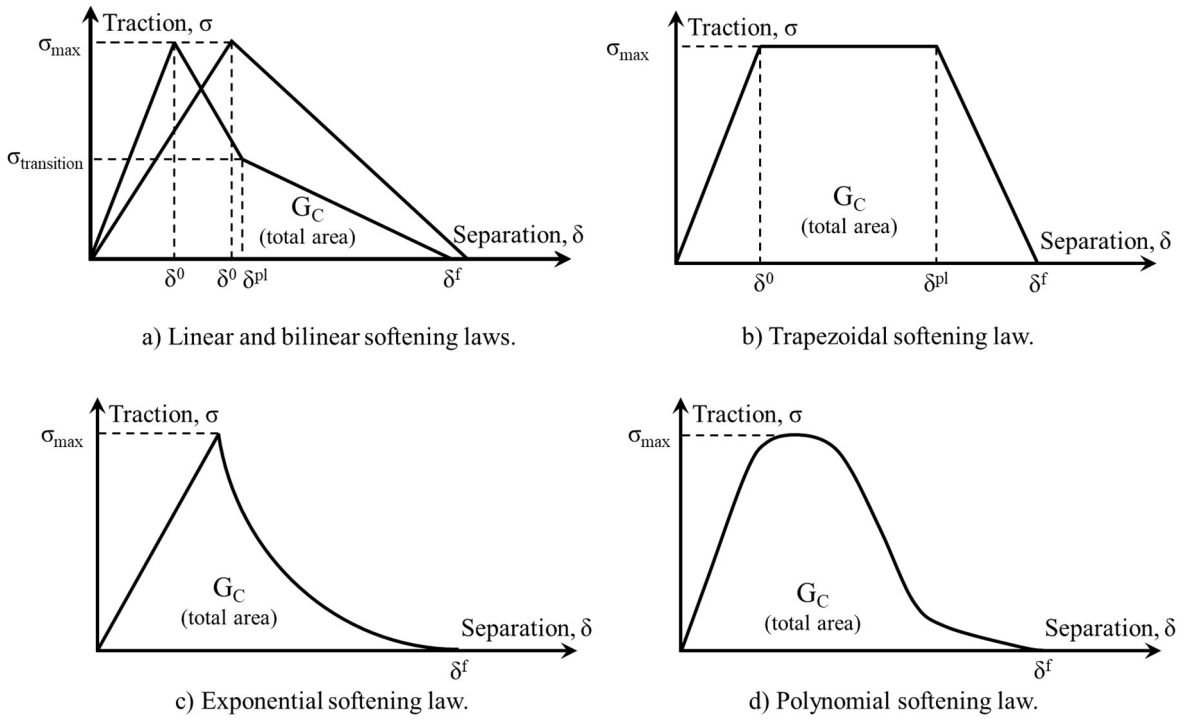

Figure 7 - Schematic representation of different softening laws.

Cohesive parameter estimation in adhesive joints

The cohesive law of any material is of great importance in the simulation of fracture processes, such that the development and study of the adhesive cohesive laws become pertinent [69]. Although CZM shows highly accurate results, a thorough determination of the parameters and shape of the cohesive law is still necessary. Yet, two main limitations may be noted: surrounding geometry-dependence of the law parameters and requirement of CZM elements' placement at the growth planes. The former may be resolved through the correct determination of the adhesive characteristics in similar constraining conditions, whereas the latter has a smaller impact because the failure paths are limited mainly in non-composite joints [70].

In general, there are three techniques suitable to estimate the cohesive properties: property identification, inverse method, and direct method. The first consists in separately calculating each parameter of CZM resorting to the adequate tests, while the second lies in an iterative fitting FE with experimental data, until reasonable compromise is reached. In both cases, the shape of the cohesive law is assumed each time a specific material is simulated, based on its behaviour in the non-elastic part of the curve [42, 53, 70]. Notwithstanding, the methods in which the cohesive law is indirectly obtained demand laborious modelling to achieve accurate cohesive parameters [42]. The third method estimates the cohesive law of each material or interface from experimental data obtained through fracture tests such as DCB or ENF [70, 71]. Furthermore, there are no made assumptions regarding the shape of the cohesive law, since the experimental data may be directly related to interface forces, rendering this approach more precise than the previous ones [53, 64].

The direct method is based on the premise that during stable crack propagation, the FPZ only translates along the specimen, ahead of the crack tip in a self-similar manner, and that the cohesive law may be deduced by differentiating the fracture toughness with respect to the initial crack tip opening [5]. In this line of thought, it is worthy to note that in 1968, Rice [27] highlighted an analytical relation between the cohesive law determined in the crack tip and the J-integral represented by $dJ/d[u_i] = t_i[u_i]$. This approach was used for different loading modes, for example, Sun and Blackman [5] in Mode I, Carvalho and Campilho [72] in Mode II, and Sørensen and Kirkegaard [49] in Mixed Mode. Even so, the experimental determination of the cohesive law is not straightforward and in recent years an effort has been made to develop diverse methods aiming to experimentally obtain it through the measurement of the CTOD, together with the J-integral values [73]. Considering the correct measurement of the crack tip opening, an essential parameter for the estimation of the cohesive law, several methods have been used, like Biel and Stigh [4] who resorted to a Linear Variable Differential

Transducer (LVDT) or Sarrado, et al. [74] who opted for DIC (Digital Image Correlation). However, when very small crack tip separations exist, difficulties emerged during the parameter measurement due to the lack of precision of the existent methods [74, 75].

Digital Image Correlation in the extraction of cohesive laws

DIC is an optical full-field and non-contact technique used to measure contour, deformation, vibration, and strain in solid materials [46]. This technique involves the application of a speckle pattern on the specimen surface, in order to produce a non-uniform grey-scale pattern. This pattern is then converted into a digital surface of grey scales, being bi-cubic splines one of the most common interpolation methods used to create a continuum digital surface. The subsequent movements of peaks and valleys are tracked to determine the surface-displacement vectors [52]. When compared to other optical approaches like Moiré's interferometry or photoelasticity, this technique presents some advantages, such as a simpler setup configuration, suitability for opaque or transparent materials, and highly precise results. Therefore, this method has been recently used in the determination of the fracture parameters in adhesive joints [76].

The development of DIC over the last decades allowed to obtain a wide range of mechanical responses, guaranteeing the monitorization of substrate deflection and rotation during the tests performed in adhesive joints [77]. Initially, this method was used to measure displacement fields, whilst the cohesive properties were estimated through an inverse FE formulation [70]. Recently, this powerful technique has been exhaustively used to study the fracture of the interface, due to the possibility of measuring local displacements near the crack tip, allowing the direct extraction of precise cohesive laws [5, 40, 51]. Even though there is plenty of research investigating the estimation of cohesive laws by DIC, the studies assessing if the CZMs are sufficient to describe the fracture behaviour of adhesive joints are still scarce [5].

3 Experimental procedures

The adhesives utilized in the present work are described in depth in the next section, as well as the manufacturing and testing techniques which have been employed. Bulk specimens, DCB, and block joints were manufactured tested for the determination of strength, fracture toughness in Mode I, and as validation tensile tests, respectively.

3.1 Materials

Two distinct epoxy-based adhesives were employed, which will be referred to as Adhesive A and Adhesive B throughout the following sections. The first is a one-component structural adhesive with crash-resistant properties, especially developed for body shop applications. It is used in automotive industry to increase the operation durability, crash performance, and the body stiffness. The second one is a structural two-component adhesive, designed for high strength and impact-resistant bonding of metallic or composite substrates. Table 2 shows the general properties of each adhesive.

Table 2 - Adhesive general properties.

Adhesive	Type of adhesive	Supplied as	Cure cycle
Adhesive A	Epoxy resin	One-part	180° / 30 min
Adhesive B	Epoxy resin	Two-part	RT / 15 days

The mechanical properties for each adhesive are listed in Table 3.

Table 3 - Adhesive mechanical properties.

Property	Adhesive A	Adhesive B
Density / g·mL^{-1}	1.26	1.07
Viscosity / Pa·s	160	430
Tensile Strength / MPa	32	30
Elongation at break / %	~6	4
Young's modulus / MPa	2100	2000

For the fracture tests, as well as for the validation tensile tests, in order to guarantee elastic deformation without plastic yielding during the loading of the specimens, hard steel was used to manufacture the substrates that were machined from DIN 40CrMnMo7. The mechanical properties of these material are presented in Table 4.

Table 4 - Steel properties.

Young's modulus / MPa	Poisson's ratio
210000	0.33

3.2 Specimen manufacturing

3.2.1 Bulk specimens

The bulk adhesive specimens for tensile strength tests were machined from cured adhesive plates with a thickness of 2 mm, prepared according to the French standard NF T 76-142 [78]. For the manufacture of the adhesive plate, uncured material was pressed between steel plates, with a silicone rubber frame contouring the material to restrain it and provide hydrostatic pressure. This procedure promotes a superior surface quality and prevents voids from appearing. In addition, the specimens were machined in accordance with British standard BS 2782 [79] to produce the configuration shown in Figure 8.

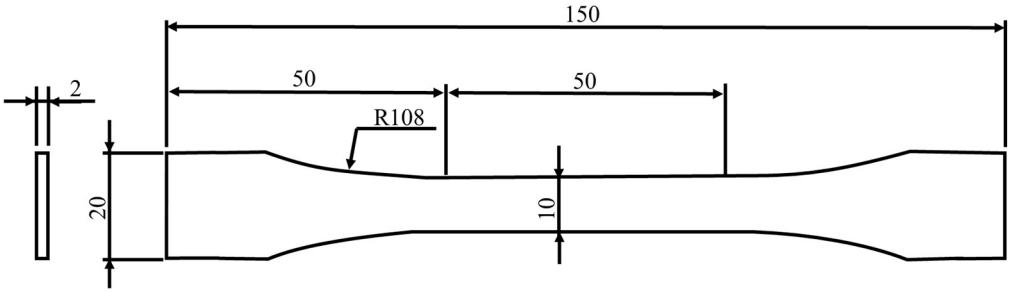

Figure 8 - Tensile specimen geometry, in mm.

3.2.2 DCB specimens

To guarantee good adhesion, both substrates were grit blasted and degreased with acetone right before the adhesive was applied. These specimens are comprised of two identical beams that are bonded together. Additionally, two loading blocks were bonded to the substrate, allowing for better data treatment using DIC analysis by relocating the loading points away from the adhesive layer. This modification was necessary due to the machine design that was used, in order to allow further DIC analysis. Figure 9 depicts a specimen with an initial section without adhesive, a, which is considered the pre-crack length. The initial pre-crack was created by placing a 0.1 mm thick sharp razor blade in the middle of the bond line. To achieve a consistent adhesive thickness, the bond line thickness was measured with calibrated tape. The constant thickness for Adhesive A and Adhesive B was 0.2 mm and 0.5 mm, respectively. Finally, to facilitate posterior DIC analysis, the specimens were coated with white matte paint and speckled with black dots.

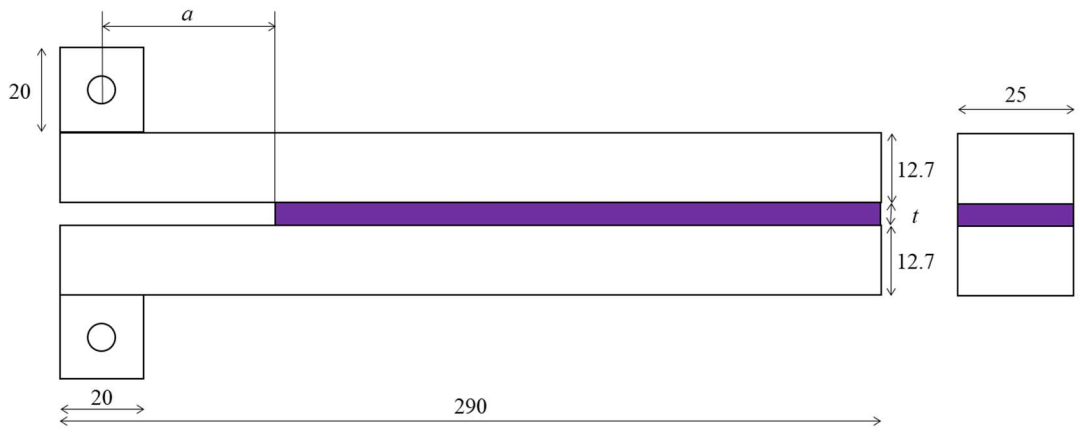

Figure 9 - DCB specimen geometry, in mm.

The mould used to cure the adhesive was also altered as a result of the DCB specimens being adapted by attaching the steel blocks at their ends. Steel bars were placed in the gaps between the substrates and the mould to provide a consistent dispersion of heat through conduction. Figure 10 shows the end outcome of a batch of DCBs that are ready to go into the hot press.

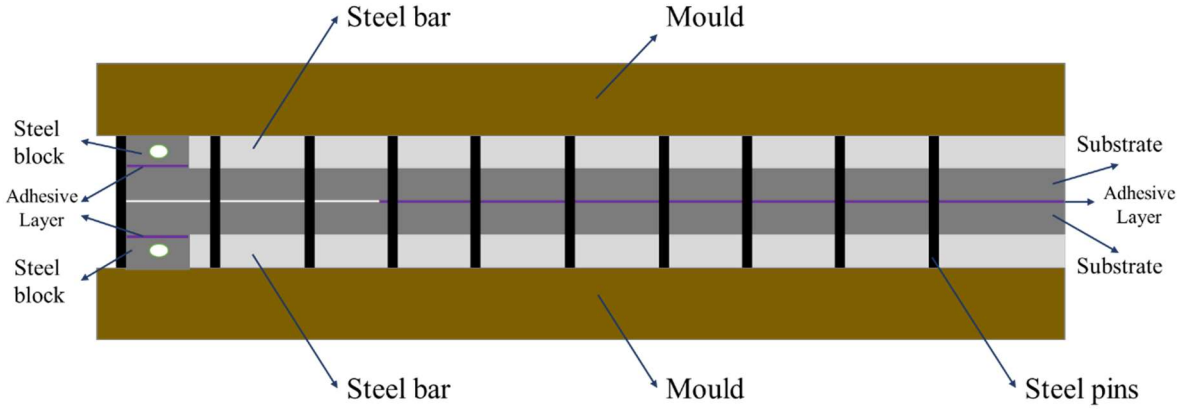

Figure 10 - Representation of the used mould.

3.2.3 ENF specimens

To guarantee good adhesion, both substrates were grit blasted and degreased with acetone right before the adhesive was applied. These specimens are comprised of two identical beams that are bonded together. Figure 11 depicts a specimen with an initial section without adhesive, a, which is considered the pre-crack length. The initial pre-crack was created by placing a 0.1 mm thick sharp razor blade in the middle of the bond line. To achieve a consistent adhesive thickness, the bond line thickness was measured with calibrated tape. The constant thickness was 0.2 mm for both the adhesives. In order to avoid friction between the two beams where there is no adhesive, a Teflon sheet embedded in oil was inserted in this

area. Finally, to facilitate posterior DIC analysis, the specimens were coated with white matte paint and speckled with black dots.

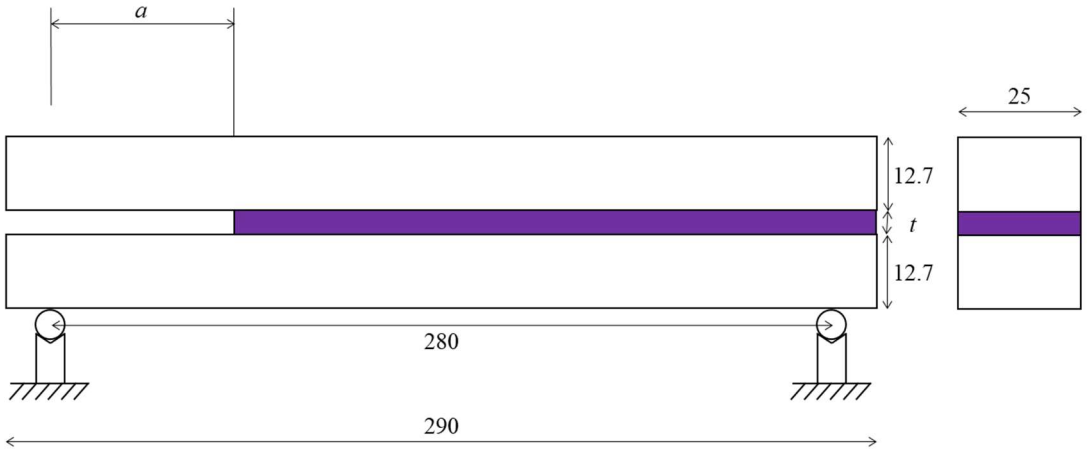

Figure 11 - ENF specimen geometry, in mm.

3.2.4 Block specimens

The substrates were manufactured from mild steel, since testing the specimens in tension should not cause high stresses in the steel, thereby reducing the possibility of plastic deformation. To guarantee optimal adhesion, both substrates were grit blasted and degreased with acetone right before the adhesive was applied. As illustrated in Figure 12, the specimens were composed by two similar blocks that were bonded together using adhesive. Finally, to facilitate posterior DIC analysis, the specimens were coated with white matte paint and speckled with black dots.

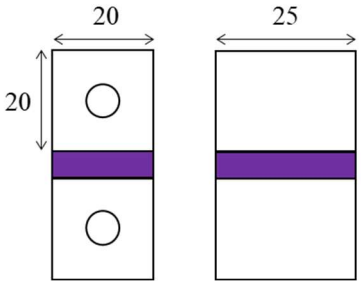

Figure 12 - Block specimen geometry, in mm.

3.3 Testing setup

Two distinct machines were used for the three types of tests: strength prediction, fracture test, and validation tensile test. A universal testing machine, INSTRON® 3367, with a load cell of 30 kN, was used for the strength prediction and validation tensile tests. An INSTRON® 8801 testing equipment with a 100 kN load cell was used for the Mode I fracture tests. The quasi-static accepted speeds for bulk tensile specimens were 1 mm/min, 20 mm/min, and 50

mm/min, while the speed for the remaining two types of specimens was 0.2 mm/min. It was necessary to synchronize the applied load and the displacement field of areas of interest for the fracture tests, as well as the validation tests. Thus, a digital camera (Canon EOS M5) equipped with a Canon EF-M 18-55 mm F/3.5-5.6 lens was placed in front of the specimens, with the lens perpendicular to the observation surface.

A laser-based approach was chosen to ensure that perpendicularity was maintained. Figure 13 depicts the completed system, which included a 3D printed part that positioned the laser perpendicularly to the test specimen. The part's positioning was the result of its geometry, as well as four magnets that kept the part from misaligning. The tripod head was adjusted by leaning a U-shaped part against a vertical plane of the machine until the laser beam was perfectly defined on the face of the same part. Figure 13 also depicts the moment after this alignment was achieved.

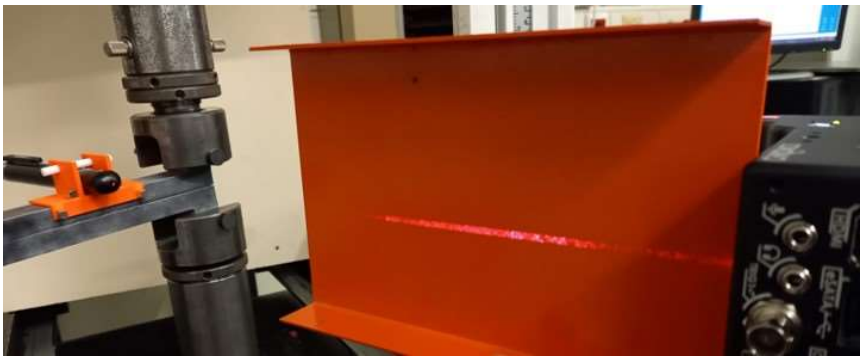

Figure 13 - Laser-based approach for perpendicularity.

In the previous section, the painting procedure for fracture and validation specimens was described. This pattern is used to perform the DIC analysis, and its quality has influences the accuracy of the measured displacements. Thus, a parametric study was conducted, in order to achieve the best quality pattern. Figure 14 shows the different results obtained for several speckles and lightning conditions. During the development of the present work, it became evident that any change, both in the speckle or in the lighting conditions, would lead to results with different quality levels. The displacement field data showed a significant improvement when the quality of the marked points was higher than 6 in a maximum of 10. In this manner, after testing a significant number of specimens with different quality points, it was settled that the speckle should have, at least, a quality of 7, to achieve the expected results. Nevertheless, there was an effort to obtain all the specimens with speckles that yielded quality points between 8 and 10, ensuring that any noise observed in the data was not due to this parameter. Additionally, the same lightning conditions were carefully reproduced for every test, to achieve a more consistent and robust testing setup.

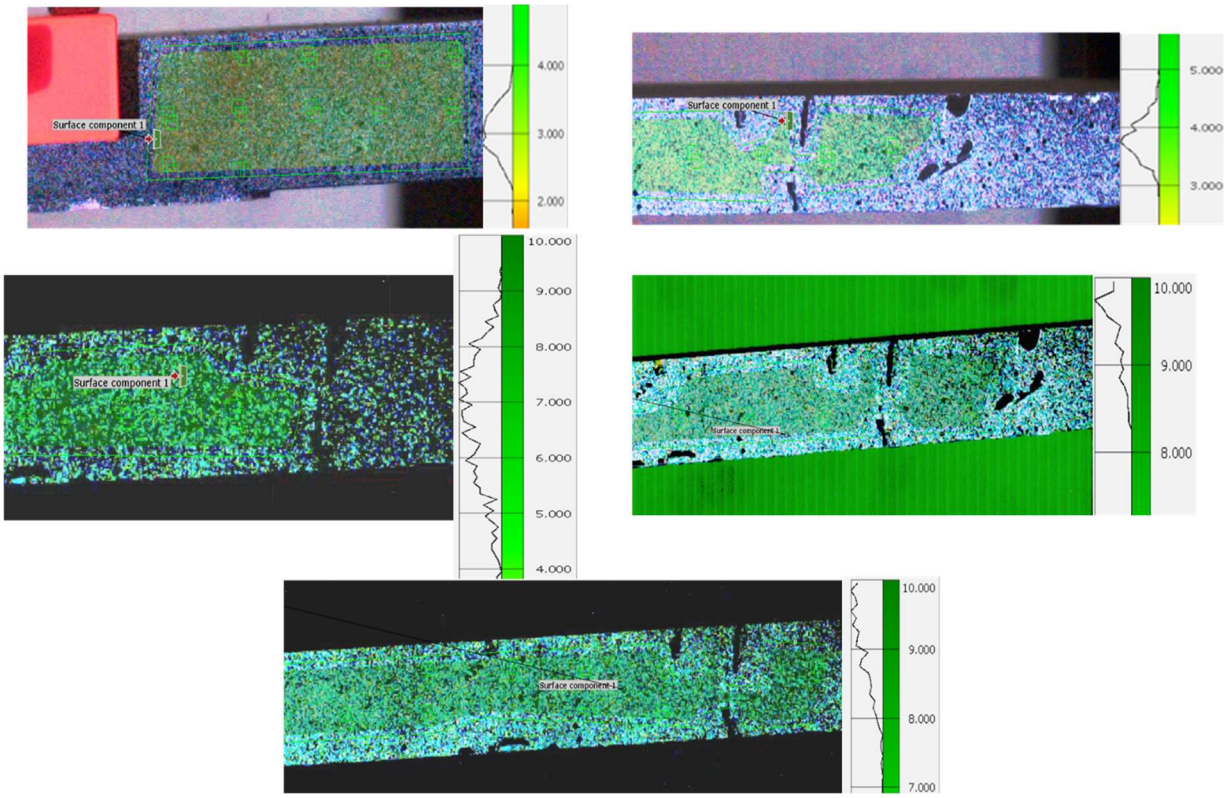

Figure 14 - Five examples of different quality patterns in DIC software.

3.3.1 Bulk tensile testing

For each test, load-displacement curves were recorded until failure occurred, with the displacement measured with an extensometer to improve measurement accuracy. The tests were carried out at the two aforementioned speeds since adhesive joints are sensitive to the strain rate. The first value was chosen as it corresponds to the standard loading rate for bulk specimens, while the second was chosen because it corresponds to the speed used in DCB tests, with the goal of replicating the actual strain rate used in a DCB. Equation (3.1) shows the parameters required to calculate the speed of bulk specimens:

$$\dot{\varepsilon} = \frac{v}{l} \tag{3.1}$$

where v represents the loading speed and l stands for the characteristic length that is under the estimated strain rate. Hence, considering that DCB tests were performed at 0.2 mm/min and that the characteristic length is the adhesive thickness, the equivalent strain rate in the bulk specimen should be 50 mm/min and 20 mm/min for the Adhesive A and Adhesive B, respectively.

3.3.2 DCB testing

The DCB specimens were mounted to the universal testing machine using stiff steel pins to connect the end-blocks to the machine attachment elements. The direct method requires synchronized monitoring of the load and two rotation angles at the load introduction points. Thereby, the Mode I fracture toughness, and later, the cohesive law, could be determined. The test machine recorded the load-displacement curve, and the displacements were recorded on video. To ensure stable crack propagation, the DCB specimens were previously loaded in tension with a small pre-load.

The J-integral approach was used to calculate the energy release rate in Mode I, which was then compared to CBBM results.

3.3.3 ENF testing

The ENF specimens were positioned in the apparatus, with two roller supports sustaining the beams. Like in the DCB test, the direct method requires the synchronized monitoring of the load and rotation angles. However, for this test, three rotations must be measured: both rotations on the support points and the rotation in the loading point, at the middle of the beam length. Thereby, the Mode II fracture toughness, and later, the cohesive law, could be determined. The test machine recorded the load-displacement curve, and the displacements were recorded on video.

The J-integral approach was used to calculate the energy release rate in Mode II, which was then compared to CBBM results.

3.3.4 Block testing

Load-displacement curves were recorded for each specimen until failure occurred, while the displacement was recorded using a camera to improve the accuracy of the measurement using DIC.

3.4 Data reduction scheme

The classic data reduction schemes used to obtain fracture energies include Compliance Calibration Method (CCM), Direct Beam Theory (DBT), and CBT, which rely on LEFM [80, 81]. For all these approaches, measuring of the crack length is needed, which can be difficult, especially for Mode II and when there is a sudden propagation of the crack. A good example of this difficulty is when extensive damage occurs, such as microcracking or fibre bridging [40]. More recently, CBBM approach, which relies in a crack equivalent concept, was applied to the fracture characterization of bonded joints by developing a data reduction scheme

method based on the beam theory and specimen compliance. In this proposed methodology, there is no need for measuring the crack length during propagation, and it accounts for the fracture process zone effects that are particularly important in ductile adhesives. The critical energy release rate is given by [80]:

$$G_{Ic} = \frac{6P^2}{b^2 h \delta_{n_t}} \left(\frac{2a_{eq}^2}{h^2 E_f} + \frac{1}{5G_f} \right) \tag{3.2}$$

where a_{eq} is the equivalent crack length, E_f is the corrected flexural modulus, and G_f is the shear modulus of the substrate.

Another approach that has been used is the resort to test specimens that are independent of the crack length, such as TDCB for Mode I, Tapered End-Notched Flexure (TENF) for Mode II, DCB specimen loaded with pure bending moments, and J-integral methods. In the present work, J-integral approach has been used to characterize the fracture behaviour of the adhesives. There are some closed-form solutions for several interlaminar fracture tests described in the literature, regarding pure Mode I, pure Mode II, and Mixed Mode. With the integral J being a path independent method, depending on the integration path chosen and the elastic assumptions made, different closed forms can be achieved. However, Paris and Paris [82] developed a closed form that does not require beam theory assumptions, using a DCB specimen for pure Mode I. They solved the J-integral along its external edge and obtained a closed-form solution that relies on the applied load and the rotation angle at the load introduction point. Considering a Mode I loading, the value of J along the exterior boundary of the DCB specimen is:

$$J_{ext} = \frac{P}{b} \cdot (\theta_{up} - \theta_{lo}\ ) \tag{3.3}$$

where P is the load, b stands for the width of the specimen, and θ_{up} and θ_{low} are the relative rotations of the upper and lower substrates at the load introduction points, respectively. Figure 15 depicts the test configurations and the required measurements.

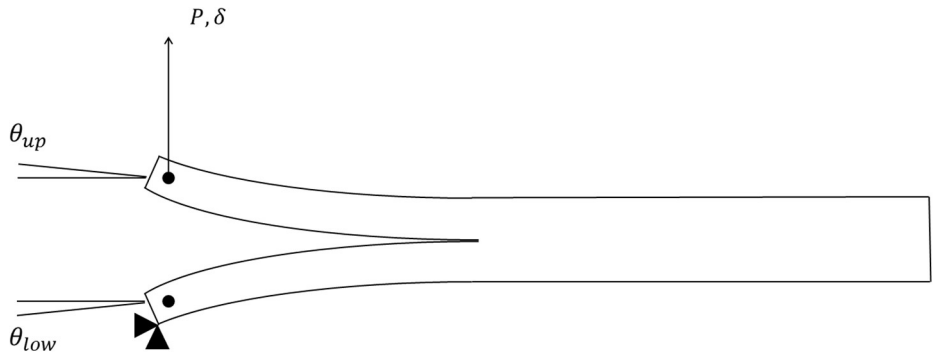

Figure 15 - DCB test configuration.

By means of a similar approach, Stigh, et al. [45] have obtained a closed-form solution for Mode II using ENF specimens, which relies on the applied load and three rotation angles. Considering a Mode II loading, the value of J along the exterior boundary of the DCB specimen is:

$$J_{ext} = \frac{P}{2b} \cdot (\theta_A - 2\theta_C + \theta_B) \tag{3.4}$$

where P is the load, b is the width of the specimen, and θ_A, θ_B, and θ_C are the rotation angles at the load introduction points, as represented in Figure 16.

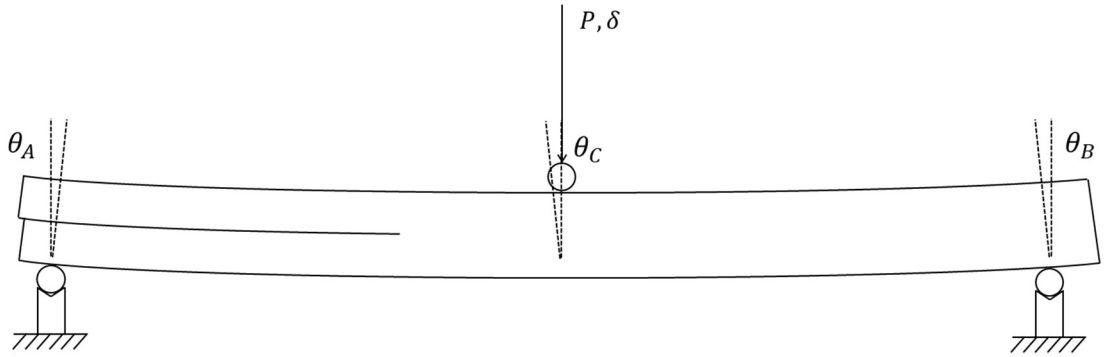

Figure 16 - ENF test configuration.

Considering the contour integral around the cohesive zone, the J-integral is given by:

$$J_{tip} = \int_0^{\delta_n^0} \sigma(\delta_n) d\delta_n \tag{3.5}$$

where δ_n is the normal or transverse displacement of the interface, σ is the normal traction across the interface, and δ_i^0 is the limiting end-opening at which the traction becomes zero. By differentiating the equation above with respect to δ_i, the traction-separation relation is obtained as shown in Equation (3.6):

$$\frac{\partial J_{tip}}{\partial \delta_i} = \sigma(\delta_i) \tag{3.6}$$

The relation $J_{ext} = J_{tip}$ is valid when considering the path independence property of the J-integral for linear and nonlinear elastic materials, and assuming that the region outside the FPZ remains elastic during fracture. As a result, by estimating the value of J_{ext}, as well as the values of δ_i during the loading, the cohesive law in Mode I or Mode II can be determined using Equation (3.6).

3.5 DIC method for the parameter measurement

To obtain the displacement field data, the recorded pictures were analysed using GOM Correlate software. A pixel in the image corresponded to 0.101 mm on the measured surface, and the facet size employed was 12 pixels. The DIC analysis allowed for the determination of both the initial crack tip opening and rotations in the loading regions.

3.5.1 Loading point rotations

Sun and Blackman [5] proposed applying DIC analysis to calculate rotations from the displacements of the inspection points in the upper and lower substrates, as shown in Figure 17. Hence, it was possible to estimate the value of the rotation of each substrate over time by computing $\theta = \frac{dy}{dx}$, by extracting the x and y displacements and then correlating their relationship in the substrates, assuming that they exhibit a linear relationship.

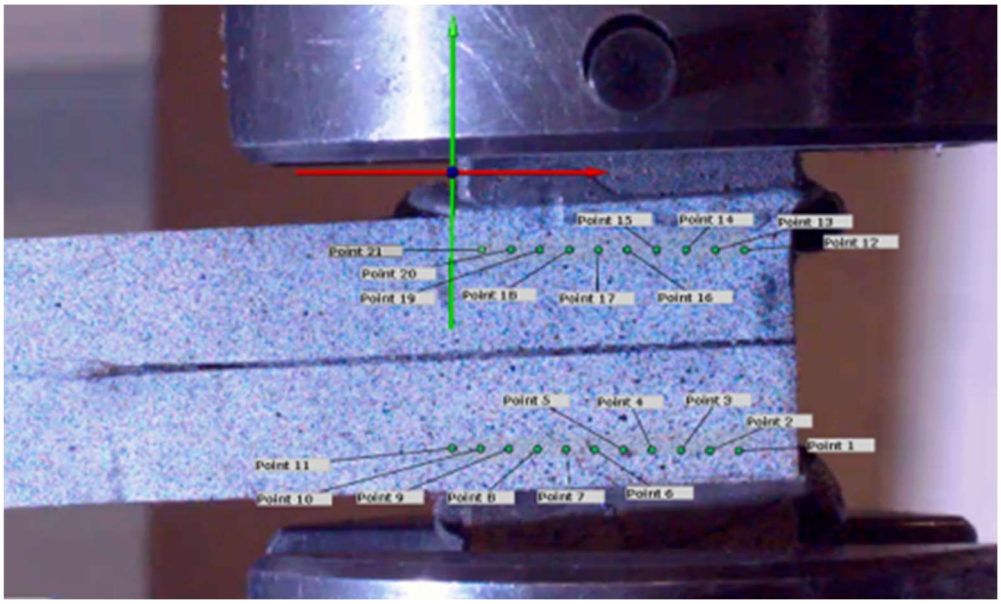

Figure 17 - Marked points in the DIC software.

Considering the premise advanced by the referred authors, a small study was conducted to ensure that the results obtained matched the expectations. The results are shown in Figure 18 and Figure 19. It is possible to verify that the values in the x direction have remained nearly constant, while their behaviour in the y direction has been nearly linear. As a result of this analysis, it was concluded that the rotations at the desired points could be reliably obtained.

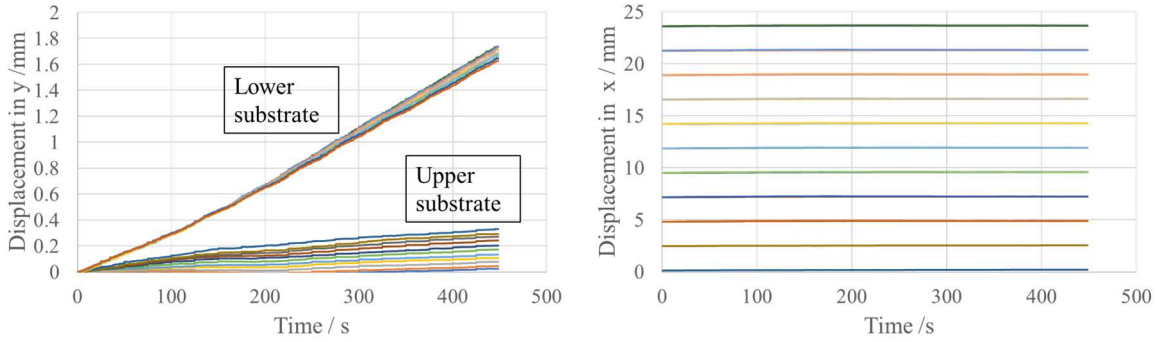

Figure 18 - Displacements of the points: y direction (left) and x direction (right).

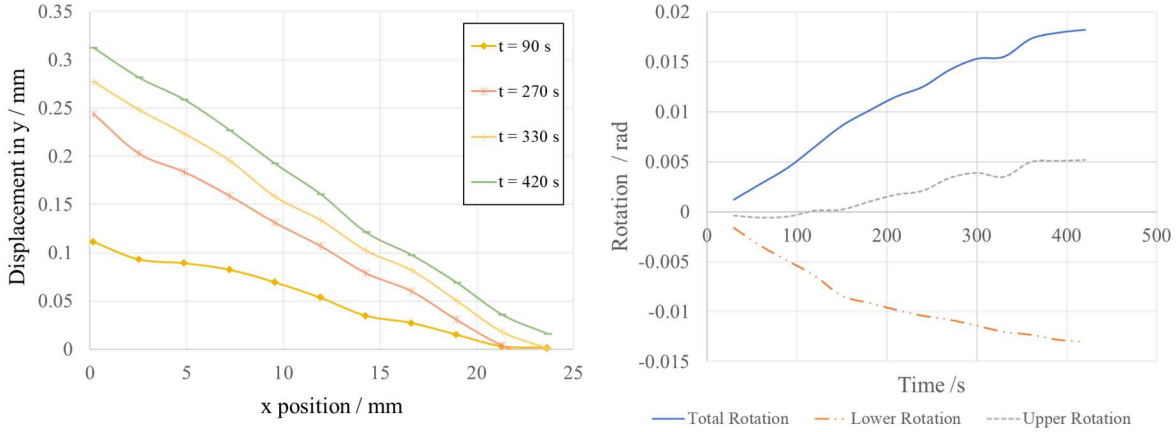

Figure 19 - Displacements in y direction with respect to displacements in x direction (left) and rotations in the substrates (right).

3.5.2 CTOD

As shown in Figure 20, the CTOD was computed by subtracting the difference between the upper and lower displacements of the inspection points. In order to ensure that the opening was measured perpendicularly to the adhesive layer orientation, the same orientation was registered in the software, and then the points were defined in the correct orientation. The CTOD, δ_n, for stiff substrates was thus calculated.

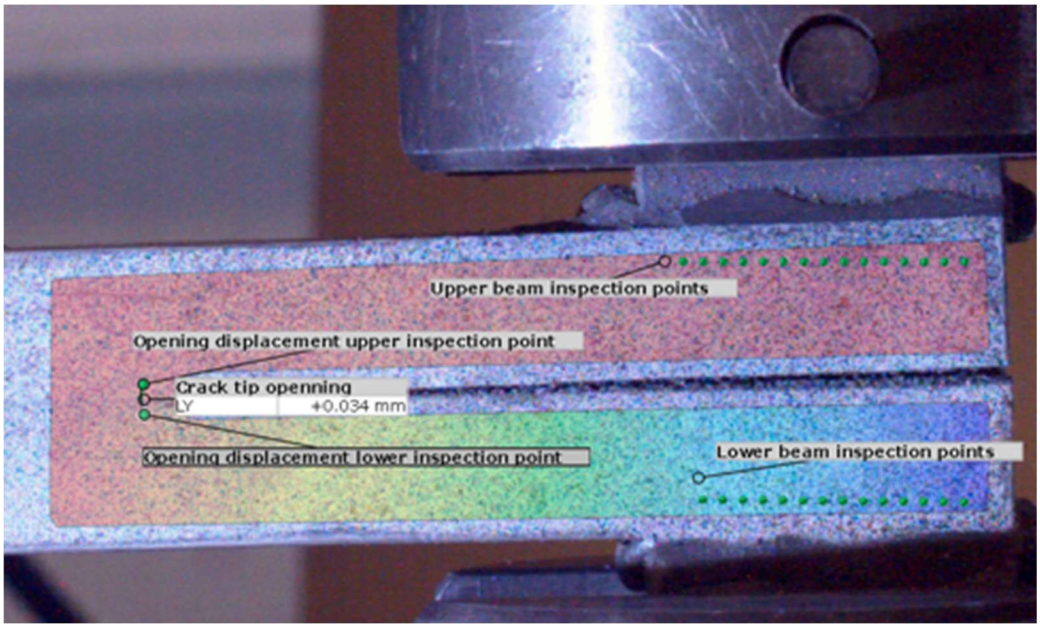

Figure 20 - CTOD measured by the DIC software.

Since the accuracy of the measurement of this parameter is of major importance for this method, it was imperative to understand if the place where it was measured interfered in the final results. The influence of the position of the points in the y direction and also in the x direction was taken into account. Figure 21 shows the positions of the points for both cases.

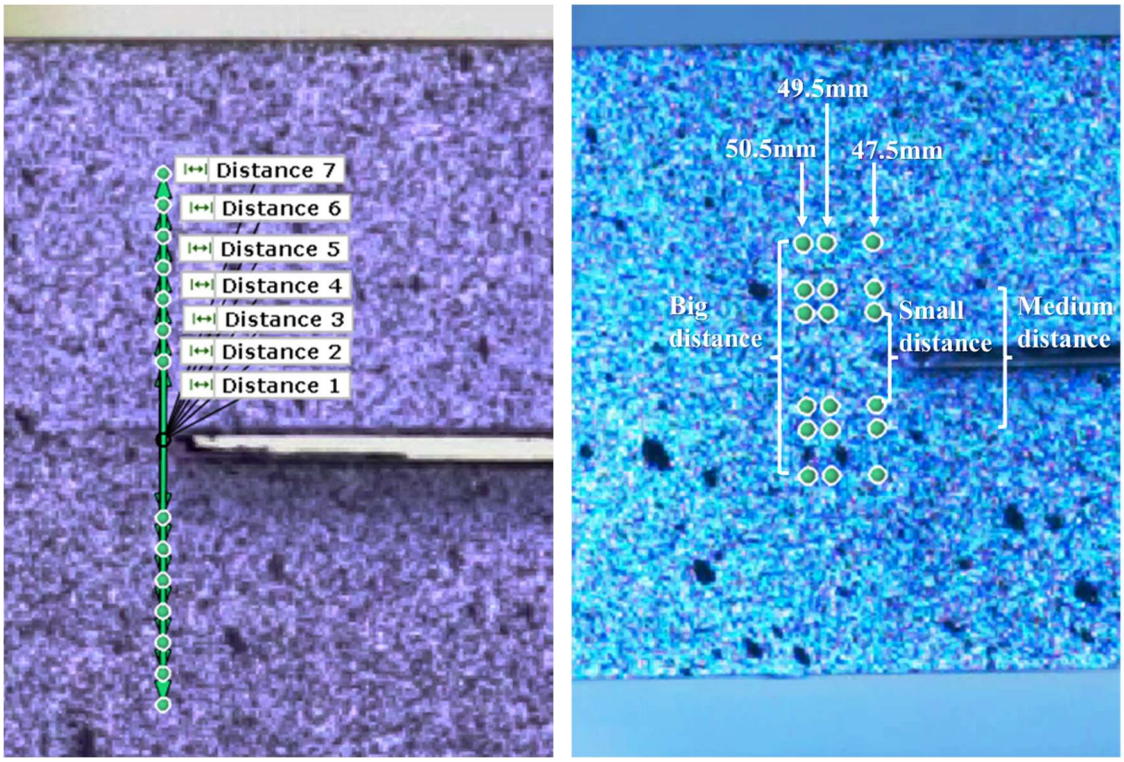

Figure 21 - Different positions for the points in the y direction (left) and in the x direction (right).

For the study of the influence of the point position in the y direction, it can be observed in Figure 22, that, generally speaking, there is good correlation between all the curves, although some fluctuations are noticed when analysed in detail. These changes are expected, since raw experimental data always has some inherent noise attached. In conclusion, the position of the points in the y direction did not seem to have a significant influence on the results, and an average of all points can be used to compute the final results.

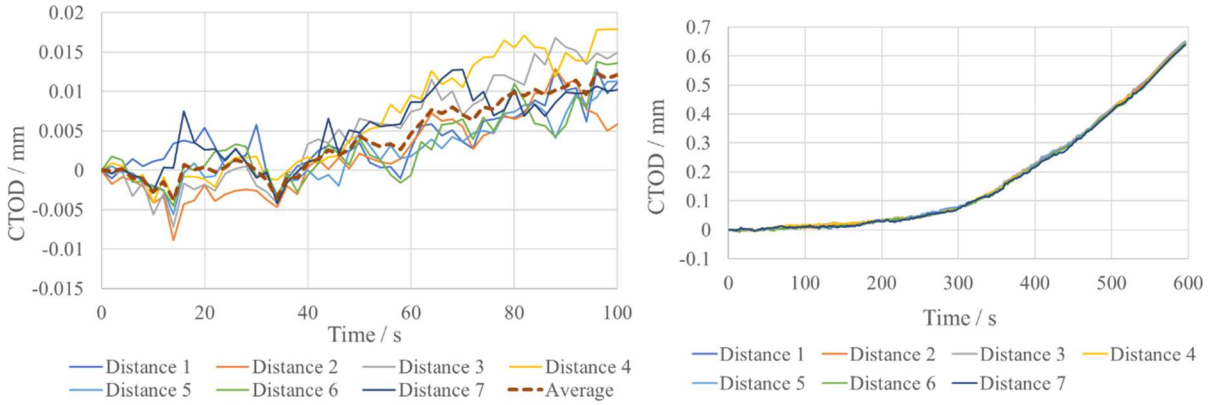

Figure 22 - CTOD for different sets of points: detailed analysis (left) and overall analysis (right).

The influence of the point position in the x direction can be observed in Figure 23, Figure 24, and Figure 25. These figures suggest that, besides the usual fluctuations in experimental data, the distance of 50.5 mm from the loading points to the crack tip exhibits a less steady result. Hence, this indicates that the x distance should be carefully measured before DIC analysis takes place.

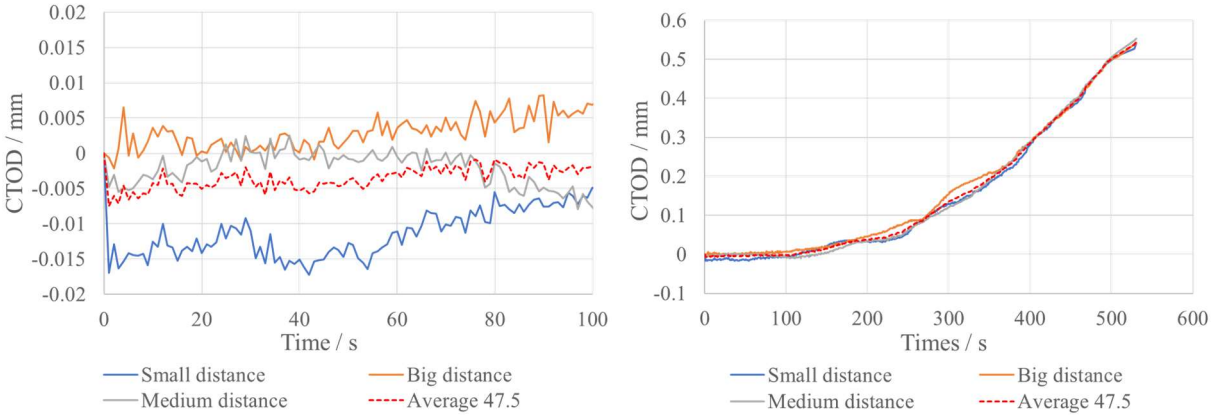

Figure 23 - CTOD for different sets of points at 47.5 mm from the loading points: detailed analysis (left) and overall analysis (right).

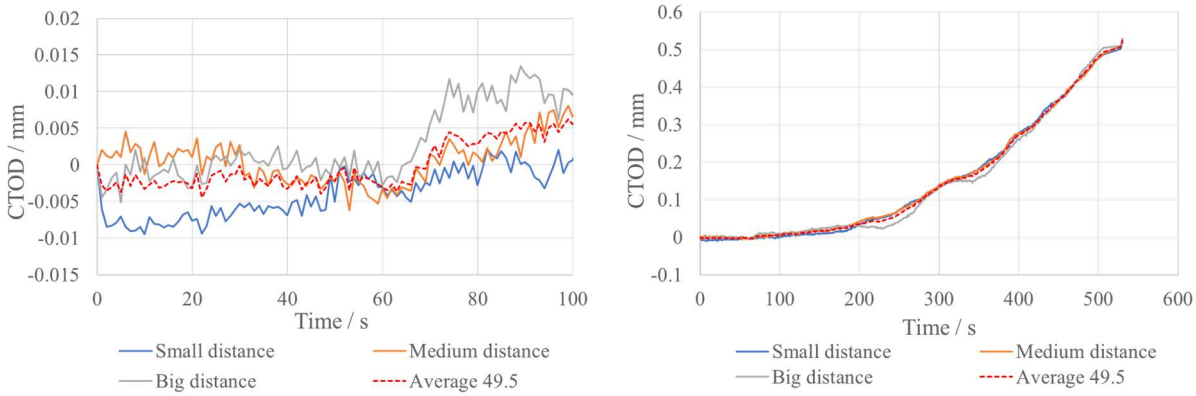

Figure 24 – CTOD for different sets of points at 49.5 mm from the loading points: detailed analysis (left) and overall analysis (right).

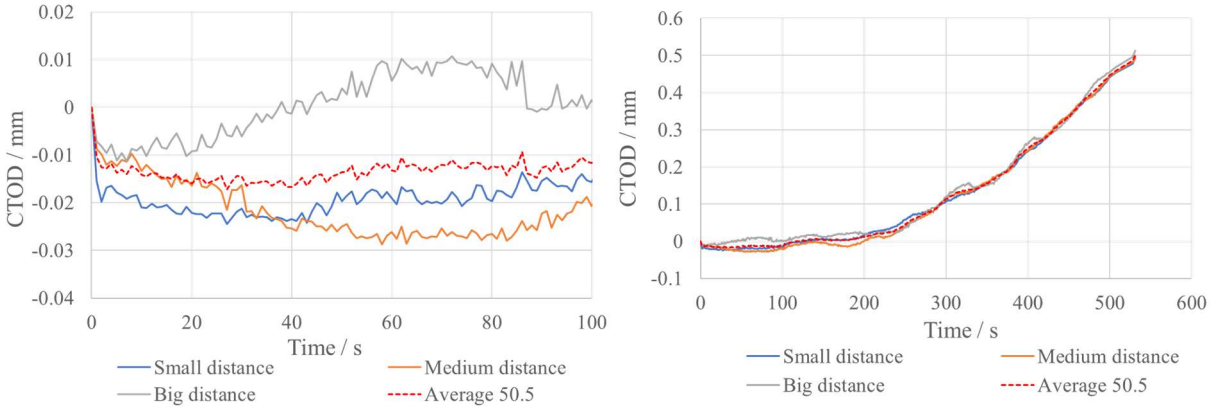

Figure 25 - CTOD for different sets of points at 50.5 mm from the loading points: detailed analysis (left) and overall analysis (right).

Figure 26 presents a comparison between the average of the three y values, in the three different x positions. There is a good agreement between the 47.5 mm and the 49.5 mm values, but the 50.5 mm values show a different trend. The previous reported trend can be better observed in these graphics, which indicate that the larger value should be discarded. Due to the method used to calculate the experimental cohesive law, which is based in a differentiation of the J values, with respect to the CTOD, the presented variations can impact severely the obtained curve.

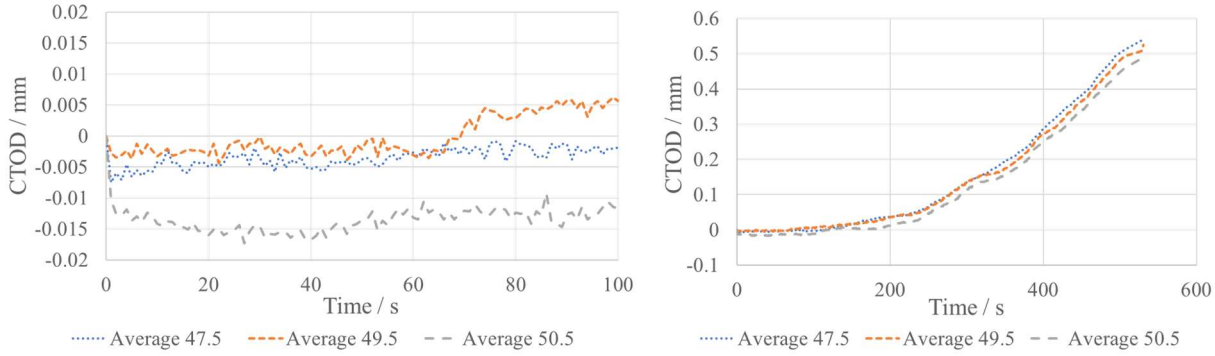

Figure 26 - Average CTOD for different sets of points at three positions from the loading points: detailed analysis (left) and overall analysis (right).

3.5.3 Cohesive law estimation

The cohesive law was estimated using the values obtained for J and the crack tip opening through the aforementioned techniques. Due to the inevitable noise present in the raw data, the Savitzky-Golay Filter was used to adjust all the parameters. The results were smoothed by adjusting the window length and polynomial order.

Direct differentiation was then used to determine the TSL:

$$\sigma = \frac{J_{t+\Delta t} - J_t}{\delta_{n_{t+\Delta t}} - \delta_{n_t}} \tag{3.7}$$

where t is time and Δt is the increment between two measurements. The increment was adjusted for each test depending on the data acquisition frequency and total time of the test.

The same filter was used for the final presentation of the cohesive law in order to achieve a smoother curve.

3.6 Code development

Based on the direct method, the estimation of a precise cohesive law consists in the differentiation of experimental results only, which introduce noise that is frequently higher than acceptable. Furthermore, the size of the DIC dataset can also be very large when using the method proposed by Sun and Blackman. As a result, a Python script was created to address these two issues by automating data processing and filtering the results appropriately. So, in order to obtain the desired estimation of the fracture toughness, as well as the cohesive law of the adhesive, the script involves different sequential steps.

The first step consists in importing the obtained files, from the GOM software, that contain the required data. Figure 27 depicts the graphical interface that first appears when the code starts running. It is necessary to import the files with the initial coordinates of the inspection

points, their displacement field, as well as the file with load-displacement values, for the test to be analysed.

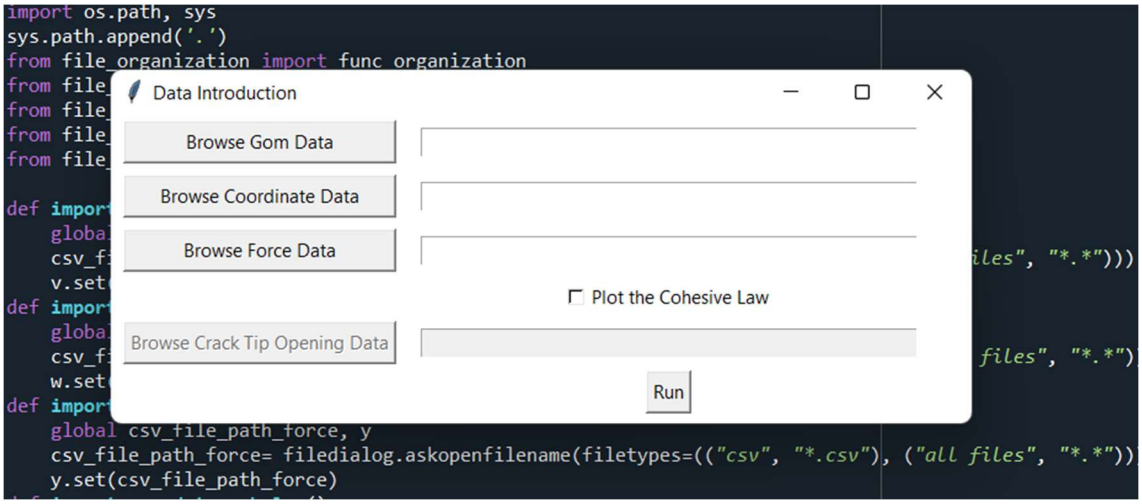

Figure 27 - Data introduction window.

By default, the program is set to only require the information to calculate the fracture toughness. However, there is a checkbox that can be marked, in order to add the extra file needed to estimate the cohesive law. When that feature is set on, the same graphical interface changes to the one that is shown in Figure 28, and the user must insert the file with the CTOD data.

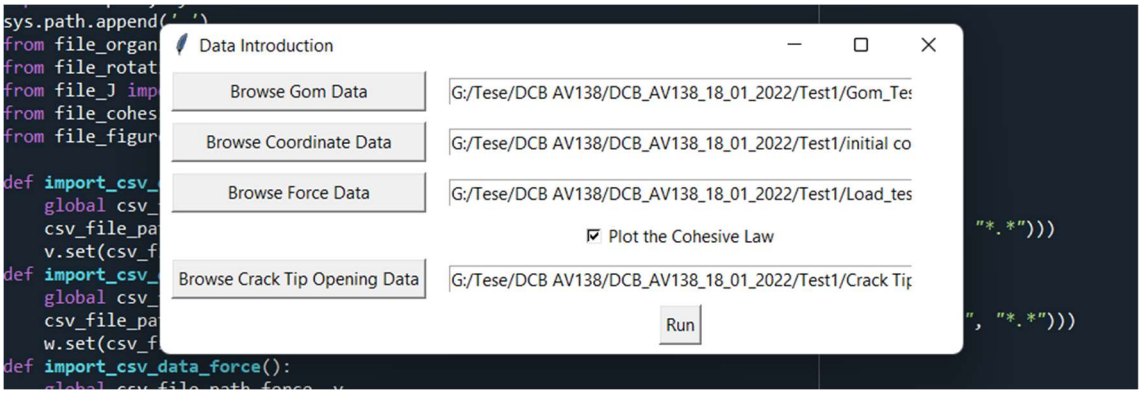

Figure 28 - Data introduction window with cohesive law option enabled.

In the end of these first steps, all of the required fields must be filled, otherwise, an error message will appear, preventing the code from running, as is shown in Figure 29.

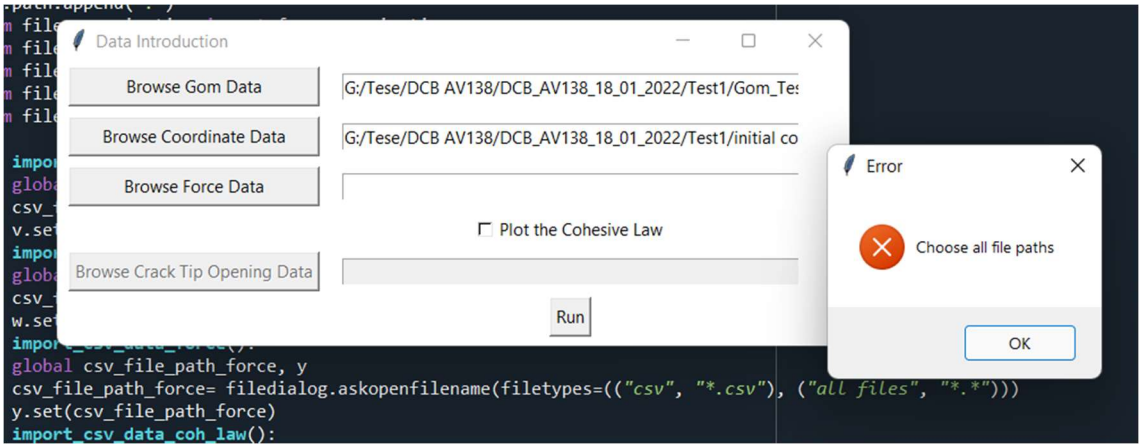

Figure 29 - Error window for missing required fields.

Additionally, when the code continues to run after all the required fields are filled, there is an internal verification of the chosen files, in order to avoid the analysis of incorrect files. Figure 30 shows an example of what would happen if one of the chosen files was the wrong one.

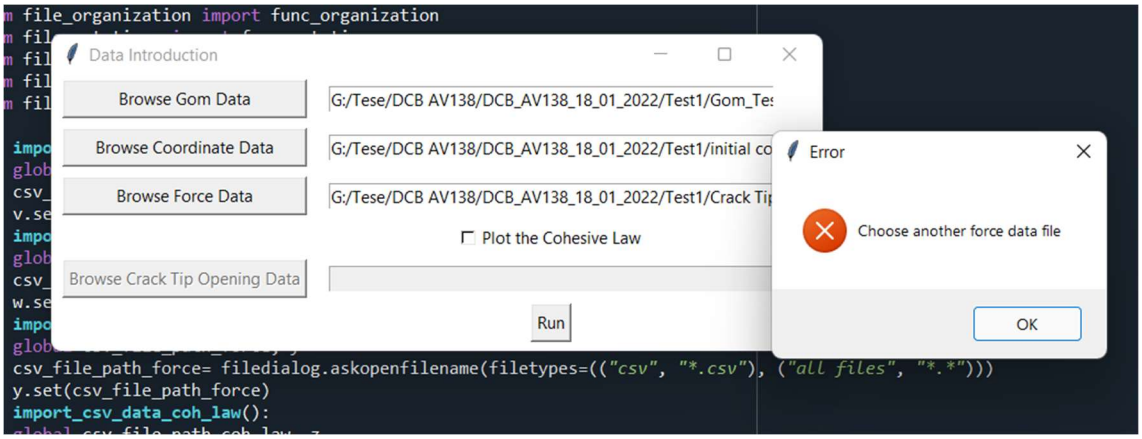

Figure 30 - Error window for wrong file.

After the first step of choosing the files imported from DIC analysis, data is computed and filtered. Then, the user can see the plots of rotation with respect to time, the J values with respect to the load point displacement, and the cohesive law with respect to the CTOD, if that option was enabled. Moreover, the plots show both raw and filtered results. An example of the resulting plots of the code can be observed in Figure 31 and Figure 32.

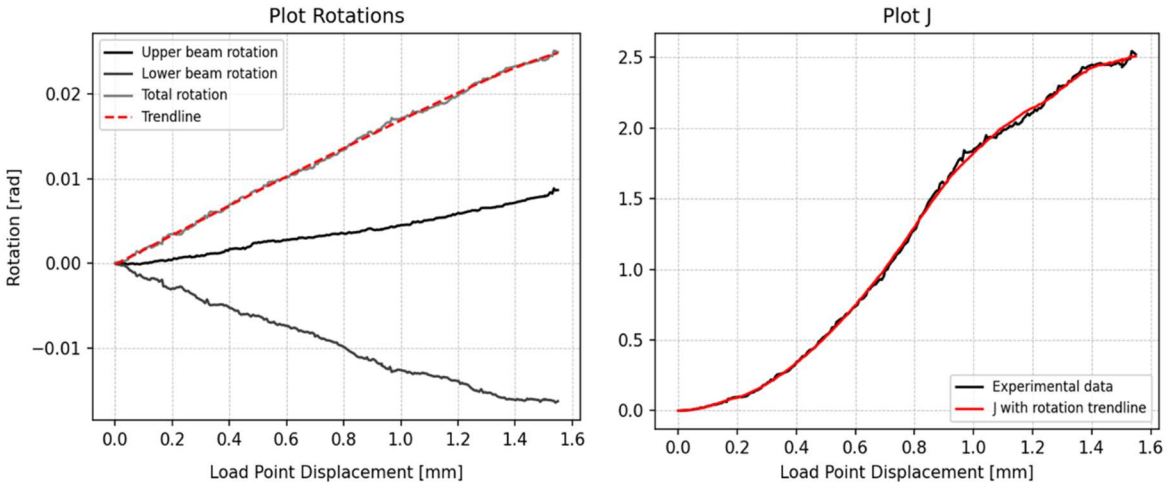

Figure 31 – Resulting plots for: rotations (left) and J-integral values (right).

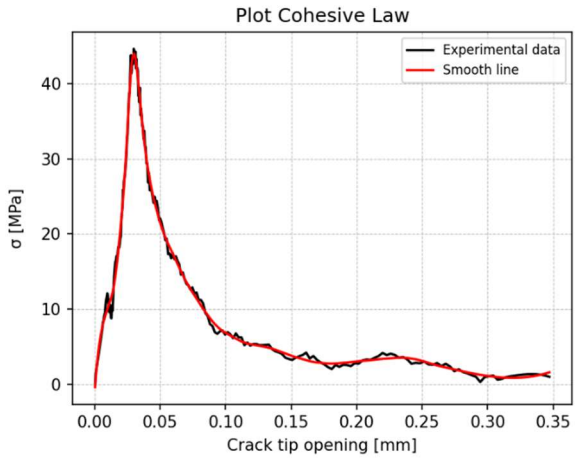

Figure 32 – Resulting plot for the cohesive law.

The third step consists in deciding if one wants to save the results or just quit the running program. Thus, there is a button in the graphical interface that should be pressed if saving the data is desired. Two different windows will sequentially appear, allowing to choose the destination folder, followed by the name of the file. Figure 33 shows the intermediate steps that precede the end of the process. When all of this is done, both the plots and the computed results are exported to the chosen file. In addition to the images, a file containing the computed results of the rotations, the J-integral values, the CTOD values, and the cohesive law results is saved. The smoothened values are also exported, in addition to the raw data.

The results obtained after this process are described in further detail in the appended **Paper**.

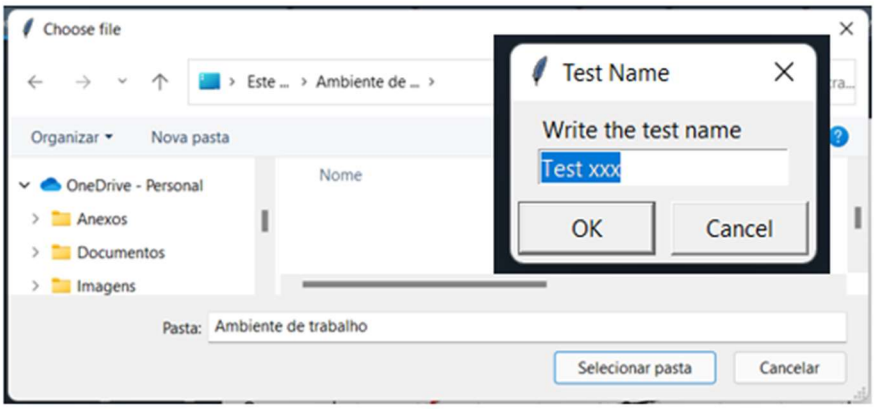

Figure 33 - Windows for the chosen folder and file name.

4 FEM analysis

A FEA was performed to validate the experimental results, attained by the application of the direct method. Before modelling the obtained cohesive laws, the average experimental results were inputted in the ABAQUS® (Dassault Systèmes, Suresnes, France) software, using only one cohesive element COH2D4, to generate the average cohesive law, computed from the average damage of each adhesive. Figure 34 shows the tabular input of the cohesive law used in this approach.

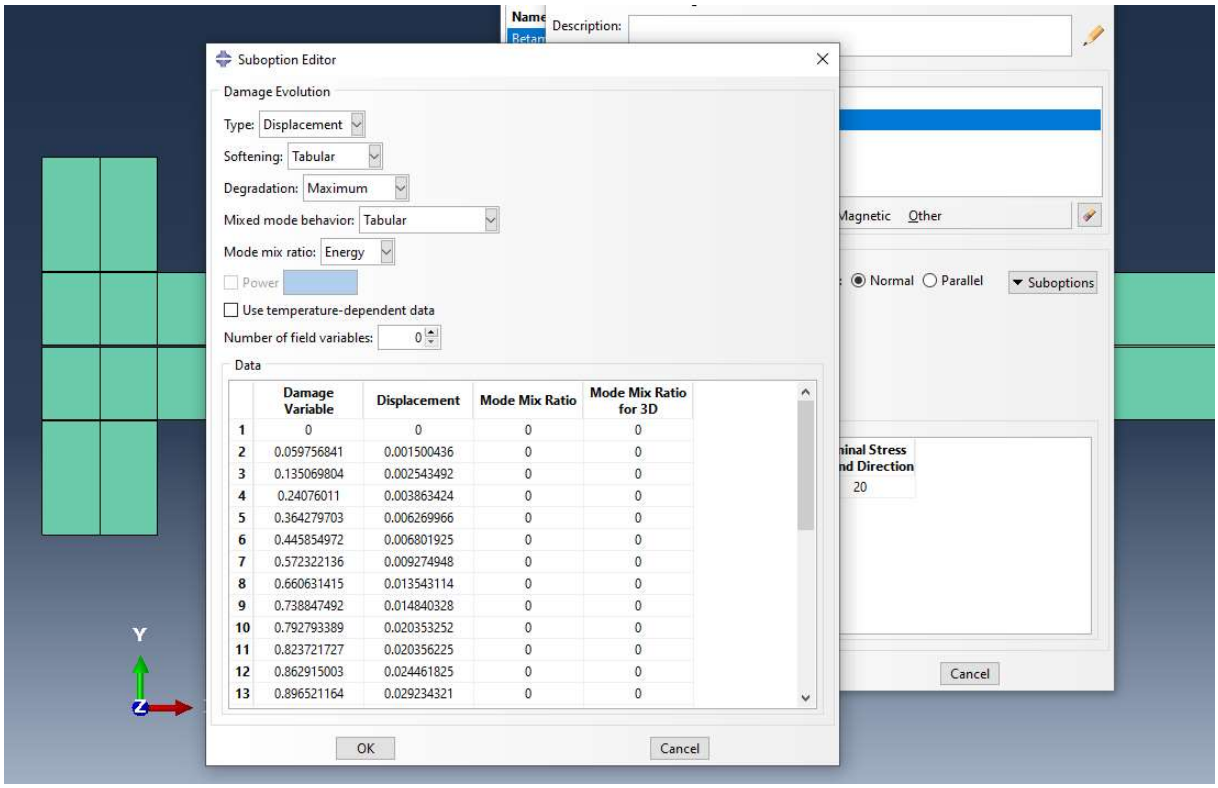

Figure 34 - Tabular input of the damage variable using Abaqus software.

4.1 Mode I – DCB model

The elastic element CPS4R was used to model the steel blocks and the substrates, while the cohesive element COH2D4 was used to model the adhesive layer. Thereafter, a 2D DCB model was used to simulate the fracture process, ensuring that the geometry of the model was identical to the one used in the fracture tests. Figure 35 represents the geometry, boundary conditions, and the mesh that was used for the simulation.

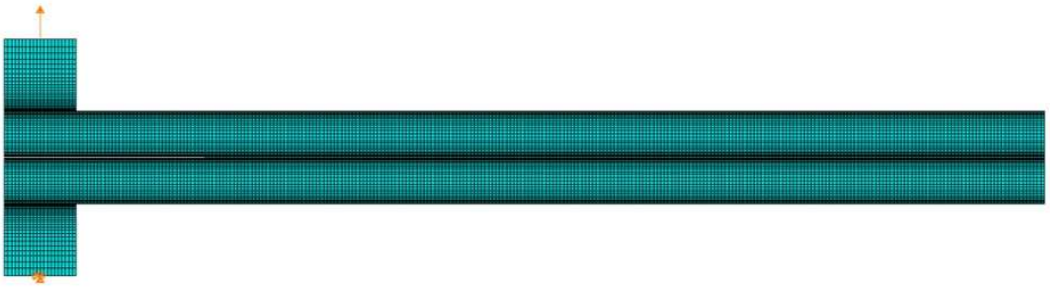

Figure 35 - DCB model for numerical simulation.

Since steel end-blocks are not commonly used in DCB tests, they are also usually not included in the respective models. However, this was not the case in the current study, so they had to be accounted for in the modelling process. In order to ensure that there was no damage in the adhesive layers between the blocks and the substrates, if the same adhesive was used, a suitable model was created. Figure 36 shows the obtained results that were then compared to the experimental data obtained. This process is described in further detail in the appended **Paper**.

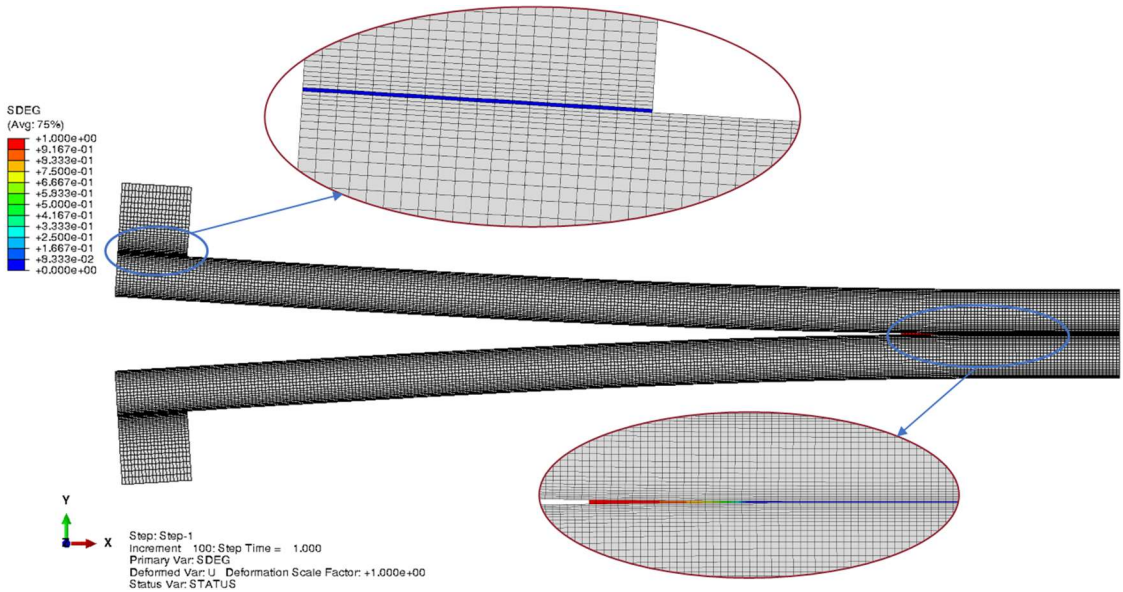

Figure 36 - Numerical result of adhesive layers analysis.

4.2 Validation in different geometry – block model

After validating the cohesive laws for a DCB specimen using the direct method, a different geometry was modelled to simulate the Adhesive A using the same experimental law.

The steel substrates were modelled using the elastic element CPS4R, while the adhesive layer was modelled using the cohesive element COH2D4. Following that, a 2D block model was used to simulate the fracture process, with a geometry that was identical to that of the tests. The geometry, boundary conditions, and mesh used in the simulation are depicted in Figure 37. The obtained results were then compared to the experimental data obtained. This process is described in further detail in the appended **Paper**.

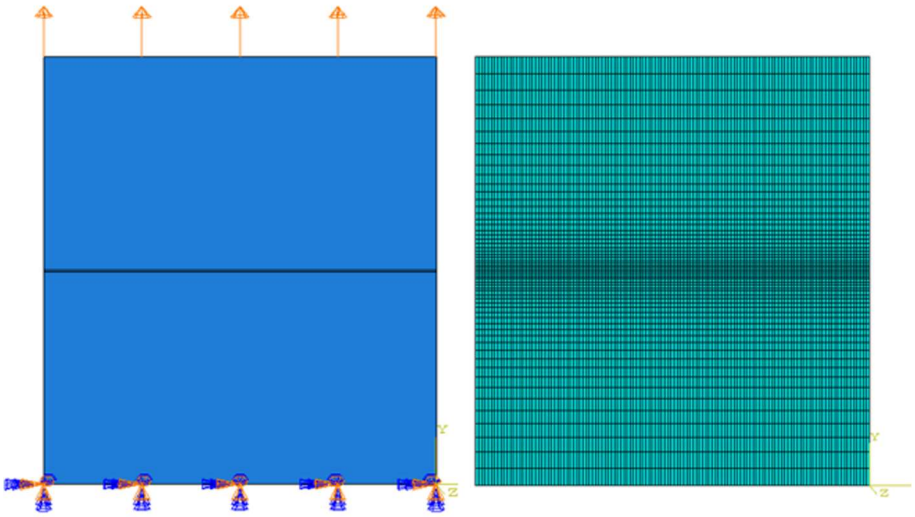

Figure 37 - Block model for numerical simulation.

4.3 Numerical validation of the inputted softening laws

The results obtained with the FEA were used to apply the direct method to the numerical values. By estimating the J values resorting to numerical load and displacement data, and differentiating them with respect to numerical CTOD, it was possible to obtain the cohesive law. This process assessed the possibility of obtaining the same cohesive law that was initially inputted in the simulation software. Figure 38 and Figure 39 depicts the chosen nodes in the DCB model, to export the numerical displacements for computing the rotations.

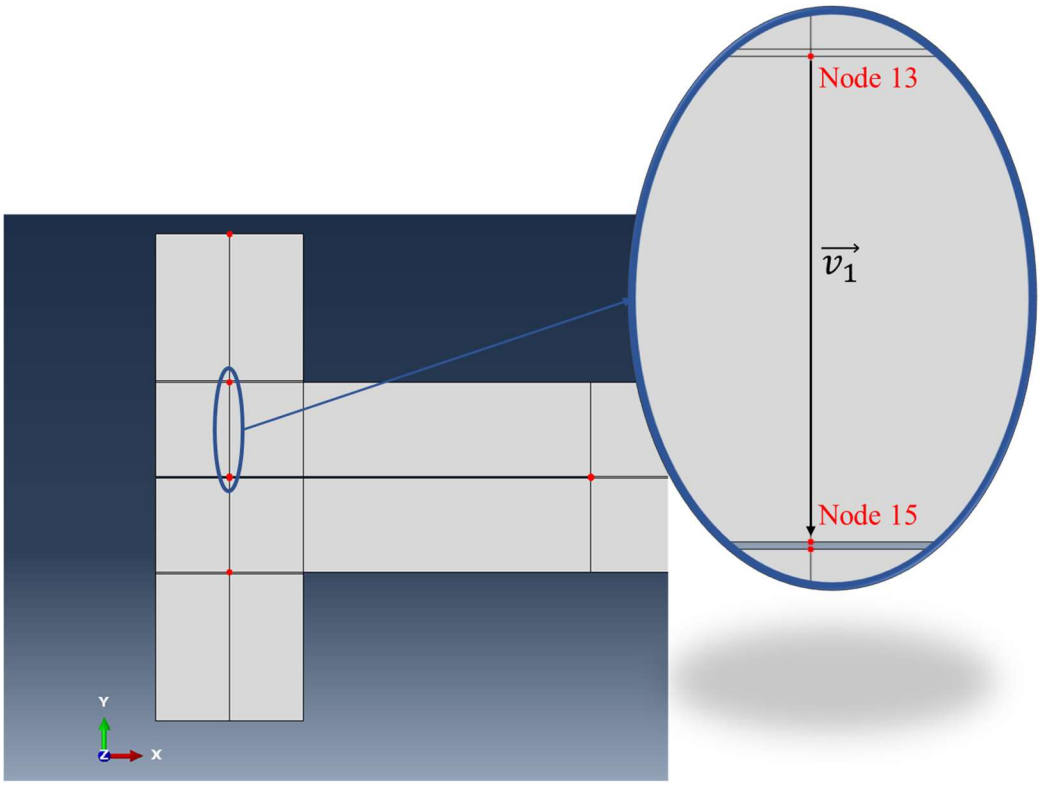

Figure 38 - Nodes used to construct the vector $\overrightarrow{v_1}$.

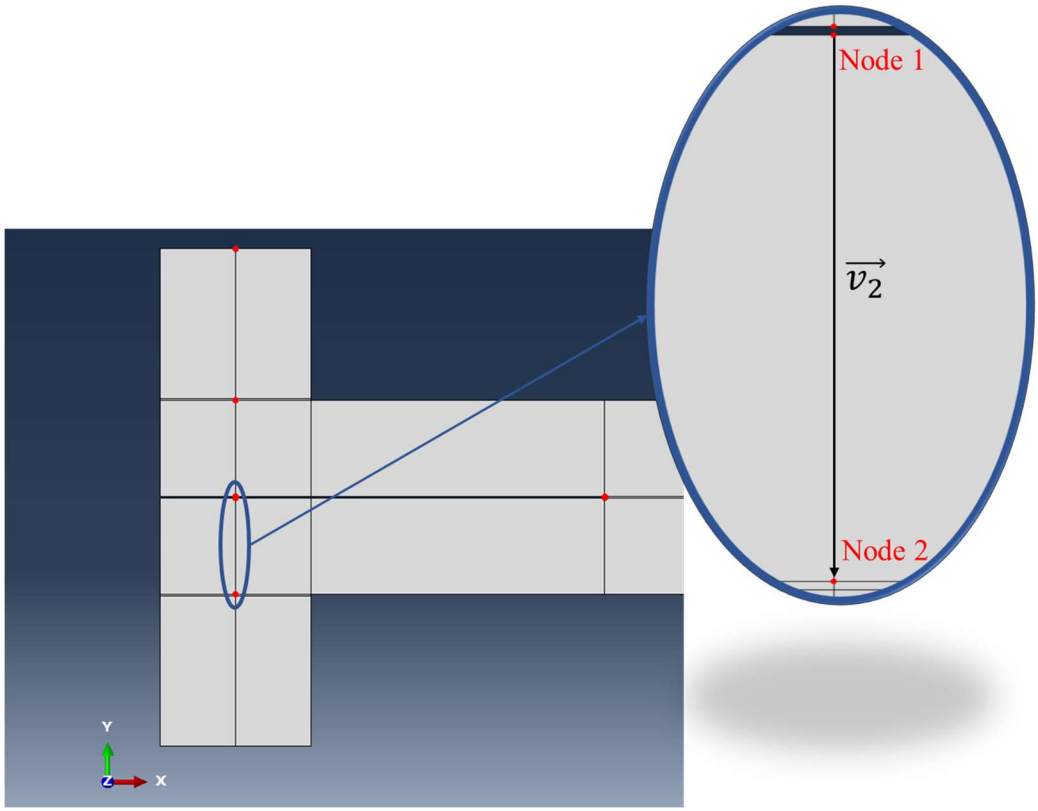

Figure 39 - Nodes used to construct the vector $\overrightarrow{v_2}$.

The rotations were calculated by defining two vectors and estimating their rotation for each increment of time. Table 5 shows the vector components and the respective used nodes.

Table 5 - Created vectors with numerical displacements.

Vector Component	Nodes
v_{1x}	(Node 13 – Node 15) U1
v_{1y}	(Node 13 – Node 15) U2
v_{2x}	(Node 1 – Node 2) U1
v_{2y}	(Node 1 – Node 2) U2

After creating the vectors, the rotations were estimated by:

$$\theta = \cos^{-1}\left(\frac{v_{1x}\cdot v_{2x} + v_{1y}\cdot v_{2y}}{\sqrt{v_{1x}^2 + v_{1y}^2}\cdot\sqrt{v_{2x}^2 + v_{2y}^2}}\right) \tag{4.1}$$

Having the numerical data for load and rotations, it was possible to estimate J values. A first comparison was performed, assuring that these values were in accordance with the experimental results. After this step, these energy values were differentiated with respect to the CTOD, measured in two nodes in the initial crack tip, as is shown in Figure 40, and the intended cohesive law was estimated. The results of this process are described in further detail in the appended **Paper**.

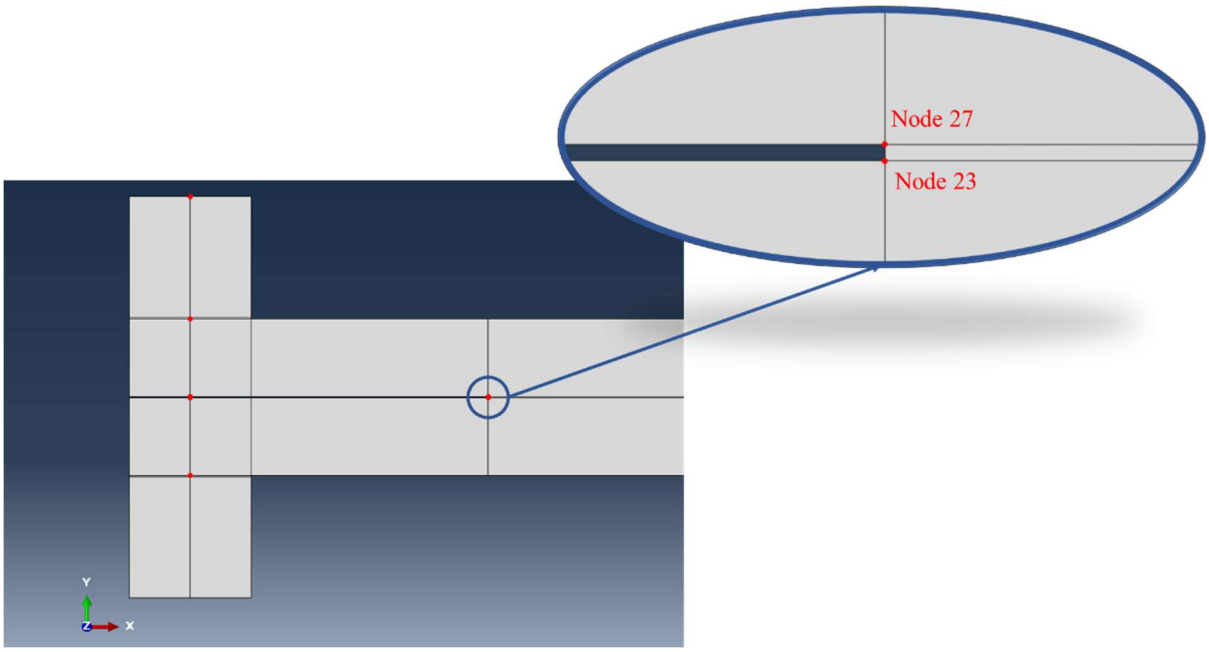

Figure 40 - Nodes used to compute the CTOD.

5 Exploratory work on Mode II

For the work on Mode II loading configuration, several adjustments on the method were performed. In spite of that, the same laser-based approach was used to attain the perpendicularity of the camera lens, regarding the specimen position. However, the solution used for Mode I, with only one camera to record both CTOD and the rotations, was found to be insufficient to provide accurate results. Moreover, the developed code needed some changes, to compute the inputted data.

5.1 Test configuration

The first ENF test was performed using the same configuration as Mode I. However, it can be observed in Figure 41 that, due to a larger area of interest in these specimens, the camera needed to be further away, and the used speckle did not have the necessary resolution for further DIC analysis. In addition, the recorded video images showed some distortion in the edge of the field of view stemming from the wide angle necessary.

Figure 41 - First ENF specimen test.

In order to overcome these obstacles, the lens of the camera, the number of cameras, and the applied speckle were all modified. Thus, a digital camera (Panasonic Lumix GX7) equipped with a Lumix G VARIO 35-100 mm ASPH f/4.0-5.6 MEGA O.I.S. tele lens was placed in front of the specimens, with the lens axis set perpendicularly to the surface under observation. For the crack tip displacement, a different digital camera (Nikon D5600) was placed in the opposite surface of the specimen. This camera was equipped with a Micro-

NiKKOR 55 mm f/3.5 macro lens, that could ensure high quality images and, hence, capture the small displacements of the crack tip. Figure 42 shows the new test configuration.

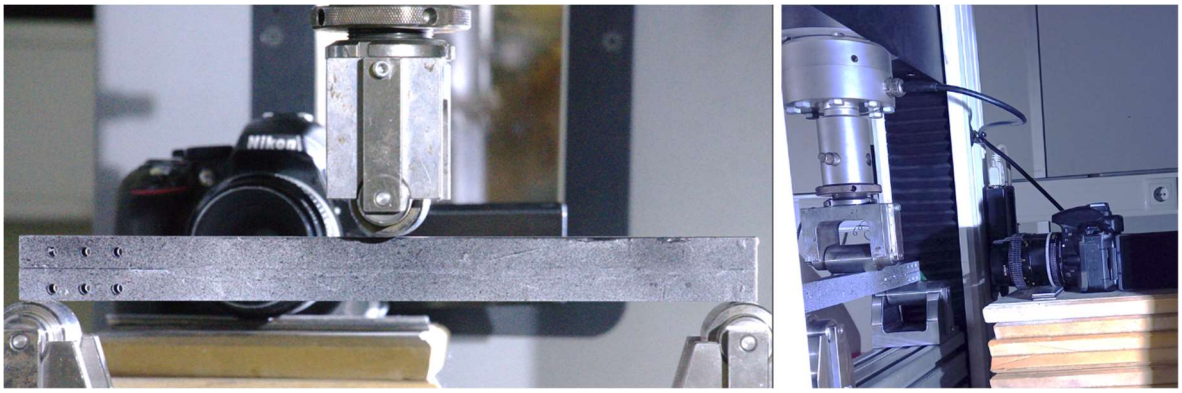

Figure 42 - Image captured with the Lumix digital camera (left) and the setup with the Nikon digital camera (right).

Figure 43 depicts the capacity of the chosen lens to capture the displacement of the crack tip, which was one of the most difficult effects to characterise in the Mode I validated process.

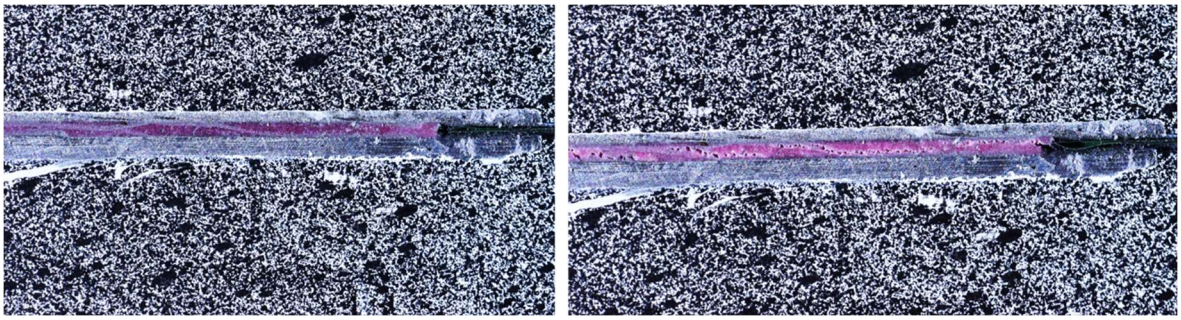

Figure 43 - Image captured in the initial moment of the test (left) and image captured after the propagation of the crack, in the final of the test (right).

5.2 Experimental results

Although the first test presented some well-known limitations, the data was still analysed, in order to understand if the results were as expected. Due to the required changes in the developed code, a comparison to Jia, et al. [30] study was made, since they used the same test configuration to obtain their results. The main goal was not to mimic the results *per se*, but to achieve the same trend within the curves. The mentioned comparison is showed in Figure 44.

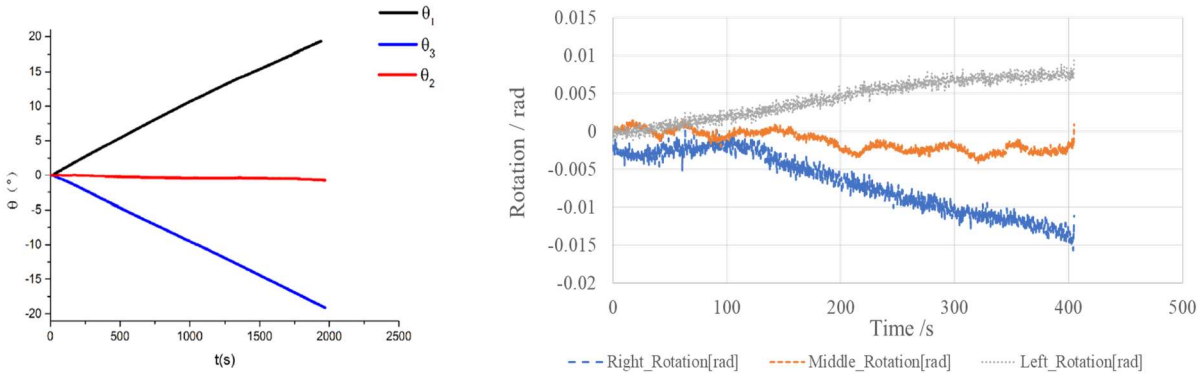

Figure 44 - Literature results [30] (left) and experimental results (right).

A similar behaviour can be observed for both results, although the ones obtained in the present work were found to have larger values of noise. As expected, the rotations measured at the edges of the specimen had similar values, with an opposite signal, turning the middle rotation into the most important for these tests. The total rotation of the specimen is given by:

$$\theta_{total} = \theta_{left} - 2\theta_{middle} + \theta_{right} \tag{5.1}$$

However, although this rotation is the most critical, it also presents the lowest values, making the precise measurement of this rotation more difficult due to a lower signal-to-noise ratio. Figure 45 shows the influence of the middle rotation in the values of the total rotation.

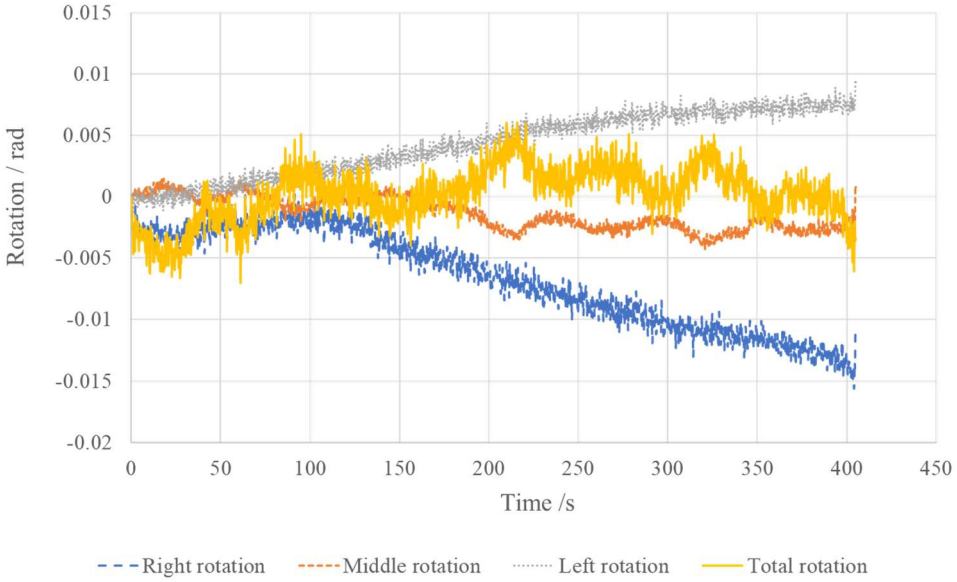

Figure 45 - Experimental results for all the rotations.

The aforementioned influence is clear, due to the oscillatory behaviour of the results, which propagates to the total rotation, besides being amplified by a factor of two. By knowing that the estimation of the cohesive law is based on a differentiation that depends on these values, this preliminary data immediately suggested that it would be very difficult to obtain the intended law with these testing conditions.

After the new setup was arranged, new tests were performed. Figure 46 shows the experimental rotations for the three performed tests, using Adhesive B.

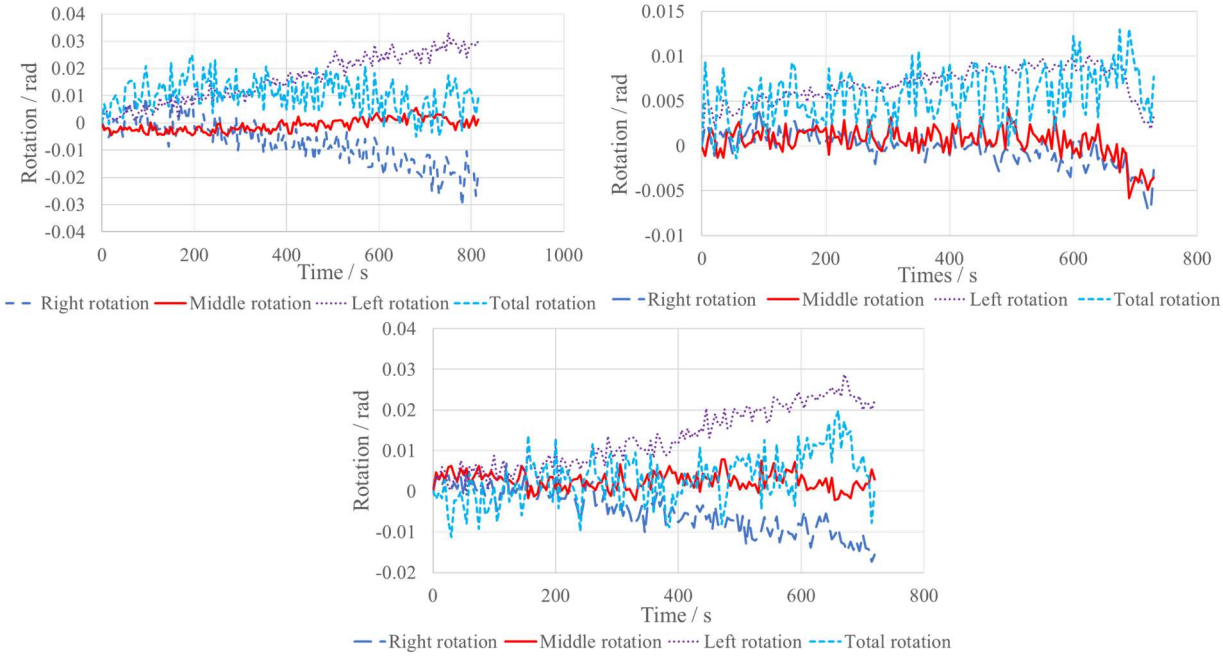

Figure 46 - Experimental rotations for Adhesive B: Test 1 (up left), Test 2 (up right) and Test 3 (bottom).

The presented results suggest that the quality of the displacement field obtained through the DIC analysis for these tests was not precise. In order to confirm it, a comparison between the CBBM and the J-integral approach, together with DIC, was performed and the results are shown in Figure 47.

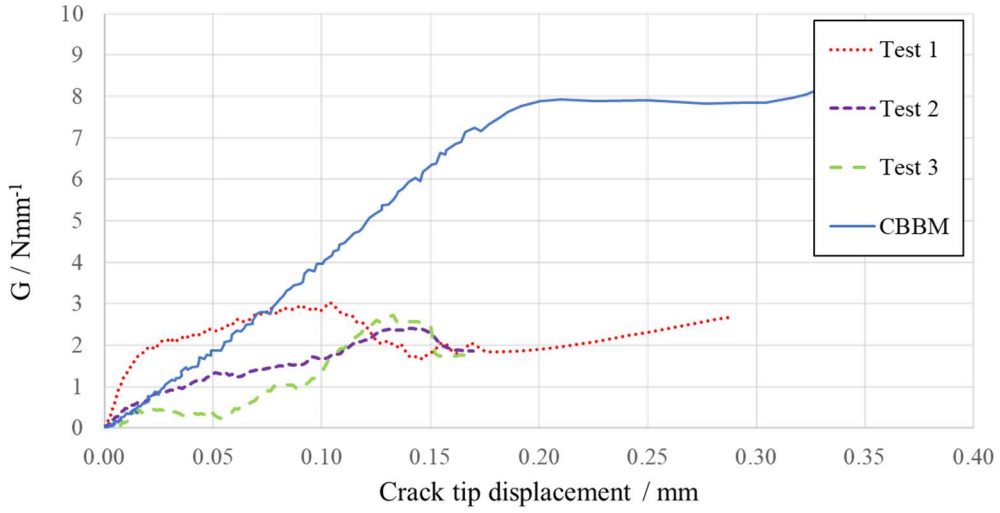

Figure 47 - Fracture toughness in Mode II comparison between the two approaches.

In the presence of such results, no determination of the cohesive laws was executed. It was assumed that with the presented data, there were no conditions to obtain acceptable results. However, the crack tip displacement was still analysed with DIC, since this procedure can still be employed in for future work with a different setup configuration. Figure 48 shows the obtained results for all the three tests, which are very good with almost no noise in the unfiltered data.

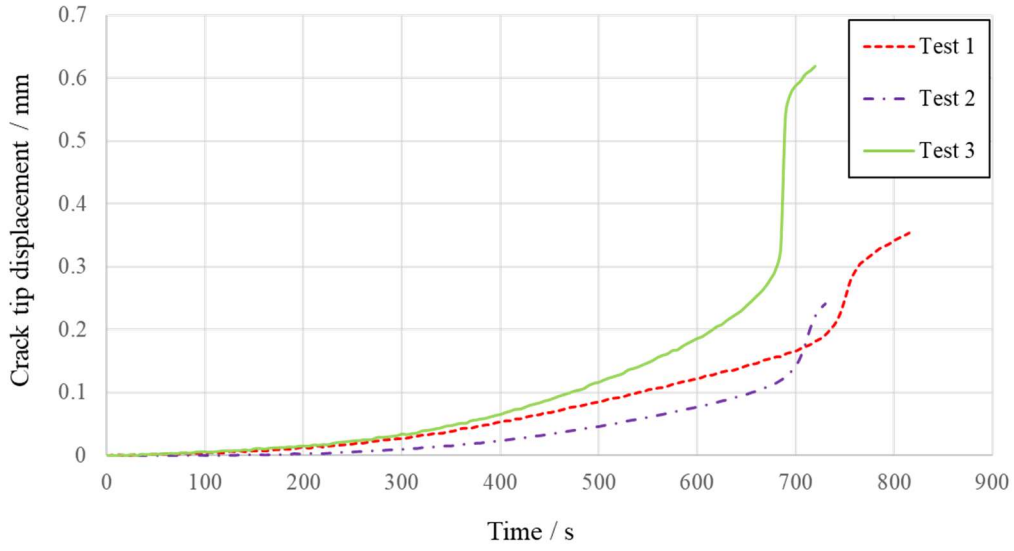

Figure 48 - Crack tip displacement for the three tests.

5.3 Final remarks

In this chapter, the Mode II fracture behaviour of the Adhesive B was evaluated, using the J-integral approach together with a DIC analysis. Moreover, the process was optimized using the developed code.

In order to adapt the test configuration to the required measurements, a different set of cameras and lenses was used, when compared to the Mode I testing configuration. The camera and the lens used to record the crack tip displacement yielded very good results, with low values of noise. However, the recorded images for the computation of the rotations did not lead to acceptable results. This can be explained by the fact that the distance between the camera and the specimen required to capture all areas of interest, did not allow for a good resolution of the painted speckle. This condition implied that the quality of the marked points in the DIC software was too low, originating high values of noise in the exported displacement field data.

Taking into account the obtained results, a different method for the measurement of the rotations should be used. Several authors [4, 21, 41, 45, 47, 74] resorted to inclinometers to directly obtain the rotations in the three required points and achieved good results. Therefore, this method could be used, together with the DIC analysis, to export the displacement field data, in order to attain the Mode II cohesive law of the adhesives.

6 Summary of the appended paper

Determination of Mode I cohesive law of structural adhesives using the direct method

This paper validates the determination of Mode I cohesive law of two structural adhesives using the direct method. DIC measurements were analysed resorting to a script developed in Python, aiming to optimize the process. Tensile tests at two different loading rates were performed, in order to compare the standard loading rate for bulk specimens and the one that seeks to replicate the actual strain rate used in a DCB. Moreover, DCB tests were used to estimate the fracture toughness of both adhesives, by using the J-integral approach, and then were compared to CBBM. Both adhesives yielded a good agreement in both methods, although some difficulties in measuring the initial compliance in CBBM have proven to influence the results for one of the adhesives. A comparison between the experimental cohesive laws and the numerical simulations proved challenging in describing with precision the failure processes by the CZM modelling, but the direct method could still predict the main features of the cohesive law. Furthermore, the experimental law was used to simulate the fracture behaviour in a different geometry and the results suggest that, for pure modes, the method is highly dependent on loading and constraining conditions.

7 Conclusion

In the present work, the direct method was applied to structural adhesives, aiming to characterize their fracture behaviour and use this data to generate cohesive zone laws. The results were obtained using DCB and ENF fracture tests, together with DIC analysis. Furthermore, a Python script was developed, in order to optimize data analysis and obtain smoothened results.

The bulk specimens for strength prediction were tested at two different loading rates, to recreate the strain rate presented in DCB tests. An increase in the strength was observed, as well as a decrease in the maximum strain. Regarding the fracture tests, both Mode I and Mode II tests were performed, and the results were analysed using the J-integral approach. The comparison between the values obtained with the J-integral and the ones obtained with CBBM validated the process for Mode I, while for Mode II, the results were not acceptable.

The cohesive laws of both adhesives were simulated, and the numerical results were compared to the experimental ones. This procedure allowed to fully validate the direct method for Mode I, although the damage process was not precisely described.

After the validation of the direct method, the determined cohesive law for the Adhesive A was used to simulate the fracture of a different geometry. The fracture behaviour of the used specimen was similar to a butt joint, so a cohesive law previously estimated for these specimens was also used in a numerical simulation.

The most significant findings of this research are:

- The strength prediction of the adhesive using bulk specimens provides different values than those derived from DCB tests.
- The J-integral approach proved to be accurate in determining the fracture toughness of the adhesives, requiring the adjustment of fewer parameters than the use of CBBM.
- The developed code allows the user to compute thousands of data from a DIC analysis, which effectively streamlines the whole characterization process.
- The direct method predicted TSLs that produced load-displacement curves with very good agreement for the peak load values, when compared to experimental results.
- The results obtained with the block specimens showed a significant dependence of the load-displacement curve on the inputted law. This indicated that the loading and constraining conditions have a significant influence on the results of the applied method.

8 Future work

The dependency of the numerical results on the shape of the inputted cohesive law suggests that there would be an interest in studying the influence of the different pure mode cohesive laws, in the simulation of adhesive joints that are under Mixed Mode loading. It would also be relevant to investigate if the numerical methods could accurately predict the fracture behaviour in these conditions.

Furthermore, it would be worthy to improve the developed script by automating the possible combinations of the parameters used in the applied filter. Moreover, these parameters could present in real time the changes in all the plots as a result of these alterations.

Additionally, in order to improve the quality of the results, the testing setup could be altered with the incorporation of inclinometers in the loading points, which would enable a more accurate measurement of the displacements. The DIC analysis could then be applied in a smaller area of interest and these results could also be improved.

References

[1] A. Khayer Dastjerdi, E. Tan, and F. Barthelat, "Direct Measurement of the Cohesive Law of Adhesives Using a Rigid Double Cantilever Beam Technique," *Experimental Mechanics,* vol. 53, no. 9, pp. 1763-1772, 2013/11/01 2013, doi: 10.1007/s11340-013-9755-0.

[2] C. d. S. P. Borges, "Fracture envelope of automotive adhesives under impact," Master, Departamento de Engenharia Mecânica, Faculdade de Engenharia do Porto, 2019.

[3] M. dos Reis, R. Carbas, E. Marques, and L. da Silva, "Functionally graded adhesive joints under impact loads," *Proceedings of the Institution of Mechanical Engineers, Part D: Journal of Automobile Engineering,* vol. 235, no. 13, pp. 3270-3281, 2021/11/01 2021, doi: 10.1177/09544070211004505.

[4] A. Biel and U. Stigh, "Comparison of J-integral methods to experimentally determine cohesive laws in shear for adhesives," *International Journal of Adhesion and Adhesives,* vol. 94, pp. 64-75, 2019/10/01 2019, doi: 10.1016/j.ijadhadh.2019.04.014.

[5] F. Sun and B. R. K. Blackman, "A DIC method to determine the Mode I energy release rate G, the J-integral and the traction-separation law simultaneously for adhesive joints," *Engineering Fracture Mechanics,* vol. 234, p. 107097, 2020/07/01 2020, doi: 10.1016/j.engfracmech.2020.107097.

[6] K. S. Alfredsson, A. Biel, and S. Salimi, "Shear testing of thick adhesive layers using the ENF-specimen," *International Journal of Adhesion and Adhesives,* vol. 62, pp. 130-138, 2015/10/01 2015, doi: 10.1016/j.ijadhadh.2015.07.008.

[7] E. M. Petrie, *Handbook of Adhesives and Sealants*. 2005, pp. 1-814.

[8] L. F. d. Silva, A. Öchsner, and R. D. Adams, *Handbook of Adhesion Technology*. Springer, 2018.

[9] *ASTM D907-15. Standard Terminology of Adhesives*, 2015.

[10] S. L. A. H. Ebnesajjad, W. Andrew, Ed. *Adhesives Technology Handbook*, 3rd ed. 2015.

[11] S. Ebnesajjad, W. Andrew, Ed. *Adhesives Technology Handbook*, 2nd ed. 2009.

[12] A. Pizzi and K. L. Mittal, *Handbook of Adhesive Technology*. CRC Press, 2017.

[13] R. Adams, *Adhesive bonding: Science, technology and applications*. 2005, pp. 1-543.

[14] P. M. G. P. Moreira, L. F. M. d. Silva, and P. M. S. T. d. Castro, *Structural Connections for Lightweight Metallic Structures*, 1st ed. 2012.

[15] L. F. M. da Silva, António G. and M. F. Moura, *Juntas Adesivas Estruturais*, 1st ed. 2007.

[16] F. Chaves, L. F. M. Silva, M. De Moura, D. Dillard, and V. Esteves, "Fracture Mechanics Tests in Adhesively Bonded Joints: A Literature Review," *The Journal of Adhesion,* vol. 90, pp. 955-992, 11/02 2014, doi: 10.1080/00218464.2013.859075.

[17] A. B Morais, A. G Magalhães, and M. FSF Moura, *Materiais Compóstios - Materiais, Fabrico e Comportamento Mecânico*, 2nd ed. 2009.

[18] A. A. Griffith, "The Phenomena of Rupture and Flow in Solids," *Philosophical Transactions of the Royal Society of London. Series A, Containing Papers of a Mathematical or Physical Character,* vol. 221, pp. 163-198, 1921.

[19] G. R. Irwin, "ANALYSIS OF STRESS AND STRAINS NEAR THE END OF A CRACK TRAVERSING A PLATE," 1957.

[20] E. Ripling, S. Mostovoy, and R. Patrick, *Application of fracture mechanics to adhesive joints*. ASTM International, 1964.

[21] C. Sarrado, A. Turon, J. Renart, and J. Costa, "An experimental data reduction method for the Mixed Mode Bending test based on the J-integral approach," *Composites Science and Technology,* vol. 117, pp. 85-91, 2015/09/29 2015, doi: 10.1016/j.compscitech.2015.05.021.

[22] M. Z. Sadeghi, J. Zimmermann, A. Gabener, and K. U. Schroeder, "The applicability of J-integral approach in the determination of mixed-mode fracture energy in a ductile adhesive," *International Journal of Adhesion and Adhesives,* vol. 83, pp. 2-8, 2018/06/01/ 2018, doi: 10.1016/j.ijadhadh.2018.02.027.

[23] D. Kimpfbeck, Z. Major, and M.-C. Miron, "Application of J Integral for the Fracture Assessment of Welded Polymeric Components," 2019.

[24] S. Goutianos and B. F. Sørensen, "The application of J integral to measure cohesive laws under large-scale yielding," *Engineering Fracture Mechanics,* vol. 155, pp. 145-165, 2016/04/01 2016, doi: 10.1016/j.engfracmech.2016.01.004.

[25] X.-k. Zhu, "J-integral resistance curve testing and evaluation," *Journal of Zhejiang University - Science A: Applied Physics & Engineering,* vol. 10, pp. 1541-1560, 11/01 2009, doi: 10.1631/jzus.A0930004.

[26] G. P. Cherepanov, "Crack propagation in continuous media: PMM vol. 31, no. 3, 1967, pp. 476–488," *Journal of Applied Mathematics and Mechanics,* vol. 31, no. 3, pp. 503-512, 1967/01/01 1967, doi: 10.1016/0021-8928(67)90034-2.

[27] J. Rice, "A Path Integral and the Approximate Analysis of Strain Concentration by Notches and Cracks," *Journal of Applied Mechanics,* vol. 35, pp. 379-386, 06/01 1968, doi: 10.1115/1.3601206.

[28] R. J. Bucci, P. C. Paris, J. D. Landes, and J. Rice, "J-integral estimation procedures," *ASTM Special Technical Publication,* pp. 40-69, 01/01 1972, doi: 10.1520/STP38818S.

[29] H. Li and N. Chandra, "Analysis of crack growth and crack-tip plasticity in ductile materials using cohesive zone models," *International Journal of Plasticity,* vol. 19, no. 6, pp. 849-882, 2003/06/01/ 2003, doi: 10.1016/S0749-6419(02)00008-6.

[30] Z. Jia, G. Yuan, D. Hui, X. Feng, and Y. Zou, "Effect of high strain rate and low temperature on mode II fracture toughness of ductile adhesive," *International Journal of Adhesion and Adhesives,* vol. 86, pp. 105-112, 2018/11/01/ 2018, doi: 10.1016/j.ijadhadh.2018.09.003.

[31] T. Ikeda , A. Yamashita , D. Lee , and N. Miyazaki "Failure of a Ductile Adhesive Layer Constrained by Hard Adherends," *Journal of Engineering Materials and Technology,* vol. 122, no. 1, pp. 80-85, 1999, doi: 10.1115/1.482769.

[32] K. N. Anyfantis and N. G. Tsouvalis, "A novel traction–separation law for the prediction of the mixed mode response of ductile adhesive joints," *International Journal of Solids and Structures,* vol. 49, no. 1, pp. 213-226, 2012/01/01 2012, doi: 10.1016/j.ijsolstr.2011.10.001.

[33] T. Siegmund and W. Brocks, "A numerical study on the correlation between the work of separation and the dissipation rate in ductile fracture," *Engineering Fracture Mechanics,* vol. 67, pp. 139-154, 2000.

[34] H. Cui, "Simulation of ductile adhesive failure with experimentally determined cohesive law," *Composites Part B: Engineering,* vol. 92, pp. 193-201, 2016/05/01 2016, doi: 10.1016/j.compositesb.2016.02.018.

[35] P. L. Rosendahl, Y. Staudt, C. Odenbreit, J. Schneider, and W. Becker, "Measuring mode I fracture properties of thick-layered structural silicone sealants," *International Journal of Adhesion and Adhesives,* vol. 91, pp. 64-71, 2019/06/01 2019, doi: 10.1016/j.ijadhadh.2019.02.012.

[36] G. Lélias, E. Paroissien, F. Lachaud, and J. Morlier, "Experimental characterization of cohesive zone models for thin adhesive layers loaded in mode I, mode II, and mixed-mode I/II by the use of a direct method," *International Journal of Solids and Structures,* vol. 158, pp. 90-115, 2019/02/01 2019, doi: 10.1016/j.ijsolstr.2018.09.005.

[37] J. Scheel and A. Ricoeur, "A comprehensive interpretation of the J-integral for cohesive interface cracks and interactions with matrix cracks," *Theoretical and Applied Fracture Mechanics,* vol. 100, pp. 281-288, 2019/04/01 2019, doi: 10.1016/j.tafmec.2019.01.016.

[38] N. Leitão and F. A. Gilabert, "A unified J-Integral-based procedure to investigate at different loading regimes the fracture by FEM simulations and image analysis," *Journal of the Mechanics and Physics of Solids,* vol. 149, p. 104318, 2021/04/01 2021, doi: 10.1016/j.jmps.2021.104318.

[39] R. D. S. G. Campilho, D. C. Moura, D. J. S. Gonçalves, J. F. M. G. da Silva, M. D. Banea, and L. F. M. da Silva, "Fracture toughness determination of adhesive and co-cured joints in natural fibre composites," *Composites Part B: Engineering,* vol. 50, pp. 120-126, 2013/07/01 2013, doi: 10.1016/j.compositesb.2013.01.025.

[40] F. Sun and B. R. K. Blackman, "Using digital image correlation to automate the measurement of crack length and fracture energy in the mode I testing of structural adhesive joints," *Engineering Fracture Mechanics,* vol. 255, p. 107957, 2021/10/01 2021, doi: 10.1016/j.engfracmech.2021.107957.

[41] M. Pérez-Galmés, J. Renart, C. Sarrado, A. Rodríguez-Bellido, and J. Costa, "A data reduction method based on the J-integral to obtain the interlaminar fracture toughness in a mode II end-loaded split (ELS) test," *Composites Part A: Applied Science and Manufacturing,* vol. 90, pp. 670-677, 2016/11/01 2016, doi: 10.1016/j.compositesa.2016.08.020.

[42] B. F. Sørensen and T. K. Jacobsen, "Determination of cohesive laws by the J integral approach," *Engineering Fracture Mechanics,* vol. 70, no. 14, pp. 1841-1858, 2003/09/01 2003, doi: 10.1016/S0013-7944(03)00127-9.

[43] C. Desai, S. Basu, and V. Parameswaran, "Determination of Traction Separation Law for Interfacial Failure in Adhesive Joints at Different Loading Rates," *The Journal of Adhesion,* vol. 92, p. 150527102921008, 05/21 2015, doi: 10.1080/00218464.2015.1046986.

[44] Y. Zhu, K. M. Liechti, and K. Ravi-Chandar, "Direct extraction of rate-dependent traction–separation laws for polyurea/steel interfaces," *International Journal of Solids and Structures,* vol. 46, no. 1, pp. 31-51, 2009/01/01 2009, doi: 10.1016/j.ijsolstr.2008.08.019.

[45] U. Stigh, S. Alfredsson, and A. Biel, "Measurement of Cohesive Laws and Related Problems," *ASME International Mechanical Engineering Congress and Exposition, Proceedings,* vol. 11, 01/01 2009, doi: 10.1115/IMECE2009-10474.

[46] J. Yu, Y. Wang, Z. Li, Q. Zhang, X. Jian, and Z. Zhang, "Using DIC technique to characterize the mode II interface fracture of layered system composed of multiple materials," *Composite Structures,* vol. 230, p. 111413, 2019/12/15 2019, doi: 10.1016/j.compstruct.2019.111413.

[47] S. Abdel Monsef, M. Pérez-Galmés, J. Renart, A. Turon, and P. Maimí, "The influence of mode II test configuration on the cohesive law of bonded joints," *Composite Structures,* vol. 234, p. 111689, 2020/02/15 2020, doi: 10.1016/j.compstruct.2019.111689.

[48] A. Arrese, N. Insausti, F. Mujika, M. Perez-Galmés, and J. Renart, "A novel experimental procedure to determine the cohesive law in ENF tests," *Composites Science and Technology,* vol. 170, pp. 42-50, 2019/01/20 2019, doi: doi.org/10.1016/j.compscitech.2018.11.031.

[49] B. F. Sørensen and P. Kirkegaard, "Determination of mixed mode cohesive laws," *Engineering Fracture Mechanics,* vol. 73, no. 17, pp. 2642-2661, 2006/11/01/ 2006, doi: 10.1016/j.engfracmech.2006.04.006.

[50] L. Loh and S. Marzi, "A novel experimental methodology to identify fracture envelopes and cohesive laws in mixed-mode I + III," *Engineering Fracture Mechanics,* vol. 214, pp. 304-319, 2019/06/01 2019, doi: 10.1016/j.engfracmech.2019.03.011.

[51] F. Sun, R. Zhang, and B. R. K. Blackman, "Determination of the mode I crack tip opening rate and the rate dependent cohesive properties for structural adhesive joints using digital image correlation," *International Journal of Solids and Structures,* vol. 217-218, pp. 60-73, 2021/05/15 2021, doi: 10.1016/j.ijsolstr.2021.01.034.

[52] J. M. Gorman and M. D. Thouless, "The use of digital-image correlation to investigate the cohesive zone in a double-cantilever beam, with comparisons to numerical and analytical models," *Journal of the Mechanics and Physics of Solids,* vol. 123, pp. 315-331, 2019/02/01 2019, doi: 10.1016/j.jmps.2018.08.013.

[53] G. Cricrì, "Cohesive law identification of adhesive layers subject to shear load – An exact inverse solution," *International Journal of Solids and Structures,* vol. 158, pp. 150-164, 2019/02/01/ 2019, doi: 10.1016/j.ijsolstr.2018.09.001.

[54] P. Rahulkumar, A. Jagota, S. J. Bennison, and S. Saigal, "Cohesive element modeling of viscoelastic fracture: application to peel testing of polymers," *International Journal of Solids and Structures,* vol. 37, no. 13, pp. 1873-1897, 2000/03/01 2000, doi: 10.1016/S0020-7683(98)00339-4.

[55] L. F. Faria Ricardo, D. Leguillon, G. Parry, and A. Doitrand, "Modeling the thermal shock induced cracking in ceramics," *Journal of the European Ceramic Society,* vol. 40, no. 4, pp. 1513-1521, 2020/04/01 2020, doi: 10.1016/j.jeurceramsoc.2019.11.071.

[56] A. Hillerborg, M. Modéer, and P. E. Petersson, "Analysis of crack formation and crack growth in concrete by means of fracture mechanics and finite elements," *Cement and Concrete Research,* vol. 6, no. 6, pp. 773-781, 1976/11/01 1976, doi: 10.1016/0008-8846(76)90007-7.

[57] R. K. Naik, S. K. Panda, and V. Racherla, "Failure analysis of metal-polymer-metal sandwich panels with wire mesh interlayers: Finite element modeling and experimental validation," *Composite Structures,* vol. 280, p. 114813, 2022/01/15 2022, doi: 10.1016/j.compstruct.2021.114813.

[58] G. Goldoni and S. Mantovani, "Damage modelling strategies for unidirectional laminates subjected to impact using CZM and orthotropic plasticity law," *Composite Structures,* vol. 275, p. 114493, 2021/11/01 2021, doi: 10.1016/j.compstruct.2021.114493.

[59] F. Ramezani, P. D. P. Nunes, R. J. C. Carbas, E. A. S. Marques, and L. F. M. da Silva, "The joint strength of hybrid composite joints reinforced with different laminates materials," *Journal of Advanced Joining Processes,* vol. 5, p. 100103, 2022/06/01 2022, doi: 10.1016/j.jajp.2022.100103.

[60] B. Erice, M. Lißner, J. Wittig, A. Hornig, M. Gude, and N. Petrinic, "On the Temperature Dependent Mechanical Response of Dynamically-loaded Shear-dominated Adhesive Structures," vol. 250, ed. Les Ulis: EDP Sciences, 2021.

[61] A. V. M. Rocha *et al.*, "Numerical analysis of mixed-mode fatigue crack growth of adhesive joints using CZM," *Theoretical and Applied Fracture Mechanics,* vol. 106, p. 102493, 2020/04/01 2020, doi: 10.1016/j.tafmec.2020.102493.

[62] J. J. M. Machado, P. D. P. Nunes, E. A. S. Marques, and L. F. M. da Silva, "Numerical study of similar and dissimilar single lap joints under quasi-static and impact conditions," *International Journal of Adhesion and Adhesives,* vol. 96, p. 102501, 2020/01/01 2020, doi: 10.1016/j.ijadhadh.2019.102501.

[63] U. T. F. Carvalho and R. D. S. G. Campilho, "Validation of a direct method to predict the strength of adhesively bonded joints," *Science and Technology of Materials,* vol. 30, no. 3, pp. 138-143, 2018/09/01 2018, doi: 10.1016/j.stmat.2017.12.002.

[64] A. B. de Morais, "Determination of the shear traction-separation law of adhesive layers using the end-notched flexure specimen," *Engineering Fracture Mechanics,* vol. 235, p. 107199, 2020/08/01 2020, doi: 10.1016/j.engfracmech.2020.107199.

[65] G. I. Barenblatt, "The Mathematical Theory of Equilibrium Cracks in Brittle Fracture," in *Advances in Applied Mechanics*, vol. 7, H. L. Dryden, T. von Kármán, G. Kuerti, F. H. van den Dungen, and L. Howarth Eds.: Elsevier, 1962, pp. 55-129.

[66] D. S. Dugdale, "Yielding of steel sheets containing slits," *Journal of the Mechanics and Physics of Solids,* vol. 8, no. 2, pp. 100-104, 1960/05/01 1960, doi: 10.1016/0022-5096(60)90013-2.

[67] A. Arrese, A. Boyano, J. De Gracia, and F. Mujika, "A novel procedure to determine the cohesive law in DCB tests," *Composites Science and Technology,* vol. 152, pp. 76-84, 2017/11/10 2017, doi: 10.1016/j.compscitech.2017.09.012.

[68] C. Wu, R. Huang, and K. M. Liechti, "Simultaneous extraction of tensile and shear interactions at interfaces," *Journal of the Mechanics and Physics of Solids,* vol. 125, pp. 225-254, 2019/04/01 2019, doi: 10.1016/j.jmps.2018.12.004.

[69] C. Shet and N. Chandra, "Effect of the Shape of T–δ Cohesive Zone Curves on the Fracture Response," *Mechanics of Advanced Materials and Structures,* vol. 11, no. 3, pp. 249-275, 2004/05/01 2004, doi: 10.1080/15376490490427207.

[70] J. C. S. Azevedo, R. D. S. G. Campilho, F. J. G. da Silva, T. M. S. Faneco, and R. M. Lopes, "Cohesive law estimation of adhesive joints in mode II condition," *Theoretical and Applied Fracture Mechanics,* vol. 80, pp. 143-154, 2015/12/01/ 2015, doi: 10.1016/j.tafmec.2015.09.007.

[71] R. M. R. P. Fernandes, J. A. G. Chousal, M. F. S. F. de Moura, and J. Xavier, "Determination of cohesive laws of composite bonded joints under mode II loading," *Composites Part B: Engineering,* vol. 52, pp. 269-274, 2013/09/01 2013, doi: 10.1016/j.compositesb.2013.04.007.

[72] U. T. F. Carvalho and R. D. S. G. Campilho, "Validation of pure tensile and shear cohesive laws obtained by the direct method with single-lap joints," *International Journal of Adhesion and Adhesives,* vol. 77, pp. 41-50, 2017/09/01 2017, doi: 10.1016/j.ijadhadh.2017.04.002.

[73] S. Abdel Monsef, A. Ortega, A. Turon, P. Maimí, and J. Renart, "An efficient method to extract a mode I cohesive law for bonded joints using the double cantilever beam test," *Composites Part B: Engineering,* vol. 178, p. 107424, 2019/12/01 2019, doi: 10.1016/j.compositesb.2019.107424.

[74] C. Sarrado, A. Turon, J. Costa, and J. Renart, "An experimental analysis of the fracture behavior of composite bonded joints in terms of cohesive laws," *Composites Part A: Applied Science and Manufacturing,* vol. 90, 07/01 2016, doi: 10.1016/j.compositesa.2016.07.004.

[75] D. Svensson, K. S. Alfredsson, A. Biel, and U. Stigh, "Measurement of cohesive laws for interlaminar failure of CFRP," *Composites Science and Technology,* vol. 100, pp. 53-62, 2014/08/21 2014, doi: 10.1016/j.compscitech.2014.05.031.

[76] M. Moazzami, M. R. Ayatollahi, S. Teixeira de Freitas, and L. F. M. da Silva, "Towards pure mode I loading in dissimilar adhesively bonded double cantilever beams," *International Journal of Adhesion and Adhesives,* vol. 107, p. 102826, 2021/06/01 2021, doi: 10.1016/j.ijadhadh.2021.102826.

[77] A. Jaillon, J. Jumel, F. Lachaud, and E. Paroissien, "Mode I cohesive zone model parameters identification and comparison of measurement techniques based on uncertainty estimation," *International Journal of Solids and Structures,* vol. 191-192, pp. 577-587, 2020/05/15 2020, doi: 10.1016/j.ijsolstr.2019.12.014.

[78] *NF T 76-142. Méthode de préparation de plaques d'adhésifs structuraux pour la réalisation d'éprouvettes d'essai de caractérisation*, 1988.
[79] "BS 2782-0:2011. Methods of testing plastics.," 2011.
[80] M. F. S. F. de Moura, R. D. S. G. Campilho, and J. P. M. Gonçalves, "Crack equivalent concept applied to the fracture characterization of bonded joints under pure mode I loading," *Composites Science and Technology,* vol. 68, no. 10, pp. 2224-2230, 2008/08/01 2008, doi: doi.org/10.1016/j.compscitech.2008.04.003.
[81] M. F. S. F. de Moura, J. J. L. Morais, and N. Dourado, "A new data reduction scheme for mode I wood fracture characterization using the double cantilever beam test," *Engineering Fracture Mechanics,* vol. 75, no. 13, pp. 3852-3865, 2008/09/01 2008, doi: 10.1016/j.engfracmech.2008.02.006.
[82] A. J. Paris and P. C. Paris, "Instantaneous evaluation of J and C," *International Journal of Fracture,* vol. 38, no. 1, pp. R19-R21, 1988.

Appendices

Appendix A Paper

Determination of Mode I cohesive law of structural adhesives using the direct method

B. D. Simões[2], P. D. P. Nunes[1], B. S. Henriques[2], E. A. S. Marques[1], R. J. C. Carbas[1], L.F.M da Silva[2]

[1]Institute of Science and Innovation in Mechanical and Industrial Engineering (INEGI), Rua Dr. Roberto Frias, 4200-465 Porto, Portugal

[2]Departamento de Engenharia Mecânica, Faculdade de Engenharia, Universidade do Porto, Rua Dr. Roberto Frias, 4200-465 Porto, Portugal

Abstract

The Mode I fracture behaviour of adhesive joints, bonded with two different epoxies, was evaluated applying the direct method together with Digital Image Correlation (DIC) analysis. The DCB (Double Cantilever Beam) test was performed to attain the load and displacement results. In order to determine the critical energy release rate, the J-integral was considered, and the direct method was used to experimentally evaluate the tensile Cohesive Zone Model (CZM) law. Additionally, DIC measurements were analysed resorting to a script developed in Python, aiming to optimize the process. Moreover, a direct comparison of the load-displacement curves between experimental and numerical results was carried out to validate the cohesive law. Despite the fact that the damage mechanism was not precisely described, the direct method could still predict the main features of the cohesive law. Also, the obtained cohesive law was used to simulate the fracture behaviour in a different geometry, to evaluate the influence of the test specimens on the results. The obtained data indicate that the direct method is dependent on the joint geometry and the constraining condition of the adhesive.

Keywords: Adhesive joints; J-integral; Cohesive law; Digital image correlation

1. Introduction

For many applications, the use of adhesives has been shown to be more advantageous than the use of classical joining processes, which is reflected in their increased usage in the automotive, aeronautical, and aerospace sectors [1]. Adhesive joints offer an attractive strength-to-weight ratio that ensures an overall reduction in weight, costs, and emissions of vehicle structures [2]. These joints enable the combination of dissimilar materials, the

elimination of stress concentrations associated to the holes necessary for mechanical joining, and grant a more uniform stress distribution [3]. Moreover, bonded connections are particularly useful for preventing galvanic corrosion between different materials and assuring some absorption of different thermal expansions, being more efficient than conventional joints to bond composite adherends [4]. Since these joints are often used in safety critical structures, it is essential to develop precise methodologies, both experimental and numerical in nature, to properly predict and characterize joint behaviour [2].

1.1. Failure prediction and Cohesive Zone Model

In tensile opening mode (Mode I), the fracture toughness of the joint is usually measured with Double Cantilever Beam (DCB) tests, suitable to quantify the fracture toughness (J_{Ic}) [5]. This is an important material parameter, typical of fracture process, that enables the evaluation of the integrity state of bonded structures [6]. Up until now, various data reduction methods have been used to obtain this material property, such as the Simple Beam Theory (SBT), Corrected Beam Theory (CBT), Experimental Compliance Method (ECM), and Compliance Based Beam Theory (CBBM). These methods are all based on Linear Elastic Fracture Mechanics (LEFM) [5] and can only be applied if the fracture process zone (FPZ) is very small comparing to the length of the component, except for CBBM. The FPZ is included in the stress field of the crack tip, that is called K-dominant zone [7]. Meanwhile, there are several proposed methods to characterize non-linear FPZ, based on the J-integral approach [8].

The J-integral determines the elastic-plastic field intensity of the crack tip. The concept was first introduced by Rice in 1968 [9], who defined it as a contour integral that describes the energy per unit area necessary to create two new surfaces on the cracked body under loading conditions. Rice also demonstrated that the J-integral is independent of the contour for any elastic or elasto-plastic material, as long as the deformation theory of plasticity is used [10]. In order to maintain its independence property, the contour must obey three conditions: it must surround the crack tip, the elastic deformation energy must not be explicitly dependent on the *x* coordinate, and there must not be other object inside the contour that may alter the body energy if it is moved in the *x* direction [11]. Considering this property, Biel and Stigh [11] applied the J-integral approach and several alternative contours. The authors observed that the two contours that assumed elastic deformation in the substrates, in the presence of plasticity, were less accurate.

Furthermore, the method with a lower number of assumptions was considered the most precise and allowed the presence of plasticity.

Given that this approach permits to overcome some LEFM limitations [5, 12-16], it has been employed in the characterization of fracture processes involving large FPZs [6, 13, 17]. It has also been used in the estimation of cohesive laws [7, 18-22] through the computation of the obtained data related to the J-integral and to the crack tip opening. Besides that, the J-integral is applied in all loading modes: Mode I [5, 7, 18, 23-25] , Mode II [8, 11, 26, 27], and Mixed Mode [21, 28-30]. Sørensen and Jacobsen [18] aimed to develop a robust approach to obtain the cohesive law from test specimens and then predict the strength of the same adhesive for other geometries. The J-integral method yielded very good results, providing a law shape that suits the micromechanical model in the problem of cross-over bridging. For this problem, as well as for the quantitative prediction of the strength of the bonded joint, a great concordance between predicted and measured strengths was accomplished.

In a study in Mode I, in which G_c, J_c, and the cohesive laws were simultaneously ascertained, Sun and Blackman [5] utilized several methods to obtain the fracture toughness of three distinct adhesives and assessed their applicability in each situation. The authors learned that for the brittle adhesive and toughened epoxy, all the values of G_c obtained through the LEFM method were in accordance with the J_c values, evidencing their validity. On the other hand, for the ductile adhesive of polyurethane, the G_c values were 15% higher than the J_c ones, indicating that the same methods are not valid.

The Finite Element Method (FEM) is the most widely accepted method for the numerical prediction of strength, through the calculation of tension and displacement fields, combined with proper failure criteria [15]. In practical applications, the failure of bonded joints is often modelled by Cohesive Zone Model (CZM) [29], which admits precise predictions of fracture growth [15], enabling the modelling of progressive degradation and failure [31]. CZMs were initially developed as a numerical tool to study fracture [32]. However, today they are increasingly used for theoretical studies and for the simulation of decohesion of structural joints or delamination in composite laminates [33] and thus, have become the most adequate method for the modelling of adhesive joints in static and fatigue models [21]. These joints have some limitations concerning the high sensitivity to imperfections and the complexity of the assessment of the different failure modes. Nonetheless, CZM is a powerful tool to simulate bonded joints, using the equivalent cohesive law that governs the mechanical behaviour of the same joints [34]. CZM can handle the non-linear zone ahead of the crack tip, which occurs due to plasticity

or micro-cracking present in many materials. Determining precise cohesive law or traction-separation law (TSL), for Mode I, is extremely important to ascertain the CZM [35], since it is used to characterize the bonded interface substrate–adhesive. However, the quantitative determination of cohesive law, under different failure modes, can be complex, since cohesive laws are sensitive to the substrate surface chemistry, as well as to bond line thickness [36].

Although CZM achieves highly accurate results, a thorough determination of the parameters and shape of the cohesive law is still necessary [37] because the prediction of adhesive joint strength is highly dependent on the CZM parameters [21]. For Mode I, the cohesive laws relate tensile tractions (t_n) to tensile relative displacements (δ_n), between homologous nodes of the cohesive element. The main cohesive laws parameters, which will be introduced in numerical models, are t_n^0 (cohesive strength in tension, providing the peak traction value) and the critical value of tensile strain energy release rate (J_{Ic}) [38]. Nowadays, different approaches are used to obtain these cohesive parameters, such as identification technique, the inverse method, and the direct method [39]. The present work will focus exclusively on the direct method to determine the cohesive law. This method is based on the premises that during stable crack propagation, the FPZ only translates along the specimen, ahead of the crack tip in a self-similar manner, and that the cohesive law may be deduced by differentiating the fracture toughness with respect to the initial crack tip opening [5]. In this line of thought, it is worthy to note that in 1968, Rice [9] highlighted an analytical relation between the cohesive law determined in the crack tip and the J-integral represented by $dJ/d[u_i] = t_i[u_i]$. This approach was used for different loading modes, for example, Sun and Blackman [16] in Mode I, Carvalho and Campilho [39] in Mode II, and Sarrado, et al. [40] in Mixed Mode. This analysis relies on a closed-form solution of the path independent J-integral and experimental measurement of crack tip opening displacement, δ_n [41]. Through this approach, it is possible to obtain the precise form of CZM laws, for a specific material or interface, since they are estimated from experimental data of fracture tests like DCB or ENF (End Notched Flexure) [41]. Even so, the experimental determination of the cohesive law is not straightforward and, in recent years, an effort has been made to develop different methods, with the aim of experimentally obtaining it through the measurement of the crack tip opening displacement, concomitantly with the J-integral values [34].

1.2. Digital Image Correlation

A crucial step to attain TSLs is measuring δ_n, that can be obtained by different methods: crack opening interferometry, digital image correlation (DIC), and laser generated stress pulses [42]. DIC methodology has become a common technique for tracking surface displacements and for associated surface strains calculation [32]. A DIC algorithm usually relates local features of a pair of digital images, searching for the displacement field that efficiently provides the best match between pixel intensities [43]. The reference image (undeformed configuration) is typically divided in two correlation domains, within which it is assumed that a grey pixel distribution defines a unique and local fingerprint of the surface, with suitable contrast and isotropy. A suitable sub-pixel correlation algorithm is then used to compute the central position of each subset in the deformed configuration, providing the displacement field across the interest zone [44]. This technique involves the application of a speckle pattern on the specimen surface, in order to produce a non-uniform grey-scale pattern. This pattern is then converted into a digital surface of grey scales, being the bi-cubic splines one of the most typical interpolation methods used to create a continuum digital surface. The subsequent movements of peaks and valleys are tracked to determine the surface-displacement vectors [32]. Recently, this powerful technique has been exhaustively used to study the fracture of the interface, due to the possibility of measuring local displacements near the crack tip, allowing the direct extraction of precise cohesive laws [5, 16, 45]. Even though several works have been carried out to quantify TSL [32, 42-44], it is still necessary to investigate if CZMs are sufficient to fully describe the failure behaviour of various adhesive joints [5].

This work strived to characterize the Mode I fracture behaviour of the adhesive joints and endeavoured to determine the cohesive law by the direct method, using DIC methodology. Additionally, a Python script was developed in an effort to optimize the whole process.

1.3. Theoretical background

1.3.1. CBBM method

The CBBM method [46], when compared with other LEFM based approaches, has the advantage of considering the effect of FPZ. This method lies in the use of an estimated equivalent crack length, extending its applicability to materials with bigger FPZs than the other classic methods. The critical energy release rate is given by:

$$G_{Ic} = \frac{6P^2}{b^2 h}\left(\frac{2a_{eq}^2}{h^2 E_f} + \frac{1}{5G_f}\right) \quad (1)$$

where a_{eq} is the equivalent crack length, E_f is the corrected flexural modulus, and G_f is the shear modulus of the substrate.

1.3.2. Direct method for the DCB tests

The direct method approach was used to attain CZM law. Based on the fundamental expression for *J*, it is possible to derive an expression for the value of J_I, applied to the DCB. Considering the contour integral around the cohesive zone, the J-integral is given by:

$$J_{tip} = \int_0^{\delta_n^0} \sigma(\delta_n) d\delta_n \quad (2)$$

where δ_n is the normal opening displacement of the interface, σ is the normal traction across the interface, and δ_n^0 is the limiting end-opening at which the traction becomes zero. By differentiating the equation above with respect to δ_n, the traction-separation relation is obtained as shown in Eq. (3):

$$\frac{\partial J_{tip}}{\partial \delta_n} = \sigma(\delta_n) \quad (3)$$

Considering a Mode I loading, the value of *J* along the exterior boundary of the DCB specimen is:

$$J_{Ext} = \frac{P}{b} \cdot (\theta_{up} - \theta_{low}) \quad (4)$$

where *P* is the applied load, *b* is the width of the specimen, and θ_{up} and θ_{low} are the relative rotations of the upper and lower substrates at the loading points, respectively. Taking into account the path independence property of the J-integral for linear and nonlinear elastic material, and assuming that the region outside the FPZ remains elastic during fracture, the relation $J_{Ext} = J_{tip}$ is valid. Therefore, the cohesive law in Mode I can be determined using Eq. (3), by estimating the value of J_{Ext}, as well as the values of δ_n during the loading.

2. Experimental procedures

The following section presents the adhesives used in the study and a detailed description of both manufacturing and testing procedures. Tensile tests, DCB, and block joints were tested for strength prediction, fracture toughness in Mode I, and validation tensile test, respectively.

2.1. Adhesives

Two different epoxy-based adhesives were used in the present work, and will be referred to in the following sections as Adhesive A and Adhesive B. The first is a one-component structural adhesive with crash-resistant properties, especially developed for body shop applications. The second is a structural two-component adhesive, designed for high strength and impact-resistant bonding of metallic or composite substrates. The cure of the first adhesive consisted of a stage at 180 °C for 30 min, as is shown in Figure 1, while the second was cured for 15 days at room temperature.

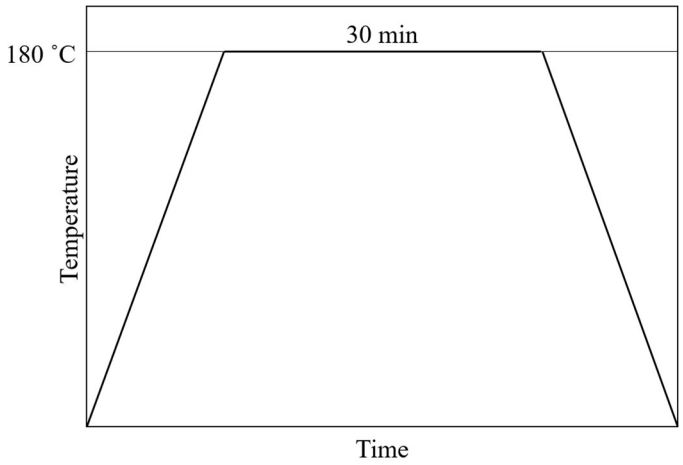

Figure 1 - Cure cycle of Adhesive A.

2.2. Specimen manufacturing

2.2.1. Bulk specimens

Bulk adhesive specimens, used in tensile strength determination tests, were machined from cured adhesive plates, manufactured considering the French standard NF T 76-142 [47], with 2 mm of thickness. For the manufacture of the adhesive plate, uncured material was pressed between steel plates, with a silicone rubber frame contouring the material to restrict it and create hydrostatic pressure. This process ensures good surface finish and prevents the appearance of voids. Furthermore, the specimens were machined following

the British standard BS 2782 [48], in order to obtain the configuration presented in Figure 2.

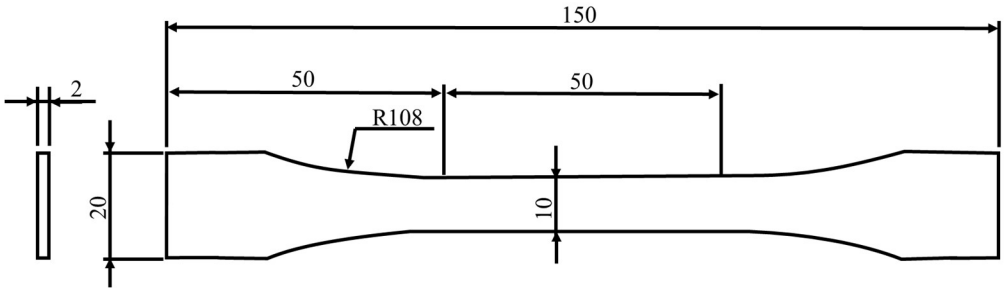

Figure 2 - Tensile specimen geometry, in mm.

2.2.2. DCB specimens

The material chosen for the substrates of the DCB specimens was hard steel, to guarantee elastic deformation without plastic yielding during the loading of the specimen. Both substrates were grit blasted and degreased with acetone immediately before the application of the adhesive, to ensure a good adhesion. These specimens consist of two identical beams that are bonded with adhesive. Additionally, two loading blocks were glued to the substrate, moving the loading points away from the adhesive layer in order to allow for improved data treatment with DIC analysis. The specimen represented in Figure 3, has an initial region without adhesive, *a*, which is the considered to be the pre-crack length. The initial pre-crack was introduced by inserting a sharp razor blade, 0.1 mm thick, at the mid-thickness of the bond line. The bond line thickness was established with calibrated tape, to ensure a constant adhesive thickness. For the Adhesive A and for the Adhesive B, the constant thickness was 0.2 mm and 0.5 mm, respectively. Finally, the specimens were coated with white matte paint and speckled with black dots to facilitate posterior DIC analysis.

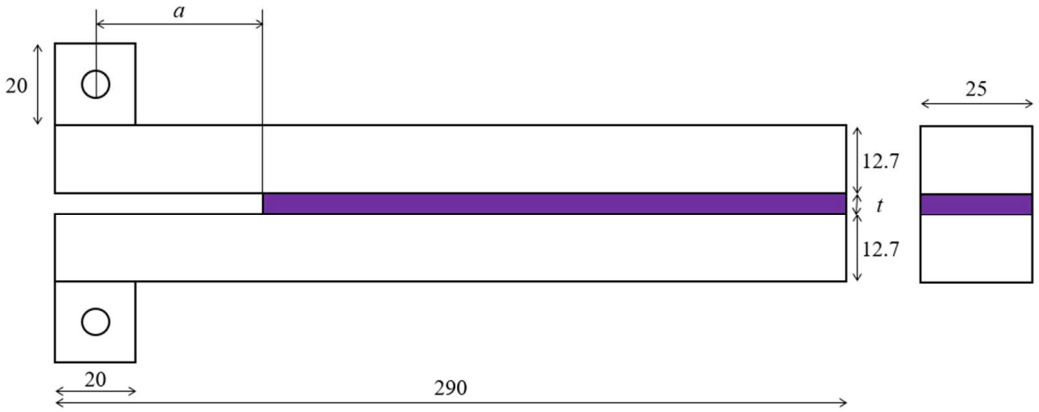

Figure 3 - DCB specimen geometry, in mm.

2.2.3. Block specimens

The substrates were fabricated using a mild steel, since testing the specimens in tension should not introduce high stresses in the steel, minimizing the risk of plastic deformation. Both substrates were grit blasted and degreased with acetone immediately before the application of the adhesive to ensure a good adhesion. The specimens consisted in two identical blocks that were bonded with adhesive, as shown in Figure 4. Finally, the specimens were coated with white matte paint and speckled with black dots to facilitate posterior DIC analysis.

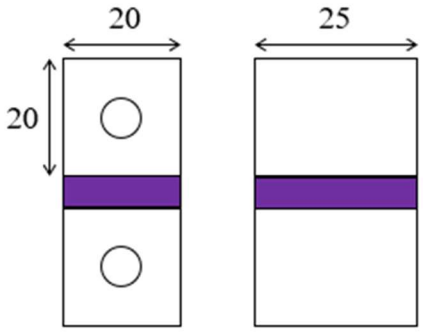

Figure 4 - Block specimen geometry, in mm.

2.3. Testing setup

For the three types of tests, strength prediction, fracture test, and validation tensile test, two different machines were used. For the strength prediction and validation tensile tests, it was used a universal testing machine, INSTRON® 3367 with a load cell of 30 kN. For the Mode I fracture tests, an INSTRON® 8801 test machine with a 100 kN load cell was used. Considering bulk tensile specimens, the quasi-static adopted speeds were 1 mm/min, 20 mm/min and 50 mm/min, and for the remaining two types of specimens the speed was 0.2 mm/min. For the fracture tests, as well as for the validation tests, it was necessary to synchronously monitor the applied load and the displacement field of areas of interest. Thus, a digital camera (Canon EOS M5) equipped with a Canon EF-M 18-55 mm F/3.5-5.6 lens was placed in front of the specimens, with the lens perpendicular to the observation surface.

For each test, at least three specimens were tested.

2.3.1. Bulk tensile testing

Load-displacement curves were recorded for each test until failure occurred, while the displacement was recorded using an extensometer to improve the accuracy of the

measurement. Since adhesive joints are sensitive to the strain rate, the tests were performed at the two aforementioned speeds. The first value was selected, since it corresponds to the standard loading rate for bulk specimens, while the second was chosen considering the speed used in DCB tests, seeking to replicate the actual strain rate used in a DCB. Eq. (5) demonstrates the necessary parameters to calculate the speed for the bulk specimens:

$$\dot{\varepsilon} = \frac{v}{l} \tag{5}$$

where v represents the loading speed and l stands for the characteristic length that is under the estimated strain rate. Hence, considering that DCB tests were performed at 0.2 mm/min and that the characteristic length is the adhesive thickness, the equivalent strain rate in the bulk specimen should be 50 mm/min and 20 mm/min for the Adhesive A and Adhesive B, respectively.

2.3.2. DCB testing

The DCB specimens were mounted to the universal testing machine by connecting the end-blocks to the machine attachment elements with stiff steel pins. The direct method requires the synchronized monitoring of the applied load and two rotation angles at the load introduction points. Thereby, the Mode I fracture toughness and later the cohesive law, could be determined. Thus, the load-displacement curve was registered by the test machine and the displacements were registered on video. The DCB specimens were previously loaded in tension with a small pre-load applied to ensure a stable crack propagation.

The energy release rate in Mode I was determined using the J-integral approach and then compared with CBBM results.

2.3.3. Block tensile testing

Load-displacement curves were recorded for each specimen until failure occurred, while the displacement was recorded using a camera to improve the accuracy of the measurement using DIC.

2.4. DIC method for the parameter measurement

The recorded images were processed using GOM Correlate software to acquire the displacement field data. The facet size used was 12 pixels and a pixel in the image

corresponded to 0.101 mm on the measured surface. The DIC analysis allowed for both the initial crack tip opening and rotations in the loading points to be registered.

2.4.1. Loading point rotations

Sun and Blackman [5] proposed a method to calculate rotations from the displacements of the inspection points, as shown in Figure 5, in the upper and lower substrates, resorting to DIC analysis. By extracting the x and y displacements and then correlating their relationship in the substrates, assuming that they exhibit a linear relationship, was possible to estimate the value of the rotation of each substrate over time by computing $\theta = \frac{dy}{dx}$.

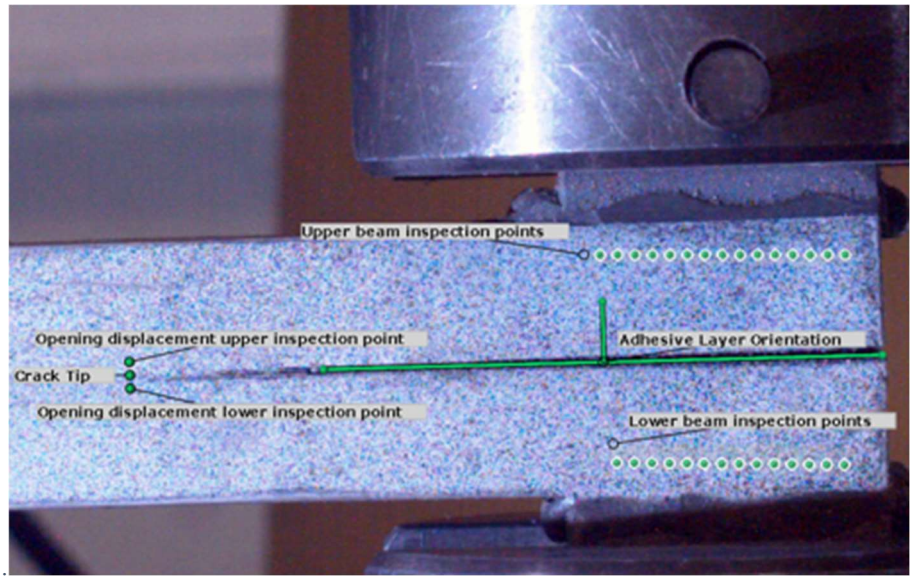

Figure 5 – Marked points in the DIC software.

2.4.2. Crack tip opening displacement

The crack tip opening displacement was measured by computing the difference between the upper and the lower inspection points, as shown in the Figure 5. In order to ensure that the opening is measured perpendicularly to the adhesive layer orientation, the same orientation was registered in the software, and then the points were defined in the correct orientation. For the stiff substrates the crack tip opening displacement, δ_n, was thus determined.

2.4.3. TSL

The values obtained for *J* and the crack tip opening using the mentioned techniques were processed to obtain the TSL. Due to the noise observed in the raw data, all the

parameters were adjusted using a Savitzky-Golay Filter. By adjusting the window length and the order of the polynomial, the results were smoothed.

The TSL was determined by direct differentiation

$$\sigma = \frac{J_{t+\Delta t} - J_t}{\delta_{n_{t+\Delta t}} - \delta_{n_t}} \tag{6}$$

where t is time and Δt is the increment between two measurements. The increment was adjusted for each test depending on the data acquisition frequency and total time of the test.

For the final presentation of the TSL, the same filter was applied in order to achieve a smoother curve in the end.

2.5. Python script

The estimation of a precise cohesive law, based on the direct method, consists in the differentiation of only experimental results, which introduce experimental noise often higher than the acceptable. Additionally, by using the method proposed by Sun and Blackman [5], the number of values within the DIC results can be in the order of thousands. Hence, a Python script was developed, aiming to address the two problems, by automating data processing and applying adequate filters to the results. Figure 6 represents the proposed algorithm.

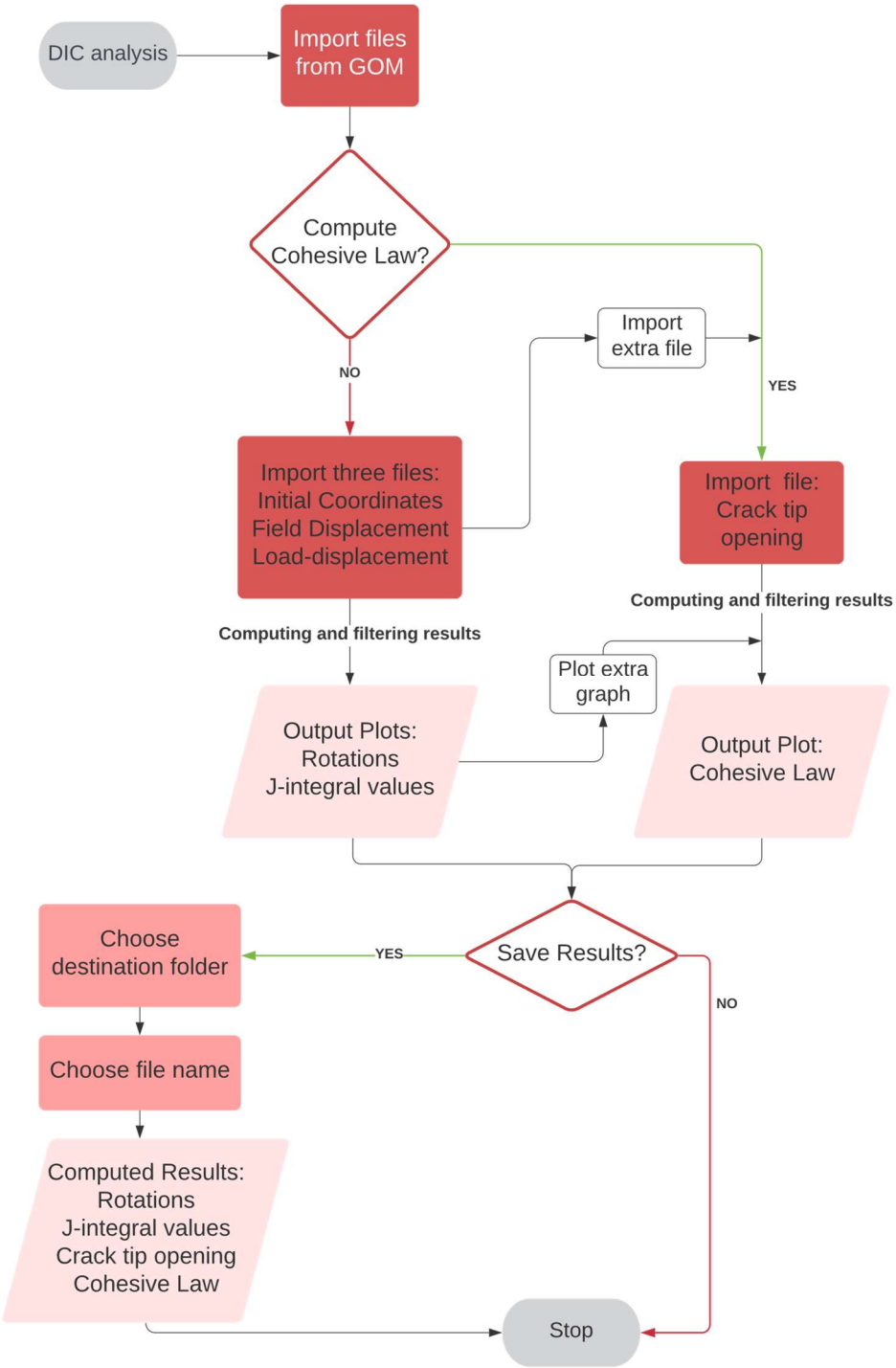

Figure 6 – Flowchart of the developed code.

3. Experimental results

3.1. Bulk tensile tests

The bulk tensile tests were performed in an effort to comprehend the influence of the different strain rates on the tensile strength and Young's modulus of the adhesives being studied.

For **Adhesive A** specimens**,** the stress-strain curves obtained, at the two loading rates, were like the ones in Figure 7. It was observed that an increase of the loading rate originated a higher strength and lower maximum strain in the adhesive.

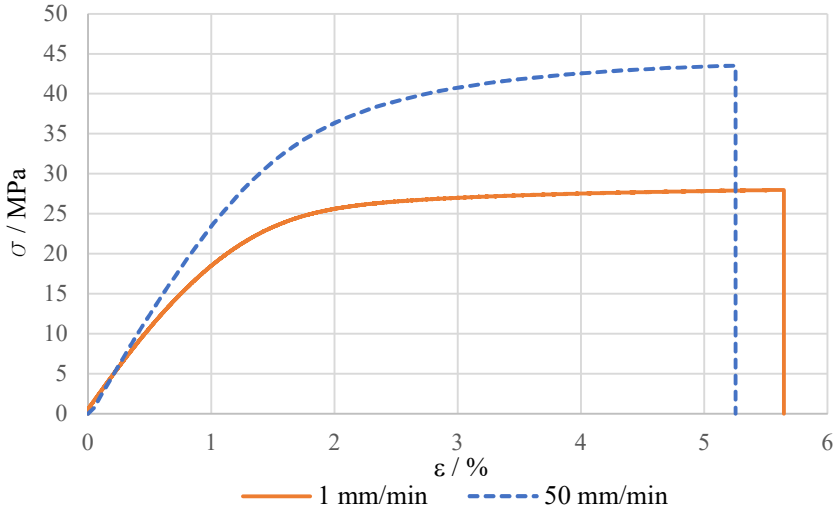

Figure 7 - Representative stress strain curves for tensile tests of Adhesive A at different loading rates.

For **Adhesive B,** a similar behaviour was observed, as shown in Figure 8.

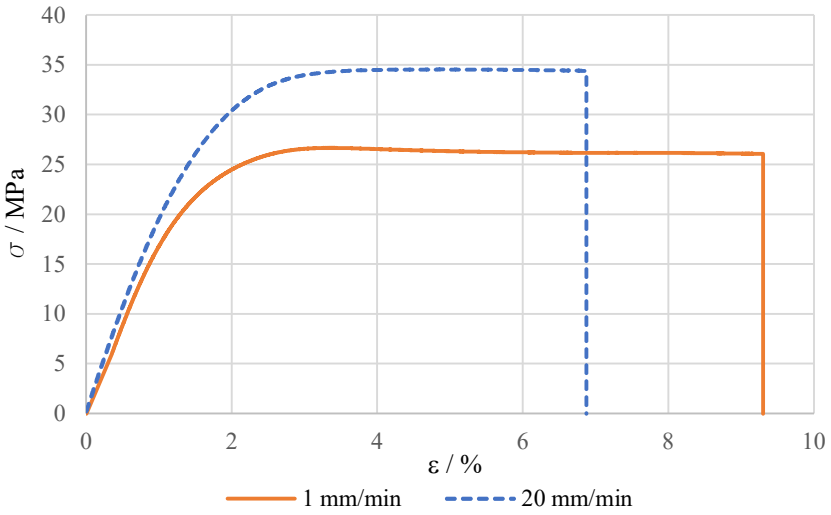

Figure 8 - Representative stress strain curves for tensile tests of Adhesive B at different loading rates.

These results seem to suggest that the strength prediction of an adhesive, based on conventional bulk tensile tests, could predict a different value than the one observed in a DCB test. The constraint posed on the adhesive by the significantly stiffer substrates restricts deformation and originates a triaxial stress state, and thus, the strength of the adhesive joint appears to be higher than the one determined in the bulk tests.

The Young's modulus for both adhesives did not reflect significant differences as it can be observed in Figure 7 and Figure 8.

3.2. DCB tests

The load-displacement curves recorded with the test machine are shown in Figure 9, by means of a representative curve, for each adhesive.

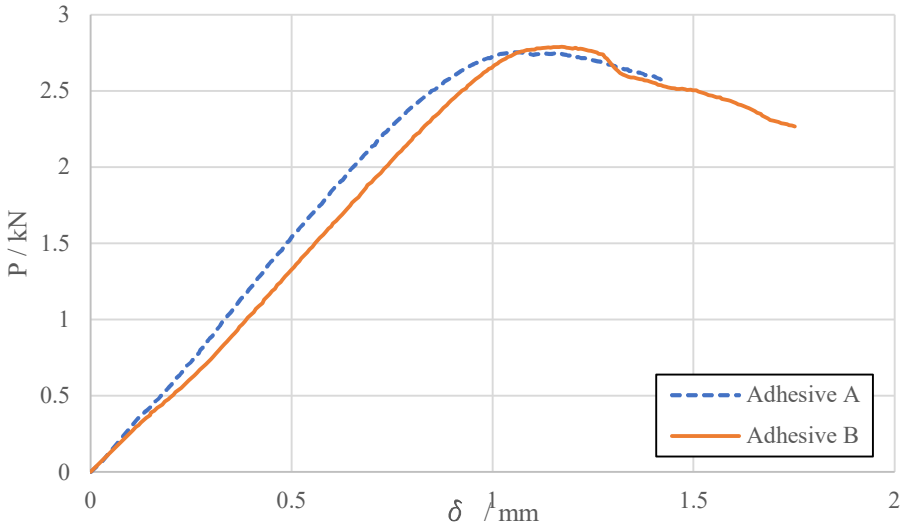

Figure 9 – Representative load-displacement curves for DCB tests of the adhesives.

The fracture toughness of each adhesive was determined with the J-integral approach, for Mode I, and then compared to the results obtained with CBBM. Additionally, to measure similar values, the displacement results used in CBBM were obtained by the displacement field of a point in the substrate, under the loading pin, with DIC analysis.

In **Adhesive A** DCB specimens, all tests exhibited a cohesive failure mode, and stable crack propagation was observed. Furthermore, crack propagation occurred in the middle-plane of the adhesive layer. Figure 10 shows the values of G and J for this adhesive. Both values steadily increased until a certain point, after which they remained approximately constant, while the displacement kept increasing. The J-integral approach was most conservative than the alternative method, although these differences could be explained by some difficulties in determining the initial compliance, C_0, in CBBM. The critical value for J_c was reached at ~2.45 N/mm. The difference between the two methods was about 6.5%.

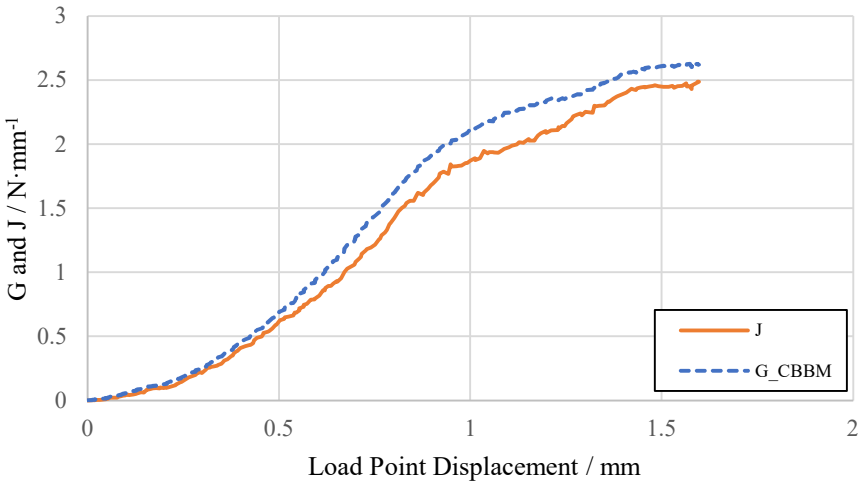

Figure 10 – Representative fracture toughness curves for CBBM and J-integral of the Adhesive A.

In **Adhesive B** DCB specimens, all tests exhibited a cohesive failure, as well as a stable crack propagation. Contrarily to the first adhesive, this epoxy did not show a crack propagation solely through the middle-plane of the adhesive layer, and some failure near the interface was observed. Notwithstanding, no adhesive failure was observed in any part of the specimen. Figure 11 shows the values of G and J for this adhesive. Both values steadily increased until a certain point, after which they remained approximately constant, while the displacement kept increasing. At this stage, the values ranged from 2.25 N/mm to 2.37 N/mm. When the critical values, G_c and J_c, were reached, both approaches estimated the same values, with an average of 2.31 N/mm.

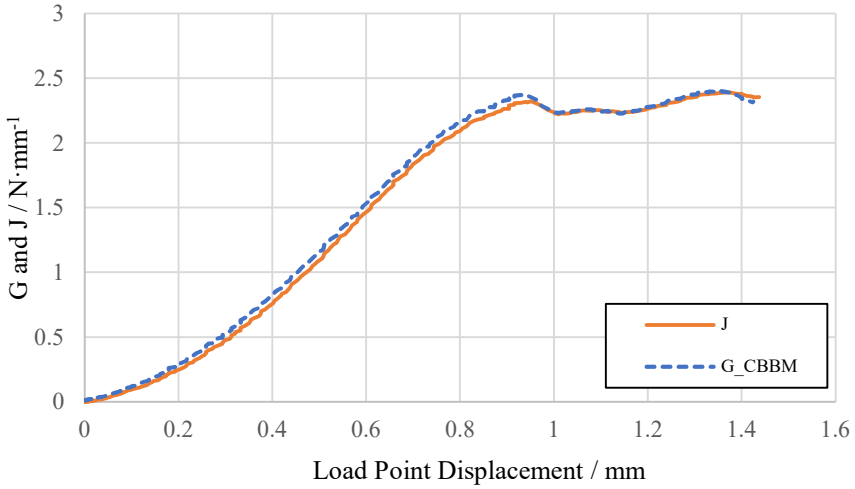

Figure 11 – Representative fracture toughness curves for CBBM and J-integral of the Adhesive B.

3.3. Traction Separation Law

A Savitzky-Golay filter was employed on the experimentally obtained data to generate a smoothened cohesive law for both adhesives. The results were found to be sensitive to the parameters used in the filter, so this procedure was carefully executed to prevent the loss of important information. However, the method proved to be highly sensitive to any change in the obtained values.

For **Adhesive A**, a maximum value for stress of 57.74 MPa was reached, at the end of the elastic part of the curve. From that point forward, there was a decreasing trend in the tension values as the damage increased. The value of the critical separation length was approximately 0.17 mm. As mentioned above, this value was higher than the one obtained through bulk tensile tests. Figure 12 shows the fracture behaviour of this adhesive.

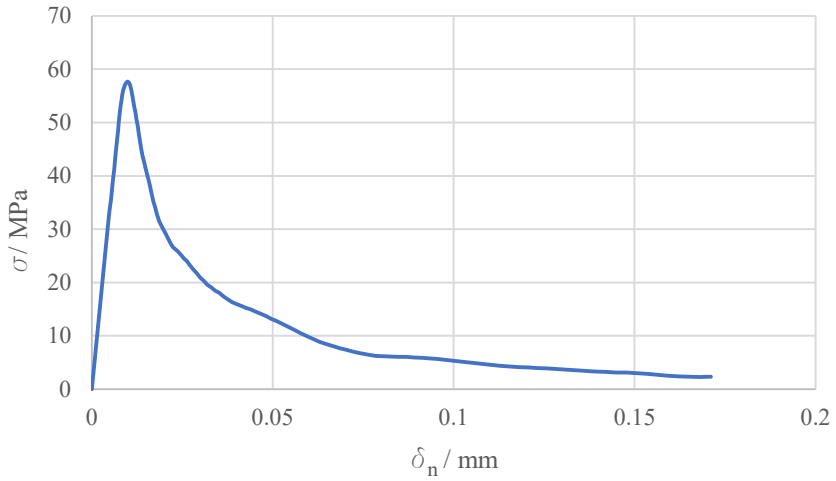

Figure 12 – Average cohesive law for the Adhesive A.

For **Adhesive B**, the maximum stress value at the end of the elastic behaviour was 36.10MPa, after which the stress quickly decreased. The value of the critical separation length was found to be approximately 0.18 mm. Figure 13 shows the fracture behaviour of this adhesive.

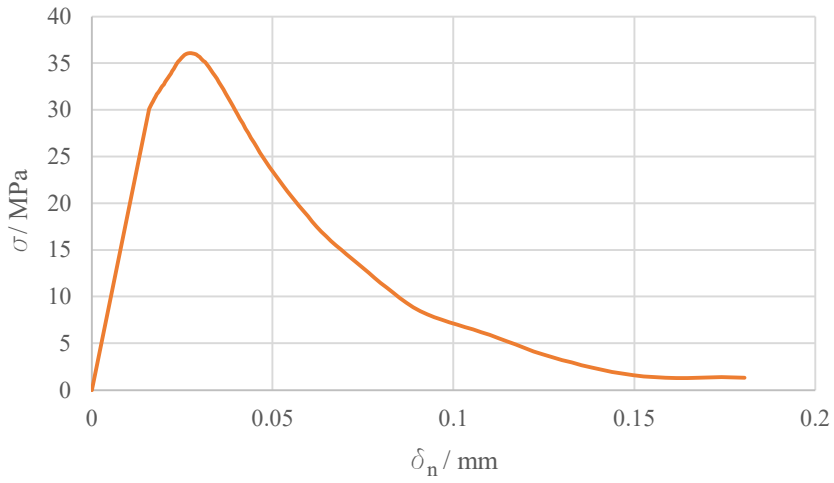

Figure 13 – Average cohesive law for the Adhesive B.

The obtained TSLs were later used to simulate the tested joints, allowing to validate the methodology. For that purpose, an average damage value for each adhesive was computed, so the average cohesive laws were inputted in the simulation and a broader solution could be achieved. Figure 14 shows these damage curves.

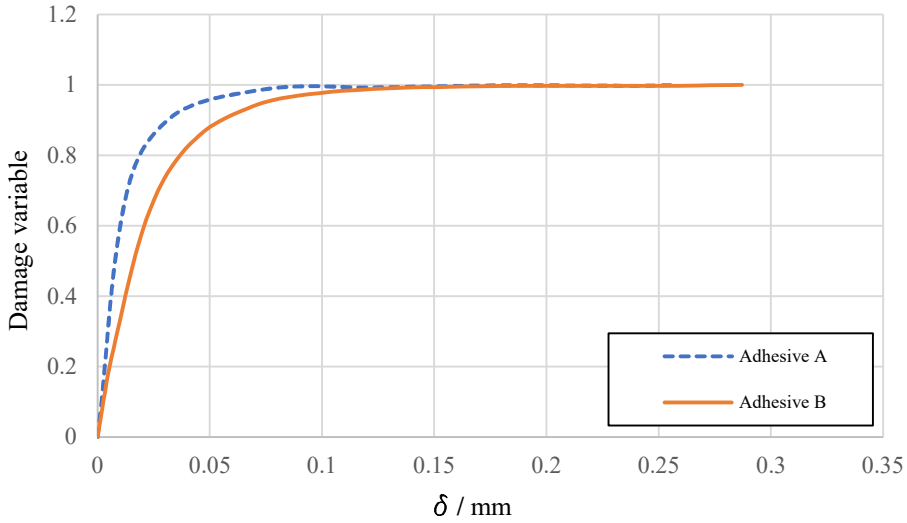

Figure 14 – Average damage evolution for the adhesives.

3.4. Block tests

As a way to further study the effect of the specimen geometry on the results obtained through the direct method, validation blocks were manufactured with the Adhesive A. Since this test is similar to a tensile butt joint test, the obtained results of the former matched the results of the latter. Assuming that, as is the case for a butt joint, the tensile test is loading all the adhesive surface at the same time, the relation between stress and

substrate displacement was determined by the expression $\sigma = F/A$, where F is the applied load and A is the area of the block that is bonded with the adhesive. A comparison between the obtained curve and the one obtained with a Slip Hopkinson Pressure Bar (SHPB) specimen [49] may be viewed in Figure 15.

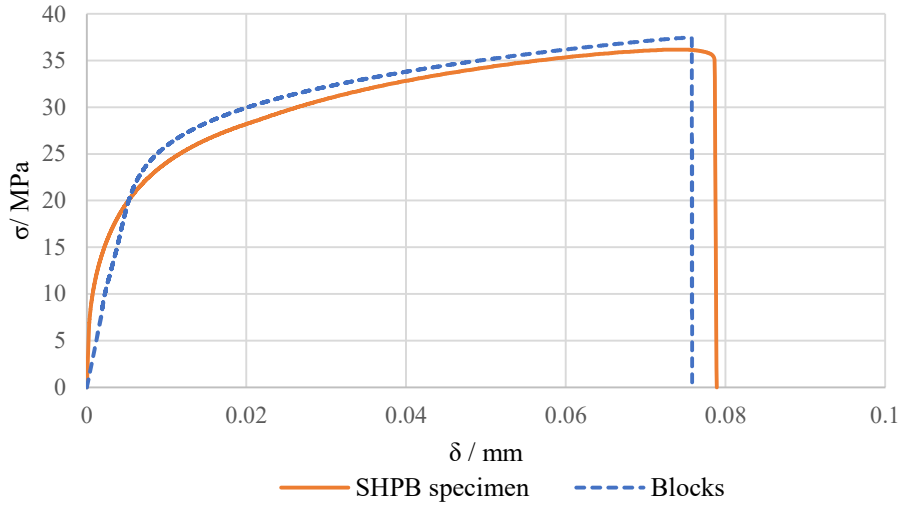

Figure 15 – Representative cohesive laws for the blocks and SHPB specimens.

4. FEM analysis

4.1. Specimen's modelling

Before modelling and simulating the obtained TSLs, the average experimental results were inputted in Abaqus software (2017), using only one cohesive element COH2D4, to generate the average cohesive law. Figure 16 shows the obtained cohesive laws for both adhesives.

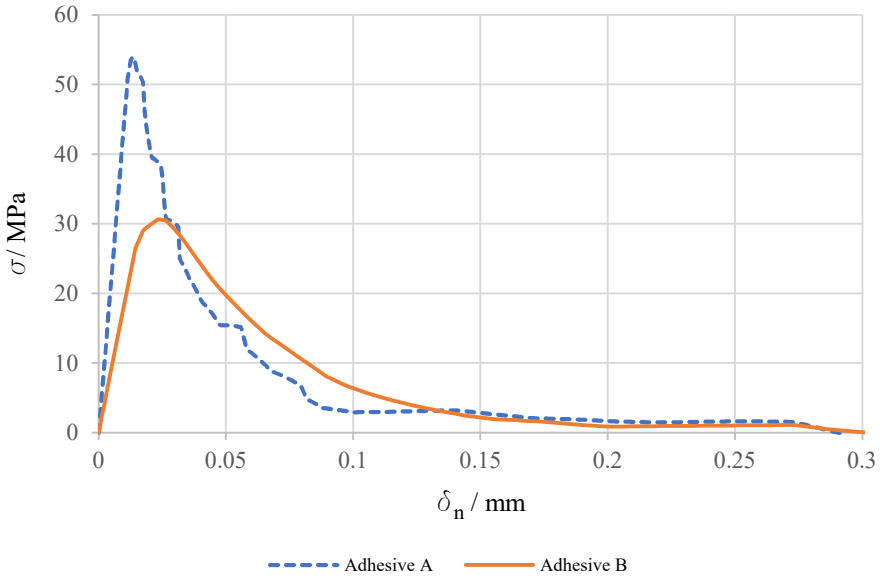

Figure 16 – Simulated average cohesive laws of the adhesives.

For the Adhesive A, the non-elastic part of the curve recorded some instabilities due to fluctuations on the average damage curve. Nonetheless, the trend of its behaviour could be easily analysed.

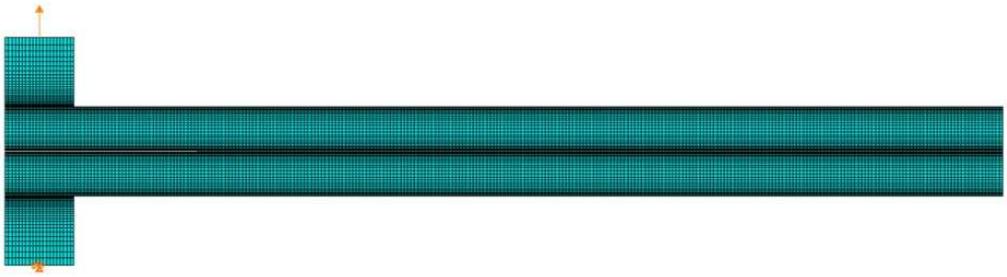

Figure 17 – DCB model for numerical simulation.

Then, the obtained TSLs were implemented in the FE software. The elastic element CPS4R was used to model the steel substrates, while the cohesive element COH2D4 was used to model the adhesive layer. Thereafter, a 2D DCB model was used to simulate the fracture process, ensuring that the geometry of the model was identical to the one used in the fracture tests. Figure 17 represents the geometry, boundary conditions, and the mesh that was used for the simulation.

4.2. Numerical validation

Regarding the numerical simulation, after the average cohesive law was used in the CZM model, its results were compared to an average load-displacement curve that represents each adhesive.

Figure 18 shows the comparison between the experimental data and the numerical simulation for the Adhesive A. The simulated model presented an overestimation of the maximum value for the load of approximately 6.3%, for the average values. For this adhesive, the fracture process was not perfectly determined by the model, since it assumes an underestimation of the damage suffered during the test. Although this behaviour was observed in the results, the tests were carried out only to capture the initiation process of crack propagation and the full damaged part of the curve could not be analysed.

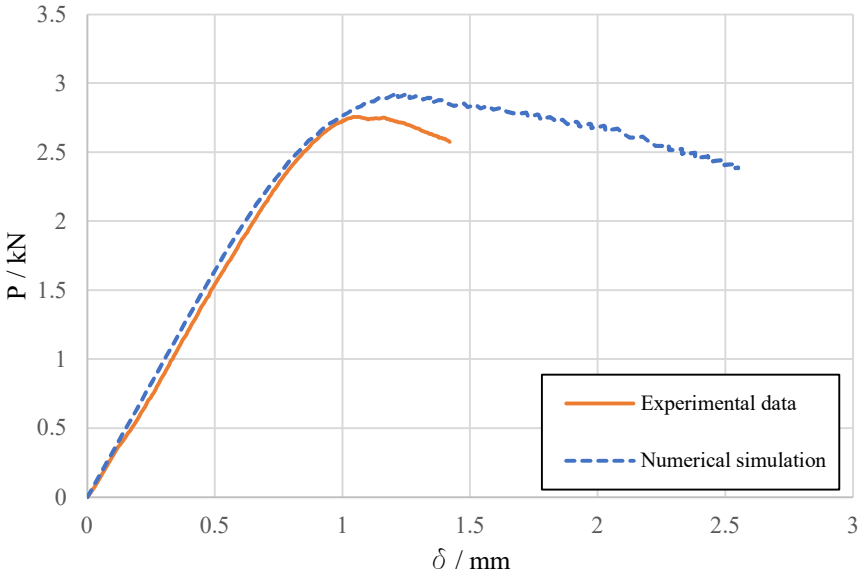

Figure 18 – Comparison between experimental and numerical load-displacement curves for the Adhesive A.

Figure 19 shows the comparison between the experimental data and the numerical simulation for the Adhesive B. The simulated model presented an exact estimation of the maximum value for the load, for the average values. Regarding the elastic part of the curve, the results indicate that the model assumed a stiffer material than the real one. For this adhesive, the simulation of the fracture process was closer to the experimental results than the previous simulation of Adhesive A. Even though these tests were also performed to capture only the initiation of fracture process, it was still possible to analyse some part of the crack propagation, allowing to observe that the numerical model did not perfectly simulate the damage process, underestimating the damage values.

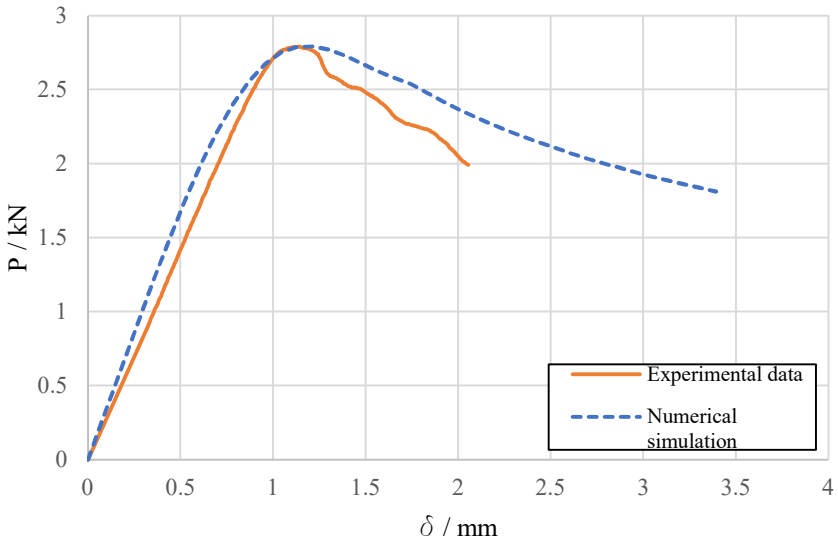

Figure 19 – Comparison between experimental and numerical load-displacement curves for the Adhesive B.

The following step was to apply the same method to the numerical values, i.e., estimating the *J* values by resorting to numerical load and displacement data, and differentiating the *J* values with respect to numerical crack tip opening displacement data. This procedure assessed the possibility of obtaining the same cohesive law that was initially inputted on the software.

Figure 20 shows both *J*-displacement and TSL curves for the average cohesive law of Adhesive A. The left curve exhibits the *J* values, which continuously increased until they reached an almost constant value. The zone with constant values shows some variations due to instabilities in the model, likely stemming from the average damage that was inputted. When compared to the average experimental data, which was ~2.4 N/mm, the result underestimated the energy value, and the difference was approximately 5%. Despite this difference, the results can still be considerable as acceptable. The right curve exhibits the comparison between the average experimental cohesive law and the obtained numerical cohesive law. It shows an almost identical linear part, with a difference between the maximum tension values of approximately 7%, from 50 MPa to 53.8 MPa. The results were similar regarding the part of the curve that represents the damage process. Overall, a good agreement between the experimental and the numerical results was observed for this adhesive.

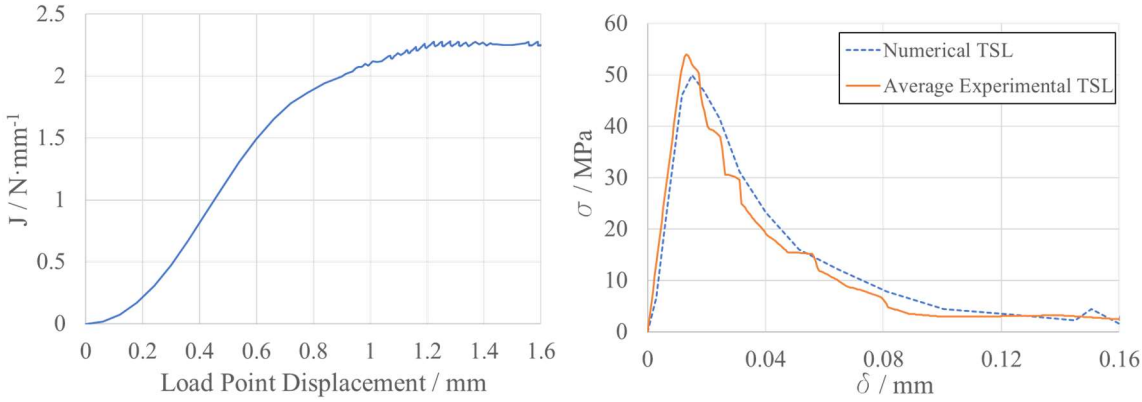

Figure 20 – Results from numerical simulation for the Adhesive A: J-integral values (left) and cohesive law (right).

Figure 21 shows both *J*-displacement and TSL curves for the average cohesive law of Adhesive B. The left curve shows the *J* values, which continuously increased until they reached a constant value that was explicitly defined. When compared to the average experimental data, which was ~2.2 N/mm, the result underestimated the energy value, and the difference was approximately 4%, which was very close to the experimental data.

The right curve exhibits the comparison between the average experimental cohesive law and the obtained numerical cohesive law. It shows two parallel linear parts, with very close values, and a difference between the maximum tension results of approximately 2%, from 30.2 MPa to 30.7 MPa. Like the elastic part, the part of the curve that represents the damage process seems to be slightly translated in the *x* direction. Overall, very good agreement was observed between the experimental and the numerical results for this adhesive.

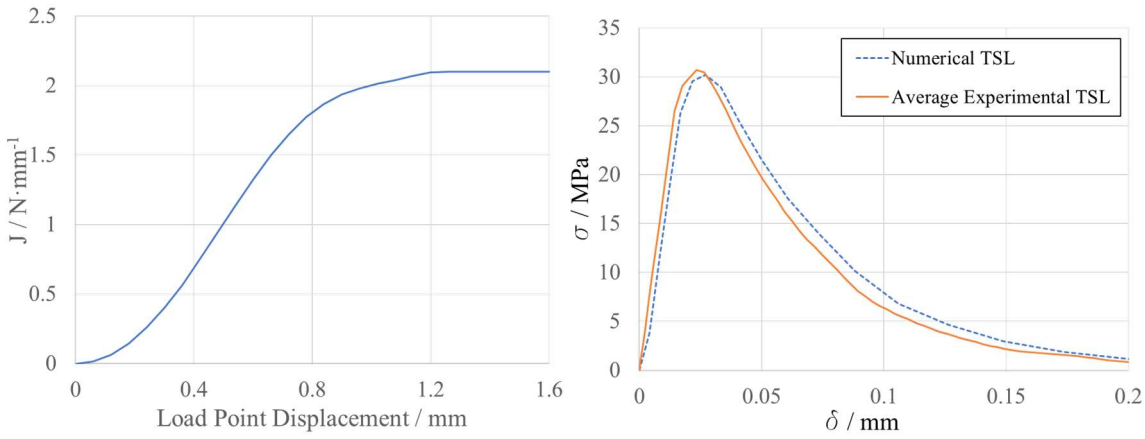

Figure 21 – Results from numerical simulation for the Adhesive B: J-integral values (left) and cohesive law (right).

The use of CZM together with the J-integral approach provided results with some deviations from the experimental values but could still be used to determine the main features of the TSL. The simulation of both adhesives could overestimate the integrity of the joint, and the simulation of Adhesive B could overestimate the stiffness of the bonded joint.

5. Validation in different geometry

After the validation of the cohesive laws, obtained through the direct method for a DCB specimen, a different geometry was modelled to simulate the Adhesive A, using the same experimental law.

5.1. Specimen's modelling

The elastic element CPS4R was used to model the steel substrates, while the cohesive element COH2D4 was used to model the adhesive layer. Thereafter, a 2D block model was used to simulate the fracture process, adopting a geometry that is identical to the one used in the tests. Figure 22 represents the geometry, the boundary conditions, and the mesh that was used for the simulation.

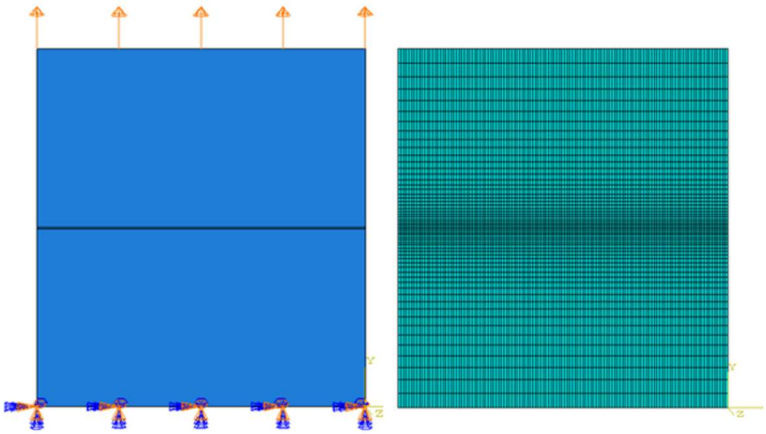

Figure 22 – Block model for numerical simulation.

5.2. Numerical validation

Regarding the numerical simulation, two cohesive laws were used in the CZM model, to simulate the joint behaviour, specifically the average experimental cohesive law and the one previously obtained [49] for a butt joint test, with the same adhesive. Since in this kind of test all the elements are loaded at the same time, the shape of the resultant curves was expected to be highly similar to the inputted laws, which was indeed the case. Figure 23 compares both the simulated load-displacement curves and the cohesive laws used to simulate the joints.

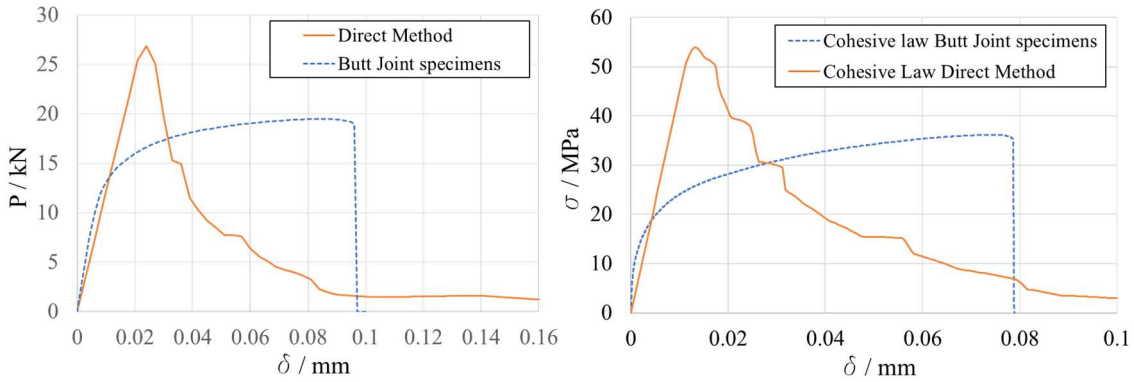

Figure 23 –Comparison of the results for the block tensile tests using Adhesive A: load-displacement curves (left) and cohesive laws (right).

As expected, the shape of the obtained load-displacement curve, for each case, was very similar to the curve that was introduced in the material properties. This result indicates that the direct method is dependent on the joint geometry and the constraining condition of the adhesive. The whole method is highly dependent on specific conditions, such as the manufacturing process of the specimens, test configuration setup, loading conditions of the specimens, and their geometry. The described situation suggests that,

for pure modes, the direct cohesive law that is obtained has practical limitations. Thus, its application should be carefully chosen.

6. Conclusion

In this work, hard steel substrates were bonded with two different epoxy-based adhesives, and the Mode I fracture behaviour of the adhesive joints was evaluated. The results were obtained using DCB tests and DIC analysis.

In order to optimize data analysis and obtain smoothened results, a Python script was developed. The appropriate setup configuration and a thorough investigation provided the opportunity to compare the J-integral results with the CBBM method, as well as to extract the direct TSL for each adhesive.

Both adhesives yielded similar fracture toughness values in both methods. Due to some difficulties in measuring the initial compliance, the fracture toughness determined with CBBM of the Adhesive A was approximately 6.5% higher than the value obtained with J-integral approach. Regarding Adhesive B, both methods attained the same value.

A comparison between the experimental TSLs and the numerical simulations showed difficulties in describing with precision the failure processes by the CZM modelling. However, the overall features were acceptable. Furthermore, the results obtained with the direct method confirmed that the strength prediction using DCB tests is different from the one obtained using bulk tensile tests.

The obtained cohesive law for the Adhesive A was used to simulate the fracture of a block specimen that behaves like a butt joint. It was concluded that the load-displacement curves were highly dependent on the shape of the inputted cohesive law. This aspect suggests that, for pure modes, the loading and constraining conditions should be carefully assessed, in order to avoid substantial differences between the experimental data and the numerical results. These results also suggest that there is interest in studying the influence of the different pure mode cohesive laws in the simulation of adhesive joints that are under Mixed Mode loading. It would also be relevant to investigate if the numerical methods could accurately predict the fracture behaviour in these conditions.

References

[1] J. Monteiro *et al.*, "Mode II modeling of adhesive materials degraded by fatigue loading using cohesive zone elements," *Theoretical and Applied Fracture Mechanics,* vol. 103, p. 102253, 2019/10/01 2019, doi: 10.1016/j.tafmec.2019.102253.

[2] M. Costa, G. Viana, R. Créac'hcadec, L. F. M. da Silva, and R. D. S. G. Campilho, "A cohesive zone element for mode I modelling of adhesives degraded by humidity and fatigue," *International Journal of Fatigue,* vol. 112, pp. 173-182, 2018/07/01 2018, doi: 10.1016/j.ijfatigue.2018.03.014.

[3] P. Zamani, A. Jaamialahmadi, and L. F. M. da Silva, "The influence of GNP and nano-silica additives on fatigue life and crack initiation phase of Al-GFRP bonded lap joints subjected to four-point bending," *Composites Part B: Engineering,* vol. 207, p. 108589, 2021/02/15 2021, doi: 10.1016/j.compositesb.2020.108589.

[4] U. T. F. Carvalho and R. D. S. G. Campilho, "Application of the direct method for cohesive law estimation applied to the strength prediction of double-lap joints," *Theoretical and Applied Fracture Mechanics,* vol. 85, pp. 140-148, 2016/10/01/ 2016, doi: 10.1016/j.tafmec.2016.08.018.

[5] F. Sun and B. R. K. Blackman, "A DIC method to determine the Mode I energy release rate G, the J-integral and the traction-separation law simultaneously for adhesive joints," *Engineering Fracture Mechanics,* vol. 234, p. 107097, 2020/07/01 2020, doi: 10.1016/j.engfracmech.2020.107097.

[6] M. Z. Sadeghi, J. Zimmermann, A. Gabener, and K. U. Schroeder, "The applicability of J-integral approach in the determination of mixed-mode fracture energy in a ductile adhesive," *International Journal of Adhesion and Adhesives,* vol. 83, pp. 2-8, 2018/06/01/ 2018, doi: 10.1016/j.ijadhadh.2018.02.027.

[7] S. Goutianos and B. F. Sørensen, "The application of J integral to measure cohesive laws under large-scale yielding," *Engineering Fracture Mechanics,* vol. 155, pp. 145-165, 2016/04/01 2016, doi: 10.1016/j.engfracmech.2016.01.004.

[8] S. Abdel Monsef, M. Pérez-Galmés, J. Renart, A. Turon, and P. Maimí, "The influence of mode II test configuration on the cohesive law of bonded joints," *Composite Structures,* vol. 234, p. 111689, 2020/02/15 2020, doi: 10.1016/j.compstruct.2019.111689.

[9] J. Rice, "A Path Integral and the Approximate Analysis of Strain Concentration by Notches and Cracks," *Journal of Applied Mechanics,* vol. 35, pp. 379-386, 06/01 1968, doi: 10.1115/1.3601206.

[10] R. J. Bucci, P. C. Paris, J. D. Landes, and J. Rice, "J-integral estimation procedures," *ASTM Special Technical Publication,* pp. 40-69, 01/01 1972, doi: 10.1520/STP38818S.

[11] A. Biel and U. Stigh, "Comparison of J-integral methods to experimentally determine cohesive laws in shear for adhesives," *International Journal of Adhesion and Adhesives,* vol. 94, pp. 64-75, 2019/10/01 2019, doi: 10.1016/j.ijadhadh.2019.04.014.

[12] D. Kimpfbeck, Z. Major, and M.-C. Miron, "Application of J Integral for the Fracture Assessment of Welded Polymeric Components," 2019.

[13] C. Sarrado, A. Turon, J. Renart, and J. Costa, "An experimental data reduction method for the Mixed Mode Bending test based on the J-integral approach," *Composites Science and Technology,* vol. 117, pp. 85-91, 2015/09/29 2015, doi: 10.1016/j.compscitech.2015.05.021.

[14] F. Chaves, L. F. M. Silva, M. De Moura, D. Dillard, and V. Esteves, "Fracture Mechanics Tests in Adhesively Bonded Joints: A Literature Review," *The Journal of Adhesion,* vol. 90, pp. 955-992, 11/02 2014, doi: 10.1080/00218464.2013.859075.

[15] R. D. S. G. Campilho, D. C. Moura, D. J. S. Gonçalves, J. F. M. G. da Silva, M. D. Banea, and L. F. M. da Silva, "Fracture toughness determination of adhesive and co-cured joints in natural fibre composites," *Composites Part B: Engineering,* vol. 50, pp. 120-126, 2013/07/01 2013, doi: 10.1016/j.compositesb.2013.01.025.

[16] F. Sun and B. R. K. Blackman, "Using digital image correlation to automate the measurement of crack length and fracture energy in the mode I testing of structural adhesive joints," *Engineering Fracture Mechanics,* vol. 255, p. 107957, 2021/10/01 2021, doi: 10.1016/j.engfracmech.2021.107957.

[17] M. Pérez-Galmés, J. Renart, C. Sarrado, A. Rodríguez-Bellido, and J. Costa, "A data reduction method based on the J-integral to obtain the interlaminar fracture toughness in a mode II end-loaded split (ELS) test," *Composites Part A: Applied Science and Manufacturing,* vol. 90, pp. 670-677, 2016/11/01 2016, doi: 10.1016/j.compositesa.2016.08.020.

[18] B. F. Sørensen and T. K. Jacobsen, "Determination of cohesive laws by the J integral approach," *Engineering Fracture Mechanics,* vol. 70, no. 14, pp. 1841-1858, 2003/09/01 2003, doi: 10.1016/S0013-7944(03)00127-9.

[19] C. Desai, S. Basu, and V. Parameswaran, "Determination of Traction Separation Law for Interfacial Failure in Adhesive Joints at Different Loading Rates," *The Journal of Adhesion,* vol. 92, p. 150527102921008, 05/21 2015, doi: 10.1080/00218464.2015.1046986.

[20] Y. Zhu, K. M. Liechti, and K. Ravi-Chandar, "Direct extraction of rate-dependent traction–separation laws for polyurea/steel interfaces," *International Journal of Solids and Structures,* vol. 46, no. 1, pp. 31-51, 2009/01/01 2009, doi: 10.1016/j.ijsolstr.2008.08.019.

[21] G. Lélias, E. Paroissien, F. Lachaud, and J. Morlier, "Experimental characterization of cohesive zone models for thin adhesive layers loaded in mode I, mode II, and mixed-mode I/II by the use of a direct method," *International Journal of Solids and Structures,* vol. 158, pp. 90-115, 2019/02/01 2019, doi: 10.1016/j.ijsolstr.2018.09.005.

[22] U. Stigh, S. Alfredsson, and A. Biel, "Measurement of Cohesive Laws and Related Problems," *ASME International Mechanical Engineering Congress and Exposition, Proceedings,* vol. 11, 01/01 2009, doi: 10.1115/IMECE2009-10474.

[23] H. Li and N. Chandra, "Analysis of crack growth and crack-tip plasticity in ductile materials using cohesive zone models," *International Journal of Plasticity,* vol. 19, no. 6, pp. 849-882, 2003/06/01/ 2003, doi: 10.1016/S0749-6419(02)00008-6.

[24] P. L. Rosendahl, Y. Staudt, C. Odenbreit, J. Schneider, and W. Becker, "Measuring mode I fracture properties of thick-layered structural silicone sealants," *International Journal of Adhesion and Adhesives,* vol. 91, pp. 64-71, 2019/06/01 2019, doi: 10.1016/j.ijadhadh.2019.02.012.

[25] J. Yu, Y. Wang, Z. Li, Q. Zhang, X. Jian, and Z. Zhang, "Using DIC technique to characterize the mode II interface fracture of layered system composed of multiple materials," *Composite Structures,* vol. 230, p. 111413, 2019/12/15 2019, doi: 10.1016/j.compstruct.2019.111413.

[26] Z. Jia, G. Yuan, D. Hui, X. Feng, and Y. Zou, "Effect of high strain rate and low temperature on mode II fracture toughness of ductile adhesive," *International Journal of Adhesion and Adhesives,* vol. 86, pp. 105-112, 2018/11/01/ 2018, doi: 10.1016/j.ijadhadh.2018.09.003.

[27] A. Arrese, N. Insausti, F. Mujika, M. Perez-Galmés, and J. Renart, "A novel experimental procedure to determine the cohesive law in ENF tests," *Composites Science and Technology,* vol. 170, pp. 42-50, 2019/01/20 2019, doi: doi.org/10.1016/j.compscitech.2018.11.031.

[28] B. F. Sørensen and P. Kirkegaard, "Determination of mixed mode cohesive laws," *Engineering Fracture Mechanics,* vol. 73, no. 17, pp. 2642-2661, 2006/11/01/ 2006, doi: 10.1016/j.engfracmech.2006.04.006.

[29] L. Loh and S. Marzi, "A novel experimental methodology to identify fracture envelopes and cohesive laws in mixed-mode I + III," *Engineering Fracture Mechanics,* vol. 214, pp. 304-319, 2019/06/01 2019, doi: 10.1016/j.engfracmech.2019.03.011.

[30] H. Cui, "Simulation of ductile adhesive failure with experimentally determined cohesive law," *Composites Part B: Engineering,* vol. 92, pp. 193-201, 2016/05/01 2016, doi: 10.1016/j.compositesb.2016.02.018.

[31] L. F. d. Silva, A. Öchsner, and R. D. Adams, *Handbook of Adhesion Technology*. Springer, 2018.

[32] J. M. Gorman and M. D. Thouless, "The use of digital-image correlation to investigate the cohesive zone in a double-cantilever beam, with comparisons to numerical and

analytical models," *Journal of the Mechanics and Physics of Solids,* vol. 123, pp. 315-331, 2019/02/01 2019, doi: 10.1016/j.jmps.2018.08.013.

[33] G. Cricrì, "Cohesive law identification of adhesive layers subject to shear load – An exact inverse solution," *International Journal of Solids and Structures,* vol. 158, pp. 150-164, 2019/02/01/ 2019, doi: 10.1016/j.ijsolstr.2018.09.001.

[34] S. Abdel Monsef, A. Ortega, A. Turon, P. Maimí, and J. Renart, "An efficient method to extract a mode I cohesive law for bonded joints using the double cantilever beam test," *Composites Part B: Engineering,* vol. 178, p. 107424, 2019/12/01 2019, doi: 10.1016/j.compositesb.2019.107424.

[35] P. Ghabezi and M. Farahani, "A cohesive model with a multi-stage softening behavior to predict fracture in nano composite joints," *Engineering Fracture Mechanics,* vol. 219, p. 106611, 2019/10/01 2019, doi: 10.1016/j.engfracmech.2019.106611.

[36] I. Katsivalis, O. T. Thomsen, S. Feih, and M. Achintha, "Development of cohesive zone models for the prediction of damage and failure of glass/steel adhesive joints," *International Journal of Adhesion and Adhesives,* vol. 97, p. 102479, 2020/03/01 2020, doi: doi.org/10.1016/j.ijadhadh.2019.102479.

[37] J. C. S. Azevedo, R. D. S. G. Campilho, F. J. G. da Silva, T. M. S. Faneco, and R. M. Lopes, "Cohesive law estimation of adhesive joints in mode II condition," *Theoretical and Applied Fracture Mechanics,* vol. 80, pp. 143-154, 2015/12/01/ 2015, doi: 10.1016/j.tafmec.2015.09.007.

[38] U. T. F. Carvalho and R. D. S. G. Campilho, "Validation of pure tensile and shear cohesive laws obtained by the direct method with single-lap joints," *International Journal of Adhesion and Adhesives,* vol. 77, pp. 41-50, 2017/09/01 2017, doi: 10.1016/j.ijadhadh.2017.04.002.

[39] U. T. F. Carvalho and R. D. S. G. Campilho, "Validation of a direct method to predict the strength of adhesively bonded joints," *Science and Technology of Materials,* vol. 30, no. 3, pp. 138-143, 2018/09/01 2018, doi: 10.1016/j.stmat.2017.12.002.

[40] C. Sarrado, A. Turon, J. Costa, and J. Renart, "An experimental analysis of the fracture behavior of composite bonded joints in terms of cohesive laws," *Composites Part A: Applied Science and Manufacturing,* vol. 90, 07/01 2016, doi: 10.1016/j.compositesa.2016.07.004.

[41] S. M. Jensen, M. J. Martos, E. Lindgaard, and B. L. V. Bak, "Inverse parameter identification of n-segmented multilinear cohesive laws using parametric finite element modeling," *Composite Structures,* vol. 225, p. 111074, 2019/10/01 2019, doi: 10.1016/j.compstruct.2019.111074.

[42] C. Wu, R. Huang, and K. M. Liechti, "Simultaneous extraction of tensile and shear interactions at interfaces," *Journal of the Mechanics and Physics of Solids,* vol. 125, pp. 225-254, 2019/04/01 2019, doi: 10.1016/j.jmps.2018.12.004.

[43] B. Blaysat, J. P. M. Hoefnagels, G. Lubineau, M. Alfano, and M. G. D. Geers, "Interface debonding characterization by image correlation integrated with Double Cantilever Beam kinematics," *International Journal of Solids and Structures,* vol. 55, pp. 79-91, 2015/03/01 2015, doi: 10.1016/j.ijsolstr.2014.06.012.

[44] G. F. Dias, M. F. S. F. de Moura, J. A. G. Chousal, and J. Xavier, "Cohesive laws of composite bonded joints under mode I loading," *Composite Structures,* vol. 106, pp. 646-652, 2013/12/01 2013, doi: 10.1016/j.compstruct.2013.07.027.

[45] F. Sun, R. Zhang, and B. R. K. Blackman, "Determination of the mode I crack tip opening rate and the rate dependent cohesive properties for structural adhesive joints using digital image correlation," *International Journal of Solids and Structures,* vol. 217-218, pp. 60-73, 2021/05/15 2021, doi: 10.1016/j.ijsolstr.2021.01.034.

[46] M. F. S. F. de Moura, R. D. S. G. Campilho, and J. P. M. Gonçalves, "Crack equivalent concept applied to the fracture characterization of bonded joints under pure mode I loading," *Composites Science and Technology,* vol. 68, no. 10, pp. 2224-2230, 2008/08/01 2008, doi: doi.org/10.1016/j.compscitech.2008.04.003.

[47] *NF T 76-142. Méthode de préparation de plaques d'adhésifs structuraux pour la réalisation d'éprouvettes d'essai de caractérisation*, 1988.

[48] "BS 2782-0:2011. Methods of testing plastics.," 2011.

[49] P. D. P. Nunes, E. A. S. Marques, R. J. C. Carbas, A. Akhavan-Safar, and L. F. M. da Silva, "Quasi-static and intermediate test speed validation of SHPB specimens for the determination of mode I, mode II fracture toughness of structural epoxy adhesives," *Engineering Fracture Mechanics,* vol. 262, p. 108231, 2022/03/01 2022, doi: doi.org/10.1016/j.engfracmech.2021.108231.

Appendix B Developed code

Main file

```
from IPython import get_ipython
get_ipython().magic('reset -f')
import matplotlib.pyplot as plt
plt.close("all")
import tkinter as tk
from tkinter import filedialog, simpledialog, messagebox, ttk
import pandas as pd
import time
import os.path, sys
sys.path.append('.')
from file_organization import func_organization
from file_rotations import func_rotations
from file_J import func_J
from file_cohesive_law import func_cohesive_law
from file_figures import func_figures

def import_csv_data_gom():
    global csv_file_path_gom, v
    csv_file_path_gom = filedialog.askopenfilename(filetypes=(("csv", "*.csv"),\
                                                    ("all files", "*.*")))
    v.set(csv_file_path_gom)
def import_csv_data_coordinates():
    global csv_file_path_coord, w
    csv_file_path_coord = filedialog.askopenfilename(filetypes=(("csv", "*.csv"),
                                                    ("all files", "*.*")))
    w.set(csv_file_path_coord)
def import_csv_data_force():
    global csv_file_path_force, y
    csv_file_path_force= filedialog.askopenfilename(filetypes=(("csv", "*.csv"),
                                                    ("all files", "*.*")))
    y.set(csv_file_path_force)
def import_csv_data_coh_law():
    global csv_file_path_coh_law, z
    csv_file_path_coh_law= filedialog.askopenfilename(filetypes=(("csv", "*.csv"),
                                                    ("all files", "*.*")))
    z.set(csv_file_path_coh_law)
def saveinfo():
    if csv_file_path_gom=='' or csv_file_path_coord=='' \
        or csv_file_path_force==''\
        or (var1.get() == 1 and csv_file_path_coh_law ==''):
        tk.messagebox.showerror(title='Error', message='Choose all file paths')
    else:
        global df_gom, df_coord, df_force, temp_gom, temp_coord, \
            temp_force, answer
        if var1.get() == 1:
            global df_coh_law, temp_coh_law
        cont=0
        temp_gom=pd.read_csv(csv_file_path_gom,sep=",")
        if temp_gom.columns[0]!='Time [s]' or temp_gom.columns[1][:6]!='Point ' \
            or temp_gom.columns[1][-8:]!='.dX [mm]':
            tk.messagebox.showerror(title='Error', message='Choose another GOM \
                                                    data file')
            cont=1
```

```
        else:
            df_gom=pd.read_csv(csv_file_path_gom,sep=",")
        temp_coord=pd.read_csv(csv_file_path_coord,sep=",")
        if temp_coord.columns[0]!='type' or temp_coord.columns[1]!='name'
\
            or  temp_coord.columns[2]!='coord-x':
            tk.messagebox.showerror(title='Error', \
                                    message='Choose another initial coordinates \
                                                data file')
            cont=1
        else:
            df_coord=pd.read_csv(csv_file_path_coord,sep=",",\
                                 usecols=['name','coord-x' ,'coord-y'])
        temp_force=pd.read_csv(csv_file_path_force,sep=",")
        if temp_force.columns[0]!='Extension' or temp_force.columns[1]!='Load' \
            or temp_force.columns[2]!='Time(s)':
            tk.messagebox.showerror(title='Error', message='Choose another force \
                                        data file')
            cont=1
        else:
            df_force=pd.read_csv(csv_file_path_force,sep=",")
        if var1.get() == 1:
            temp_coh_law=pd.read_csv(csv_file_path_coh_law,sep=",")
            if temp_coh_law.columns[0]!='Time [s]' \
                or temp_coh_law.columns[1][:6]!= 'Point ' \
                    or temp_coh_law.columns[3]!='Crack tip openning.LY [mm]':
                tk.messagebox.showerror(title='Error', \
                                        message='Choose another crack \
                                                    tip opening data file')
                cont=1
            else:
                df_coh_law=pd.read_csv(csv_file_path_coh_law,sep=",",\
                                       usecols=['Time [s]',\
                                                'Crack tip openning.LY [mm]'])
        if cont==0:
            answer = var1.get()
            root.destroy()
def button_enable():
    if var1.get() == 1:
        btn5.configure(state = 'normal')
        entry_4.configure(state = 'normal')
    elif var1.get() == 0:
        btn5.configure(state = 'disabled')
        global csv_file_path_coh_law, z
        csv_file_path_coh_law = ''
        z.set(csv_file_path_coh_law)
        entry_4.configure(state = 'disabled')

root = tk.Tk()
root.title('Data Introduction')
root.geometry('700x250')
root.configure(background='white')
v = tk.StringVar(); w = tk.StringVar(); y = tk.StringVar(); z = tk.StringVar()
var1 = tk.IntVar()
csv_file_path_gom=''; csv_file_path_coord=''; csv_file_path_force='';
\ csv_file_path_coh_law=''
btn1=tk.Button(root,text='Browse Gom Data',\
               command=import_csv_data_gom).grid(row=0, column=0,padx=10,\
                                                 sticky=tk.W+tk.E)
```

```
btn2=tk.Button(root,text='Browse Coordinate Data', \
               command=import_csv_data_coordinates).grid(row=1, column=0,padx=10,\
                                                         sticky=tk.W+tk.E)
btn3=tk.Button(root,text='Browse Force Data',\
               command=import_csv_data_force).grid(row=2, column=0,padx=10, \
                                                   sticky=tk.W+tk.E)
btn5=tk.Button(root,text='Browse Crack Tip Opening Data',\
               command=import_csv_data_coh_law,state='disabled')
btn5.grid(row=4, column=0,padx=10,sticky=tk.W+tk.E)
btn4=tk.Button(root,text='Run',command=saveinfo).grid(column=1, row=5)
entry_1 = tk.Entry(root,textvariable=v,width=50).grid(row=0, column=1, padx=10, \
                                                      pady=10)
entry_2 = tk.Entry(root,textvariable=w,width=50).grid(row=1, column=1, padx=10, \
                                                      pady=10)
entry_3 = tk.Entry(root,textvariable=y,width=50).grid(row=2, column=1, padx=10, \
                                                      pady=10)
entry_4 = tk.Entry(root,textvariable=z,width=50,state='disabled')
entry_4.grid(row=4, column=1, padx=10, pady=10)
c1 = tk.Checkbutton(root, text='Plot the Cohesive Law',variable=var1, \
                    command=button_enable, onvalue=1, offvalue=0, \
                        bg='white').grid(row=3, column=1, padx=10)
root.eval('tk::PlaceWindow . center')
root.mainloop()

try:
    del temp_gom, temp_force, temp_coord, btn1, btn2, btn3, btn4, btn5, entry_1, \
        entry_2, entry_3, entry_4, c1, var1, root, v, w, y, z, csv_file_path_coord, \
            csv_file_path_force, csv_file_path_gom
    if answer == 1:
        del temp_coh_law, csv_file_path_coh_law

    start=1
    root_3 = tk.Tk()
    root_3.title("Progressbar")
    root_3.geometry('200x70')
    progress = tk.ttk.Progressbar(root_3, orient = 'horizontal',length = 100, \
                                  mode = 'determinate')

    def my_progress(df_gom, df_coord, df_force):
        global figure1, figure2, ax1, ax2, df_final, px

        if answer==1:
            df_final = pd.DataFrame(index=range(len(df_gom)),
            columns=['Time[s]','Upper_Rotation[rad]',\'Lower_Rotation[rad]',
                     'Total_Rotation[rad]','Total_Rotation_Trend[rad]','Force[kN]',
                     'Load_Point_Disp[mm]','J[N/mm]','J(Rot_Trend)[N/mm]',
                     'Delta_Trend_Zero[mm]','Stress[MPa]','Stress_Smooth[MPa]'])
        else:
            df_final = pd.DataFrame(index=range(len(df_gom)),
            columns=['Time[s]','Upper_Rotation[rad]','Lower_Rotation[rad]',
                      'Total_Rotation[rad]','Total_Rotation_Trend[rad]','Force[kN]',
                      'Load_Point_Disp[mm]','J[N/mm]','J(Rot_Trend)[N/mm]'])

        #Computing inputs
        df_upper, df_lower, up_points, low_points = func_organization(df_coord,\
                                                                      df_gom)
        df_final['Time[s]'] = df_gom['Time[s]']

        progress['value'] = 10
```

```
        value_label.config(text = '10 %')
        root_3.update()
        time.sleep(0.5)

        #Rotations
        coef_up = func_rotations(df_upper, up_points)
        progress['value'] = 40
        value_label.config(text = '40 %')
        root_3.update()
        time.sleep(0.5)

        coef_low = func_rotations(df_lower, low_points)
        del df_upper, df_lower, up_points, low_points
        progress['value'] = 70
        value_label.config(text = '70 %')
        root_3.update()
        time.sleep(0.5)

        #Final dataframe
        df_final['Upper_Rotation[rad]'] = coef_up
        df_final['Lower_Rotation[rad]'] = coef_low
        df_final['Total_Rotation[rad]'] = df_final['Upper_Rotation[rad]']- \
                                          df_final['Lower_Rotation[rad]']
        df_final['Force[kN]'] = df_force['Load']
        df_final['Load_Point_Disp[mm]'] = df_force['Extension']
        del coef_up, coef_low

        #J
        df_final = func_J(df_final)

        #Cohesive Law
        if answer==1:
            func_cohesive_law(df_coh_law, df_final)
            global figure3, ax3

        progress['value'] = 90
        value_label.config(text = '90 %')
        root_3.update()
        time.sleep(0.5)

        # Plots
        if answer==1:
            figure1, figure2, figure3 = func_figures(df_final, answer)
        else:
            figure1, figure2 = func_figures(df_final, answer)

        progress['value'] = 100
        value_label.config(text = '100 %')
        root_3.update()
        time.sleep(1)
        root_3.destroy()

    progress.pack(pady = 10)
    txtvar=tk.StringVar()
    value_label = ttk.Label(root_3, text=txtvar)
    value_label.pack()
    root_3.eval('tk::PlaceWindow . center')
    root_3.after(start, my_progress(df_gom, df_coord, df_force))
    root_3.mainloop()
```

```
    del start, df_coord, df_gom, df_force, progress, txtvar, value_label, root_3

    from matplotlib.backends.backend_tkagg import FigureCanvasTkAgg

    def saveinfo2():
        global dir_name, test_name
        dir_name = filedialog.askdirectory(title='Choose file')
        if dir_name!='':
            cont=0
            while cont==0:
                test_name=simpledialog.askstring(title="Test Name",
                            prompt="Write the test name",initialvalue='Test xxx')
                if test_name==None:
                    dir_name=''; test_name=''; cont=1
                elif test_name!=None:
                    if os.path.exists(dir_name+'/'+test_name+ \
                                      ' - Plot Rotations.tiff')==0 \
                        and os.path.exists(dir_name+'/'+test_name+ \
                                           ' - Plot J.tiff')==0:
                        figure1.savefig(dir_name+'/'+test_name+ \
                                        ' - Plot Rotations.tiff', \
                                            dpi=150, format="tiff")
                        figure2.savefig(dir_name+'/'+test_name+' - Plot J.tiff', \
                                        dpi=150, format="tiff")
                        df_final.to_csv(dir_name+'/'+test_name+ \
                                        ' - Calculations.csv',index=False)
                        if answer==1:
                            figure3.savefig(dir_name+'/'+test_name+ \
                                            ' - Plot Cohesive Law.tiff', \
                                                dpi=150, format="tiff")
                        cont=1
                        root_2.destroy()
                    else:
                        quest=tk.messagebox.askquestion(title='Error', message= \
                                                        'There is already a file \
for '+ \test_name+'. \
Do you want to \
overwrite it?')
                        if quest=='yes':
                            figure1.savefig(dir_name+'/'+test_name+' - \
Plot Rotations.tiff',\
                                            dpi=150, format="tiff")
                            figure2.savefig(dir_name+'/'+test_name+' - \
Plot J.tiff', dpi=150, format="tiff")
                            df_final.to_csv(dir_name+'/'+test_name+ \
                                            ' - Calculations.csv',index=False)
                            if answer==1:
                                figure3.savefig(dir_name+'/'+test_name+\
                                            ' - Plot Cohesive Law.tiff', dpi=150, \
                                                format="tiff")
                            cont=1
                            root_2.destroy()
                        else:
                          cont=0

    def on_closing():
        global str
        bol=messagebox.askokcancel("Quit", "Do you want to quit?")
        if bol==1:
```

```
            root_2.destroy()

    root_2 = tk.Tk()
    root_2.title('Data Plots'); root_2.geometry('2000x580'); \
        root_2.configure(background='white')

    dir_name=''; test_name=''

    if answer==1:
        figure_1 = FigureCanvasTkAgg(figure1, root_2); \
            figure_1.get_tk_widget().grid(row=1,column=1)
        figure_2 = FigureCanvasTkAgg(figure2, root_2); \
            figure_2.get_tk_widget().grid(row=1,column=2)
        figure_3 = FigureCanvasTkAgg(figure3, root_2); \
            figure_3.get_tk_widget().grid(row=1,column=3)
    else:
        figure_1 = FigureCanvasTkAgg(figure1, root_2); \
            figure_1.get_tk_widget().grid(row=1,column=1)
        figure_2 = FigureCanvasTkAgg(figure2, root_2); \
            figure_2.get_tk_widget().grid(row=1,column=3)

    btn1=tk.Button(root_2,text='Save Results',font=('Calibri', 10),padx=6,\
                   pady=6,bg='#4a7abc',fg='yellow', activebackground='green', \
                       activeforeground='white', \
                           command=saveinfo2).grid(row=2, column=2, pady=8)
    root_2.protocol("WM_DELETE_WINDOW", on_closing)
    root_2.eval('tk::PlaceWindow . center')
    root_2.mainloop()

except NameError:
    del btn1, btn2, btn3, btn4, btn5, entry_1, entry_2, entry_3, entry_4, c1, \
        var1, root, v, w, y, z, csv_file_path_coord, csv_file_path_force,\
            csv_file_path_gom, csv_file_path_coh_law
```

Function *func_organization*

```
def func_organization(df_coord, df_gom):

    import pandas as pd
    df_coord.columns = df_coord.columns.str.replace('␣', '')
    df_coord_ord = df_coord.sort_values('coord-x').reset_index(drop=True)
    up_coord_value = df_coord_ord['coord-y'].max()
    low_coord_value = df_coord_ord['coord-y'].min()
    df_gom.columns = df_gom.columns.str.replace('␣', '')

    #organize points
    up_points = []; low_points = []
    for pt in range(len(df_coord_ord)):
        if df_coord_ord.iloc[pt,2] == up_coord_value:
            up_points.append(df_coord_ord.iloc[pt,0])
        elif df_coord_ord.iloc[pt,2] == low_coord_value:
            low_points.append(df_coord_ord.iloc[pt,0])

    #dataframe with time length and 2*number of points of the upper beam
    df_upper = pd.DataFrame(index=range(len(df_gom)), \
                            columns=range(2*len(up_points)))
    for pts in range(len(up_points)):
        str = up_points[pts].replace('␣','')+('.dX[mm]')
        for pt_u in range(len(df_coord_ord)):
            if up_points[pts] == df_coord_ord.at[pt_u,'name']:
                df_upper[pts] = df_gom[str]+df_coord_ord.iloc[pt_u,1]
                df_upper = df_upper.rename(columns={pts:up_points[pts]+ \
                                                    '.xup'})
        str2 = up_points[pts].replace('␣','')+('.dY[mm]')
        df_upper[pts+len(up_points)] = df_gom[str2]
        df_upper = df_upper.rename(columns={pts+len(up_points):up_points[pts]+ \
                                            '.yup'})
    df_lower = pd.DataFrame(index=range(len(df_gom)), \
                            columns=range(2*len(low_points)))
    for pts2 in range(len(low_points)):
        str = low_points[pts2].replace('␣','')+('.dX[mm]')
        for pt_l in range(len(df_coord_ord)):
            if low_points[pts2] == df_coord_ord.at[pt_l,'name']:
                df_lower[pts2] = df_gom[str]+df_coord_ord.iloc[pt_l,1]
                df_lower = df_lower.rename(columns={pts2:low_points[pts2]+ \
                                                    '.xup'})
        str2 = low_points[pts2].replace('␣','')+('.dY[mm]')
        df_lower[pts2+len(low_points)] = df_gom[str2]
        df_lower = df_lower.rename(columns={pts2+len(low_points):low_points[pts2]+ \
                                            '.yup'})

    return df_upper, df_lower, up_points, low_points
```

Function *func_rotations*

```
def func_rotations(df, points):

    import numpy as np
    df = df.astype(float)
    coef = []
    for pt in range(len(df)):
        c = np.polyfit(df.iloc[pt,0:len(points)],df.iloc[pt,len(points):2* \
                                                         (len(points))],1)
        coef.append(c[0])

    return coef
```

Function *func_J*

```
def func_J(df_final):

    import numpy as np
    import pandas as pd
    from scipy import signal

    df_final['J[N/mm]'] = (df_final['Force[kN]'] / 25) *  \
        df_final['Total_Rotation[rad]']
    coef_rot = np.polyfit(df_final['Load_Point_Disp[mm]'], \
                          df_final['Total_Rotation[rad]'],6)
    fit_rot = np.poly1d(coef_rot)
    rot_trend = fit_rot(df_final['Load_Point_Disp[mm]'])
    df_final['Total_Rotation_Trend[rad]'] = rot_trend
    df_final['J(Rot_Trend)[N/mm]'] = (df_final['Force[kN]'] / 25) * \
        df_final['Total_Rotation_Trend[rad]']


    return df_final
```

Function *func_cohesive_law*

```
def func_cohesive_law(df_coh_law, df_final):

    import pandas as pd
    import numpy as np
    from scipy import signal
    import matplotlib.pyplot as plt
    df_coh_law.columns = df_coh_law.columns.str.replace('␣', '')
    coef_opening = np.polyfit(df_final['Time[s]'], \
                              df_coh_law['Cracktipopenning.LY[mm]'], 6)
    fit_opening = np.poly1d(coef_opening)
    open_trend = fit_opening(df_final['Time[s]'])
    df_coh_law['Delta_Trend[mm]'] = open_trend
    df_final['Delta_Trend_Zero[mm]'] = open_trend

    delta = signal.savgol_filter(df_final['Delta_Trend_Zero[mm]'], 53, 1)
    df_final['Delta_Trend_Zero[mm]'] = delta
    plt.plot(df_final['Time[s]'],df_final['Delta_Trend_Zero[mm]'])
```

```
    # Fit
    J = signal.savgol_filter(df_final['J(Rot_Trend)[N/mm]'], 53, 4)
    df_final['J(new)'] = J
    L = [0]
    L1 = [0]
    for var_i in range(len(df_final) - 1):
        diff = abs(df_final['J(new)'][var_i] - df_final['J(new)'][var_i+1])
        L.append(diff)
        diff2 = abs(df_final['Delta_Trend_Zero[mm]'][var_i] - \
                    df_final['Delta_Trend_Zero[mm]'][var_i+1])
        L1.append(diff2)
    df_final['Diff_J'] = L
    df_final['Diff_Delta'] = L1
    df_final['Stress[MPa]'] = df_final['Diff_J'] / df_final['Diff_Delta']
    df_final['Stress[MPa]'][0] = 0
    czmsmooth = signal.savgol_filter(df_final['Stress[MPa]'],53, 4),
    df_aux = pd.DataFrame(czmsmooth)
    df_final['Stress_Smooth[MPa]'] = df_aux.T

    return df_final
```

Function *func_figures*

```
def func_figures(df_final, answer):

    import matplotlib.pyplot as plt
    mls_1 = '-'; mls_2 = '--'#; mls_3 = '-.';
    mls_4 = '-o'; mls_5 = '-*'; mls_6 = '-x' # tipos de linhas
    colors = [[0,0,0],[0.25,0.25,0.25],[0.5,0.5,0.5],[1,0,0]] # line colours
    px = 1/plt.rcParams['figure.dpi']  # pixel in inches

    # Plot Rotations
    figure1 = plt.Figure(figsize=(520*px,420*px), dpi=120)
    ax1 = figure1.add_subplot(111)
    ax1.plot(df_final['Load_Point_Disp[mm]'],df_final['Upper_Rotation[rad]'], \
             mls_1,color=colors[0],lw=1.5) #Up
    ax1.plot(df_final['Load_Point_Disp[mm]'],df_final['Lower_Rotation[rad]'], \
             mls_1,color=colors[1],lw=1.5) #Low
    ax1.plot(df_final['Load_Point_Disp[mm]'],df_final['Total_Rotation[rad]'], \
             mls_1,color=colors[2],lw=1.5) #Total
    ax1.plot(df_final['Load_Point_Disp[mm]'], \
             df_final['Total_Rotation_Trend[rad]'],mls_2, \
                 color=colors[3],lw=1.5) #Trend
    ax1.legend(['Upper beam rotation','Lower beam rotation','Total rotation', \
                'Trendline'],fontsize = 8,loc='upper left')
    ax1.set_title('Plot Rotations', fontsize = 12)
    ax1.grid(color = '0.75', ls = '--', lw = 0.5) # Set up the gridlines
    ax1.xaxis.set_ticks_position('bottom')
    ax1.set_xlabel('Load Point Displacement [mm]',fontsize = 10, \
                   labelpad = 10) # x axis label
    ax1.set_ylabel('Rotation [rad]',fontsize = 10,labelpad = 5) #  y axis label
    figure1.tight_layout()

    # Plot J
    figure2 = plt.Figure(figsize=(520*px,420*px), dpi=120)
    ax2 = figure2.add_subplot(111)
    ax2.plot(df_final['Load_Point_Disp[mm]'],df_final['J[N/mm]'],mls_1, \
```

```
        color=colors[0],lw=1.5) #Exp
ax2.plot(df_final['Load_Point_Disp[mm]'],df_final['J(Rot_Trend)[N/mm]'], \
        mls_1,color=colors[3],lw=1.5) #Trend
ax2.legend(['Experimental data', 'J with rotation trendline'],fontsize = 8, \
          loc='lower right')
ax2.set_title('Plot J', fontsize = 12)
ax2.grid(color = '0.75', ls = '-', lw = 0.5)
ax2.xaxis.set_ticks_position('bottom')
ax2.set_xlabel('Load Point Displacement [mm]', fontsize = 10, labelpad = 5)
ax2.set_ylabel('J [N/mm]', fontsize = 10, labelpad = 10)
figure2.tight_layout()

# Plot Cohesive Law
if answer==1:
    figure3 = plt.Figure(figsize=(520*px,420*px), dpi=120)
    ax3 = figure3.add_subplot(111)
    ax3.plot(df_final['Delta_Trend_Zero[mm]'],df_final['Stress[MPa]'],mls_1, \
             color=colors[0],lw=1.5) #Experimental
    ax3.plot(df_final['Delta_Trend_Zero[mm]'],df_final['Stress_Smooth[MPa]'], \
             mls_1,color=colors[3],lw=1.5) #Trend
    ax3.legend(['Experimental data', 'Smooth line'],fontsize = 8, \
               loc='upper right')
    ax3.set_title('Plot Cohesive Law', fontsize = 12)
    ax3.grid(color = '0.75', ls = '-', lw = 0.5) # Set up the gridlines
    ax3.xaxis.set_ticks_position('bottom')
    # Define the x axis label
    ax3.set_xlabel('Crack tip opening [mm]', fontsize = 10, labelpad = 5)
    # Define the y axis label
    ax3.set_ylabel(u'\u03C3 [MPa]', fontsize = 10, labelpad = 10)
    #ax3.set_xlim([0,0.3]) - only if window adjustment is needed
    #ax3.set_ylim([0,80]) - only if window adjustment is needed
    figure3.tight_layout()

if answer==1:
    return figure1, figure2, figure3
else:
    return figure1, figure2
```